

**WIND GUSTS DISTURBANCE REJECTION FOR A
QUADROTOR WITH TILTED ROTORS**

BY

ABDULRAHMAN ALIYU

A Thesis Presented to the
DEANSHIP OF GRADUATE STUDIES

KING FAHD UNIVERSITY OF PETROLEUM & MINERALS

DHAHRAN, SAUDI ARABIA

In Partial Fulfillment of the
Requirements for the Degree of

MASTER OF SCIENCE

In

SYSTEMS AND CONTROL ENGINEERING


April 2016

KING FAHD UNIVERSITY OF PETROLEUM & MINERALS

DHAHRAN- 31261, SAUDI ARABIA

DEANSHIP OF GRADUATE STUDIES

This thesis, written by **ABDULRAHMAN ALIYU** under the direction of his thesis advisor and approved by his thesis committee, has been presented and accepted by the Dean of Graduate Studies, in partial fulfillment of the requirements for the degree of **MASTER OF SCIENCE IN SYSTEMS & CONTROL ENGINEERING.**

 17-5-2016

Dr. Hesham K. Al-Fares
Department Chairman

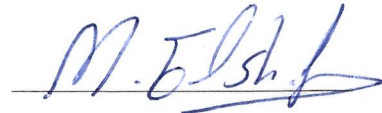


Dr. Salam A. Zummo
Dean of Graduate Studies

19/5/16

Date





Dr. Moustafa El-Shafei
(Advisor)



Dr. Magdi S. Mahmoud
(Member)



Dr. AbdulWahid Al-Saif
(Member)



Dr. Muhammad Faizan
Mysorewala
(Member)



Dr. Sayyid Anas Vaqar
(Member)

© Abdulrahman Aliyu

2016

Dedication

To my family

ACKNOWLEDGMENTS

With utmost gratitude to Allah (SWT) whose might cannot be quantified. May His peace and blessings be upon our beloved prophet Muhammad (PBUH), his household and companions (Peace upon them), ameen.

Special gratitude to my parent and family members for their invaluable support. May Allah grant them the highest rank in paradise, ameen.

I would like to thank all those through whom I gained every bit of knowledge to this day and always. Knowledge is indeed light.

Sincere gratitude to my Advisor Dr. Moustafa El-Shafie and all committee members for giving their backing at the time of need.

High appreciation to KFUPM and her entire faculty and staff for the opportunity to build my career. I would also like to thank Saudi Government for generously funding my study.

I would like to thank the Deanship of Scientific Research (DSR) at KFUPM for their support through research group project number IN141048.

Lastly high gratitude to well-wishers and the Nigerian community for contributing to the liveliness of my stay in KFUPM.

TABLE OF CONTENTS

ACKNOWLEDGMENTS	v
TABLE OF CONTENTS	vi
LIST OF TABLES	viii
LIST OF FIGURES	ix
LIST OF ABBREVIATIONS	xi
ABSTRACT	xii
ملخص الرسالة	xiv
CHAPTER 1 INTRODUCTION	1
1.1 Concept of Quadrotor	2
1.2 Conventional Quadrotors	3
1.3 Tiltrotor Quadrotor	6
1.4 MOTIVATION	8
1.5 CONTRIBUTION	10
1.6 Thesis Structure	10
CHAPTER 2 LITERATURE REVIEW	11
2.1 Conventional Quadrotor Modelling and Control	11
2.2 Tiltrotor/Wing Quadrotor Modeling and Control	13
2.3 Wind Disturbance Rejection	14
2.4 Optimization Techniques	15
CHAPTER 3 MODELLING	17
3.1 Quadrotor Aerodynamics and Moments	17
3.1.1 Thrust Force	17
3.1.2 Blade Element Theory	17
3.1.3 Drag Forces and Moments	18

3.2	Quadrotor Kinematics	19
3.2.1	Rotation Matrix	20
3.3	Quadrotor Dynamic Modelling	21
3.3.1	Dynamic Equations of Conventional Quadrotor	22
3.3.2	Dynamic Equations of Tiltrotor Quadrotor	27
CHAPTER 4 WIND GUST MODELLING		33
4.1	Dryden Wind Gust Model	34
4.2	Von Karman Wind Gust Model	36
4.3	Macro Approach for Wind Gust Model	39
CHAPTER 5 CASCADE CONTROL IMPLEMENTATION		44
5.1	PID Control	44
5.1.1	Altitude Controller	46
5.1.2	Wind Force Cancellation Strategy	46
5.2	Controller Parameter Optimization by Differential Evolution	47
5.3	Simulation Results and Discussion	52
CHAPTER 6 DECENTRALIZED BACKSTEPPING CONTROL IMPLEMENTATION		61
6.1	Decentralized Control	61
6.1.1	Model Presentation	62
6.1.2	Model Decomposition - Coordination	63
6.1.3	Backstepping Control	68
6.2	Decentralized Backstepping Control of Tiltrotor Quadrotor	70
6.3	Simulation Results and Discussion	74
CHAPTER 7 CONCLUSION AND RECOMMENDATION		92
References		94
Vitae		101

LIST OF TABLES

Table 1 PID controller parameters for primary loop	46
Table 2 PD controller parameters for the secondary loop	47
Table 3 DE Algorithm Parameters.....	51
Table 4 Dynamic Parameters used for Cascade Control	52
Table 5 Results of tiltrotor quadrotor under wind disturbance	60
Table 6 Parameters used for Decentralized Backstepping control	75
Table 7 Results comparison between Cascade Control and Decentralized Backstepping Control under wind disturbance	79

LIST OF FIGURES

Figure 1 Conventional Quadrotor [26].	3
Figure 2 Roll-Pitch-Yaw Formulations of Quadrotor [6].	5
Figure 3 Eight Input structure for Tilt-wing configuration [36].	6
Figure 4 Eight Input Structure for tiltrotor configuration [38]	7
Figure 5 Eight Input Structure for tiltrotor configuration [39]	7
Figure 6 Twelve Input Structure for tiltrotor configuration [40].	7
Figure 7 Quadrotor Coordinate System/ Free Body Diagram [6].	20
Figure 8 Quadrotor structure [40]	28
Figure 9 Artificial wind gust generation setup [45].	34
Figure 10 Wind velocity in inertial coordinate that results from the Dryden wind gust model developed in MATLAB.	36
Figure 11 Effect of wind on the quadrotor body [49]	40
Figure 12 Simulation showing wind velocity before and after wind gust	41
Figure 13 Cascade Control Block Diagram	45
Figure 14 DE Flowchart (Vesterstro and Thomsen).	50
Figure 15 Crossover Procedure (Vesterstro and Thomsen).	51
Figure 16 Convergence of DE algorithm.	52
Figure 17 Position control without rotor tilting	54
Figure 18 Error between x-y positions without tilting the rotors.	54
Figure 19 Quadrotor Altitude x, y, and z without rotor tilting	55
Figure 20 Quadrotor position with rotor tilting	55
Figure 21 Error between x-y positions without tilting the rotors.	56
Figure 22 Quadrotor Altitude x, y, and z with rotor tilting.	56
Figure 23 Quadrotor attitude ($\varphi \theta \psi$)	57
Figure 24 Plots of orientation axes, α_i	57
Figure 25 Multitasking Quadrotor	58
Figure 26 Forward speed of multitasking Quadrotor.	59
Figure 27 Block diagram of decentralized backstepping control	74
Figure 28 Convergence of DE algorithm for Decentralized Control gains	74
Figure 29 Elevation to [0,0,50]m under wind gust	76
Figure 30 3D plot of Elevation to [0,0,50]m under wind gust.	76
Figure 31 Position plots of elevation to [0,0,50]m under wind gust.	77
Figure 32 Velocity plots of elevation to [0,0,50]m under wind gust	77
Figure 33 Orientation angles plots of elevation to [0,0,50]m under wind gust	78
Figure 34 Angular rates of elevation to [0,0,50]m under wind gust.	78
Figure 35 Elevation to height of 50m	80

Figure 36 3D plot of target [10,10,50]m.....	81
Figure 37 Collapsed View of 3D plot.....	81
Figure 38 Plots of positions, x, y, and z for the coordinate [10,10,50]m.....	82
Figure 39 Velocities of x, y, z for the coordinate [10,10,50]m.....	82
Figure 40 Orientation plots for the coordinate [10,10,50]m.....	83
Figure 41 Plots of velocities, phi, theta and psi, for the coordinate [10,10,50]m.....	83
Figure 42 Position of elevation and thrust further to a [10,0,50]m location under wind gust	84
Figure 43 3D plot of Quadrotor position for elevation and thrust further to a [10,0,50]m location under wind gust	85
Figure 44 Collapsed view for elevation and thrust further to a [10,0,50]m location under wind gust	85
Figure 45 x, y and z position for elevation and thrust further to a [10,0,50]m location under wind gust	86
Figure 46 Velocities for elevation and thrust further to a [10,0,50]m location under wind gust	86
Figure 47 Orientation angles for elevation and thrust further to a [10,0,50]m location under wind gust	87
Figure 48 Angular velocities for elevation and thrust further to a [10,0,50]m location under wind gust	87
Figure 49 Height position for elevation, hovering and moving at an angle and then hover at an angle.....	88
Figure 50 3D plot for elevation, hovering and moving at an angle and then hover at an angle	89
Figure 51 Collapsed 3D plot for elevation, hovering and moving at an angle and then hover at an angle.....	89
Figure 52 x, y and z position for elevation, hovering and moving at an angle and then hover at an angle.....	90
Figure 53 Velocities for elevation, hovering and moving at an angle and then hover at an angle	90
Figure 54 Orientation angles for elevation, hovering and moving laterally at an angle and then hover at an angle (pi/6 rad).....	91
Figure 55 Angular velocities for elevation, hovering and moving at an angle (pi/6 rad) and then hover at an angle	91

LIST OF ABBREVIATIONS

CoG	:	Centre of Gravity
CR	:	Crossover Factor
D	:	Problem Dimension
DE	:	Differential Evolution
DOF	:	Degrees of Freedom
F	:	Mutation Factor
GA	:	Genetic Algorithm
ISE	:	Integral Square Error
LQR	:	Linear Quadratic Regulator
MAE	:	Maximum Absolute Error
MIMO	:	Multi Input Multi Output
MSE	:	Mean Square Error
NP	:	Number of Population
PID	:	Proportional Integral Differential
PSO	:	Particle Swarm Optimization
QTR	:	Quad Tilt Rotor
SMC	:	Sliding Mode Control
UAVs	:	Unmanned Aerial Vehicles
VTOL	:	Vertical Take-off and Landing

ABSTRACT

Full Name : [Abdulrahman Aliyu]
Thesis Title : [Wind Gusts Disturbance Rejection for a Quadrotor With Tilted Rotors]
Major Field : [Systems and Control Engineering]
Date of Degree : [April 2016]

Conventional unmanned quadrotor aerial vehicles have a plethora of applications for civilian and military purposes. Quadrotors as the name implies usually have four input variables (fixed rotors) which are used to drive six outputs (i.e. 3 translational and 3 rotational motions), and this leads to coupling between motions. Tilt- rotor quadrotors are more versatile because they have more input variables to independently control its orientation and position without coupling.

This work is constituted into three major parts; a suitable tiltrotor quadrotor modeling was first presented. Secondly, different wind modeling techniques are discussed. Thirdly, different control methods were applied namely, cascade control method and decentralized backstepping control method. In cascade control method, additional rotor tilting inputs are utilized and successfully used to mitigate the effect of wind gust disturbance. Cascade control consists of multiple nested loops and the tiltrotor quadrotor orientation axis was used for mobility and wind disturbance rejection while the rotor speed was used to generate thrust. We evaluated the performance of quadrotor with tilted rotor under wind gusts and compared its performance with conventional quadrotor.

The decentralized backstepping control approach is used to generate a new set of inputs capable of independently and simultaneously achieve decoupling of motions while rejecting wind disturbances. The tiltrotor quadrotor dynamic is first decentralized to achieve six subsystems. Controller inputs for each subsystem are generated via Lyapunov based backstepping method. Thereafter, a Differential Evolution (DE)

algorithm is used to estimate the controller parameters. Simulation results from both control methods shows that the developed decentralized backstepping controller exhibits better robustness capability against wind disturbance.

ملخص الرسالة

الاسم الكامل: عبد الرحمن عليوة

عنوان الرسالة: هبوب الرياح اضطراب رفض لرباعية الدوار المائل مع الدوار

التخصص: أنظمة وهندسة التحكم

تاريخ الدرجة العلمية: أبريل 2015

السيارات التقليدية رباعية الدوار بدون طيار لديها عدد كبير من التطبيقات لأغراض مدنية وعسكرية. رباعية الدورات كما يوحي الاسم وعادة ما يكون أربعة متغيرات المدخلات (الدورات الثابتة) التي تستخدم لدفع ستة مخرجات (أي 3 متعدية و 3 حركات الدوران)، وهذا يؤدي إلى اقتران بين الاقتراحات. إمالة الدوار رباعية الدورات هي أكثر تنوعا لأن لديهم المزيد من المتغيرات إدخال للتحكم بشكل مستقل التوجه والموقف دون اقتران.

يتكون هذا العمل إلى ثلاثة أجزاء رئيسية. وقد قدمت لأول مرة إمالة الدوار النمذجة رباعية الدوار مناسبة. ثانيا، وتناقش مختلف تقنيات النمذجة الرياح. ثالثا، تم تطبيق طرق المكافحة المختلفة وهي طريقة المتحكم المتسلسل ومركزية العودة يخطو أسلوب التحكم. في أسلوب التحكم تتالي، وتستخدم الدوار يميل مدخلات إضافية واستخدامها بنجاح للتخفيف من أثر اضطراب عاصفة الرياح. تتكون السيطرة سلسلة من حلقات متداخلة متعددة واستخدام إمالة الدوار محور التوجه رباعية الدوار للتنقل والرياح اضطراب الرفض في حين تم استخدام سرعة الدوار لتوليد قوة الدفع. قمنا بتقييم أداء رباعية الدوار مع الدوار يميل تحت هبوب الرياح ومقارنة أدائها مع التقليدية رباعية الدوار.

يتم استخدام نهج السيطرة التراجع لا مركزية لتوليد مجموعة جديدة من مدخلات قادرة على بشكل مستقل وفي نفس الوقت تحقيق فصل الاقتراحات في حين رفض اضطرابات الرياح. واللامركزية الميل الدوار رباعية الدوار ديناميكية أول من تحقيق ستة الأنظمة الفرعية. يتم إنشاؤها المدخلات تحكم عن كل نظام فرعي عبر يابونوف أساس طريقة التراجع. بعد ذلك، يتم استخدام التفاضلية تطور (DE) خوارزمية لتقدير المعلمات وحدة تحكم. نتائج

المحاكاة من كل طرق المكافحة يدل على أن اللامركزية تحكم، خطوة إلى الوراء وضعت المعارض القدرة متانة
أفضل ضد اضطراب الرياح.

CHAPTER 1

INTRODUCTION

Unmanned Aerial Vehicles (UAVs) recently attracted enormous research and development interest, especially VTOL (Vertical Take-off and Landing) aircraft. One of the most recent areas of research is the autonomous quadrotor development. Quadrotors UAVs have been extensively used for various civilian and military purposes. Examples of such applications are pick and place objects, delivery, surveillances, traffic monitoring, construction purposes for example pick and place objects, rescue missions, patrolling forests in case of fire outbreak, warfare, and other risky missions. However, the more adapted they are to an environment the more versatile they become. A major advantage of UAVs is that it does not require a particular air field base. Regular quadrotors have coupled motion. For instance, they have to change their body angles to achieve a particular orientation. For some critical missions, this is not desired.

The quad tilt rotor [QTR] enables transition from helicopter mode to aircraft mode by tilting the rotor at the same time along the axis perpendicular to the front direction of the vehicle (pitch angle). This highly non-linear system is difficult to characterize due to its complex aerodynamic system. A linear technique as expected, would perform poorly because of its inability to compensate for non-linear phenomenon affecting vehicle dynamics. Linear models perform perfectly around the region which they are linearized but deteriorate extensively outside equilibrium points or whenever subjected to perform

aggressive maneuvers and are thus unable to satisfactorily handle perturbations. However, a non-linear controller is better suited to handle perturbations and allow for trajectory tracking considering its multiple equilibrium nature (smooth switching).

1.1 Concept of Quadrotor

Advancement in Multirotor design emanated from the various design techniques from the past. The quadrotor is preferred more widely used over conventional mini-helicopters because they have more lift thrusts. In addition, they have high maneuverability and are easy to build. Moreover, it can easily attain vertical take-off and landing (VTOL) due its multi-rotor non-coaxial nature. Adjusting the speed of the rotors, one can attain flight attitude control.

Quadrotor UAVs has a more compact structure because it has no tail compared with the twin-rotor helicopter. In addition, flight attitude is more stable because the lifting force of four rotors is more uniform than a single rotor. In comparison with fixed-wing aircraft, the take-off requirement are less and can also hover with better adaptability to its surroundings. However, a more recent design, tilt-wing quadrotor complements some of the drawbacks of the quadrotor especially with the decoupling of motion.

To study the most resent design which is the quadrotor with tilted propellers, it is important to first understand the theory of conventional quadrotor.

1.2 Conventional Quadrotors

Conventional quadrotors are an under-actuated system having four independent control inputs to track six Degrees of Freedom (DOF), i.e. six co-ordinates outputs. Three of the six coordinate points are used for translation while the remaining are used for rotational position or orientation as shown below.

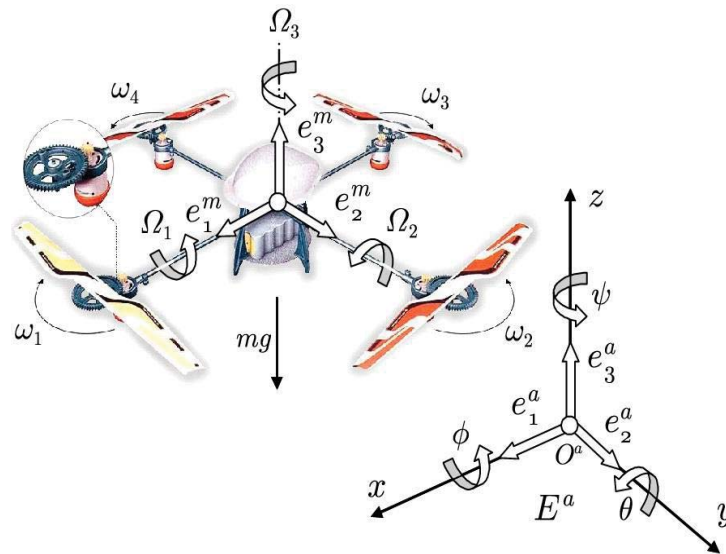


Figure 1 Conventional Quadrotor [26].

All propellers axes of revolution are fixed. Moreover, they have fixed-pitch blades and airflow is downwards (for an upward lift). This a rigid structure and the propeller speeds can vary. However, the propeller velocities are directly related to the moments. For instance, the front and rear propellers are considered pair, which rotates in one direction, while the other pair, left and right ones which rotates in opposite direction. In hovering condition, all propellers have the same speed.

The four propellers spin and generate thrust i.e. the upward force. Air is pushed vertically downward to the area around them as the propellers spin. According to Newton's third law of motion, air applies equal and opposite reaction force to the propellers, i.e. vertically upward and hence thrust is generated. In order to bank, one propellers rotates marginally faster than the other opposite one, this creates a horizontal force and with one force opposing gravity so the vehicle moves sideward.

To make the quadcopter rotate in its perpendicular axis, two pair of rotors spin slightly faster than the other two, this causes a torque (clockwise or anticlockwise, depending on the rotation of that pair of rotors) which pushes the quadcopter in the opposite direction of the direction in which the torque was generated, thus the quad copter rotates about its perpendicular axis. When all four rotors increase spinning in one direction, then the vehicle moves upwards and vice versa.

Unlike conventional rotorcrafts that use complex mechanism to alter blade pitch to direct thrust and steer the craft, the quadrotor uses simpler differential thrust mechanism to control the three angles, i.e. roll, pitch and yaw.

Roll:

Rotation about x- axis is known as roll. Roll is actuated by difference in speed of right and left rotors, which results in a moment about x-axis. During roll the overall thrust remains the same as for hovering.

Pitch:

Rotation about y-axis is known as pitch. Pitch is actuated by difference in speed of front and rear rotors, which results in a moment about y-axis. During pitch, the overall thrust remains the same as hovering.

Yaw:

Rotation about z-axis is known as yaw. Yaw is different from roll and pitch as it involves all the four instead of two motors. It is achieved by varying the balance between moments generated by all four rotors. Increasing the speed of the front-rear pair of motors while decreasing the speed of the left-right pair actuates yaw and vice versa. The yaw movement is generated because of the way that the left-right propellers turn clockwise while the front-back ones pivot counterclockwise. Therefore, when the overall torque is unbalanced, the quadrotor turns on itself. The total perpendicular thrust is the same as in hovering.

An illustration of roll, pitch and yaw is shown below.

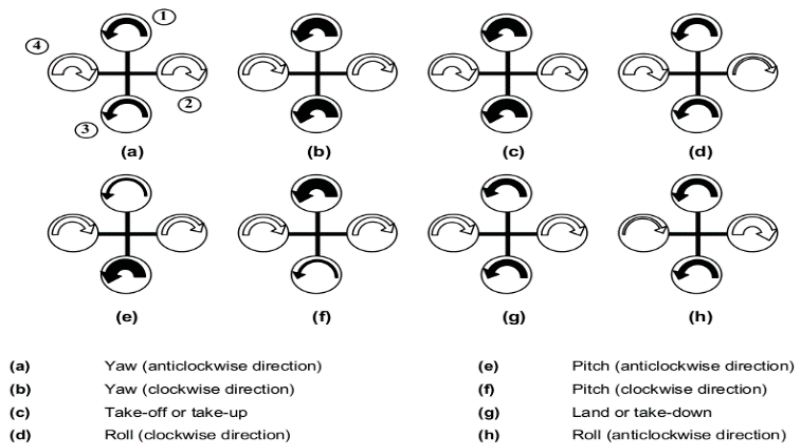


Figure 2 Roll-Pitch-Yaw Formulations of Quadrotor [6].

1.3 Tiltrotor Quadrotor

Unlike the conventional quadrotor, the tilt rotor quadrotor is able to achieve forward flight, or move sideways without having to yaw, roll or pitch as the case may be. Additional inputs may go from 4 to 8 depending on the degree of freedom of the tilting axes. This flight mode concept is imperative for performing more clinical tasks in cluttered environment in real life applications taking also environmental factors into consideration. However, the concept of vertical take-off is same with conventional quadrotor, tilting is used to achieve decoupling of motion to make it a fully or over actuated system. Fig. 3 gives the structure of various tilt-wing design with eight inputs capable of obtaining airplane flight mode. The design presented in Figs. 4 and 5 gives the structure of tiltrotor designs with eight inputs also but the additional inputs are used to decouple altitude and attitude. Fig. 6 presents the tiltrotor quadrotor with twelve inputs also which is has fault tolerance capability in addition to motion decoupling.

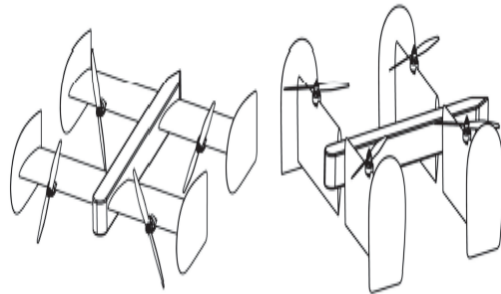


Figure 3 Eight Input structure for Tilt-wing configuration [36]

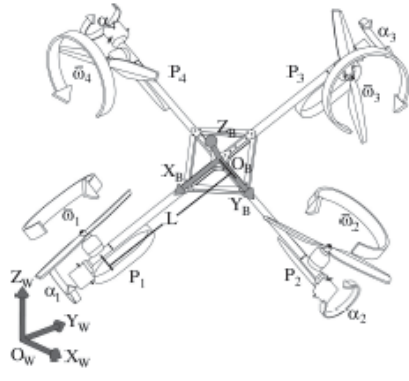


Figure 4 Eight Input Structure for tiltrotor configuration [38]

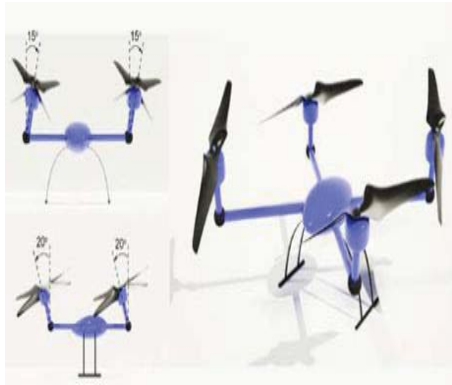


Figure 5 Eight Input Structure for tiltrotor configuration [39]

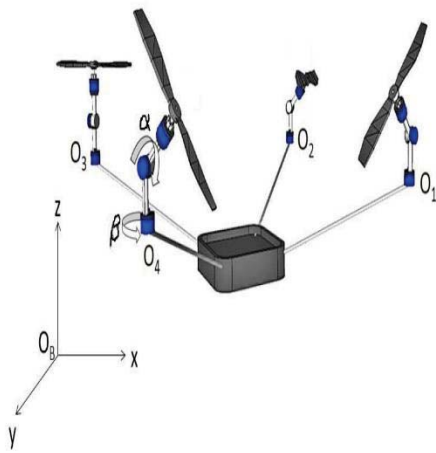


Figure 6 Twelve Input Structure for tiltrotor configuration [40]

1.4 MOTIVATION

Wind gusts have tremendous effect when flying quadrotor outdoors during certain critical missions. Although, some works have been done to address the issue of atmospheric factors like wind gust when flying conventional quadrotors. Unfortunately, for the tiltrotor quadrotor, the issues of wind disturbance is yet to be addressed especially with those with twelve inputs.

Wind disturbances term are usually incorporated in the quadrotor modelling equation. The same approach will be considered with the conventional quadrotor as this represents a pragmatic approach. Various wind modelling techniques such as the Dryden, Von Karman, and a macro approach exist for simulation purpose but it is imperative to select a suitable model for the work so as to explore the capability of the tiltrotor quadrotor. However, in experimental setups, wind disturbances are generated from a set of electric fans, through wind tunnels.

Wind disturbances affects the quadrotor body mainly by displacing its axes from a desired set point. A tiltrotor quadrotor has more advantages because its additional inputs can be utilized to mitigate wind effect and decouple motion as well.

Control methodologies are aimed at keeping the quadrotor on track or at least within a barest minimum error in position and orientation. The additional inputs of a tiltrotor quadrotor, if adequately controlled, can greatly reduce the effect of wind disturbance felt while maintaining a desired set point. A single loop controller exhibits good performance but deteriorates due external disturbance acting on the system. The concept of cascade

control is very useful in annulling such disturbances. Therefore it is fascinating to apply such control technique to showcase the advantages of having additional inputs in the tiltrotor quadrotor.

Nonlinear control strategies exhibits a great deal of robustness against external disturbance. However, the significance of finding a technique to drive six output variables of interest (position and orientation) cannot be overemphasized. This is because conventional quadrotors are incapacitated due to their coupling nature. For the tiltrotor quadrotor, a control technique that would independently effect quadrotor output gives rise to the need apply a decentralized approach. A decentralized approach is required to split the tiltrotor quadrotor dynamic into six subsystems, each relating to a single output which enables easy application of a nonlinear control technique called the backstepping control. Therefore, a decentralized backstepping control method is an important strategy do deal with model complexity and wind disturbance rejection.

The need to evaluate the performance of the tiltrotor quadrotor is of paramount importance in order to judge the effectiveness of any controller developed. For instance, metrics such as the Confidence Interval (CI), Mean Square Error (MSE) and Maximum Absolute Error (MAE) can effectively interpret the quality of control methods. However, performance evaluation will also open room for improvements and comparisons with the future controllers that may be developed.

1.5 CONTRIBUTION

A quadrotor with tilted rotor is proposed to study the performance of various control systems taking wind disturbance into account as follows;

- Modeling of the quadrotor is presented from the literature; the goal is to incorporate wind disturbances into tiltrotor quadrotor modelling equations.
- Study various wind gust modelling technique; the aim being to select a suitable wind disturbance amongst different wind modelling techniques used for both experimental and simulation purposes and are discussed.
- Position and attitude control with wind gust rejection; the objective is to design controllers to successfully mitigate the effect of wind disturbance.
- Performance evaluation and comparison; the aim being to evaluate the performances of the controllers.

1.6 Thesis Structure

This thesis is organized as follow: Chapter 2 presents the literature review. Modelling of both conventional and tilt rotor quadrotor is presented in Chapter 3. In chapter 4 wind gusts modelling techniques are discussed. Chapter 5 presents Cascade control of the tilt rotor quadrotor under wind gusts. Chapter 6 presents decentralized backstepping control of the tilt rotor quadrotor under wind gust. Finally, concluding remarks and future recommendations are given in Chapter 7.

CHAPTER 2

LITERATURE REVIEW

UAVs have been extensively used for various civilian and military purposes. Examples of such applications as earlier mentioned are pick and place objects, delivery, surveillances, traffic monitoring, rescue missions, patrolling forests in case of fire outbreak, warfare, and other risky missions [1],[2],[3],[4],[5].

2.1 Conventional Quadrotor Modelling and Control

A comprehensive history on the evolution of UAVs is presented in [6]. Quadrotor UAVs, have attracted more attention because of its compact nature and versatility. Modeling of conventional quadrotors exists in numerous literature mainly based on Euler-Lagrange or Newton-Euler formalism [6], [7], [8]. These modeling techniques presented various work [9], [10], [11], [12], [13], [14], [15], [16], were controlled by different PID controller schemes to achieve various flight modes. For instance, in [9], a gain scheduling PID was used to control the quadrotor while demonstrating fault tolerance capabilities. Also, a gain scheduling PID and a Model Reference Adaptive Control (MRAC) are adopted. In [11], a PID was used for visual based tracking for a hybrid system (Quadrotor and Pushcart carrier). In [12], a Linear Quadratic Regulator (LQR) controller was used alongside PID with a microcontroller for hover control. [13] Presented a self-tuning fuzzy PID controller with obstacle avoidance. In [14], a nonlinear PID methodology was used for attitude and position tracking. Also, [15] used a cascade PID and Generalized

Predictive Control (GPC) for path tracking. In [16], a comparative study was carried out on PID, LQR and Model Predictive Control (MPC) where PID exhibited more robustness.

However various nonlinear control methods have been applied as described in [17]. In [18] and [19] a feedback linearization technique and fuzzy/static feedback linearization were employed for attitude and position control. In [20] and [21], Sliding Mode Control (SMC) technique was used for trajectory tracking. In [22], Backstepping control was compared to SMC technique on a conventional quadrotor which shows that former is able to better control orientation angles in the presence of high perturbations. Backstepping control have also been used in some other research works [23], [24], [25], [26], [27], [28], [29]. In [23] a State Dependent Riccati Equation (SDRE) and backstepping controllers are used to find control inputs where the friction term of the quadrotor dynamic was first neglected in order to simplify the solution. In [24] backstepping and adaptive control where used in order to tackle disturbances and model uncertainties. In [25], [26], [27], [28], [29], backstepping control with various disturbance methods are adopted. Hybrid controller structure have also been used in [30], where and adaptive and SMC methods were applied. In [31] also, a hybrid feedback linearization and SMC are used whereas in [32], a hybrid backstepping and feedback linearization control via visual feedback are employed all for trajectory tracking purposes.

Various decentralized nonlinear control strategies have been applied in various fields as described in [33]. In [34], a decentralized adaptive control method was applied to find independent controllers for altitude and attitude, whereby there is no exchange of information. Another decentralized backstepping was applied in [35] for a class of

nonlinear MIMO systems but the controller parameters are empirically selected. In [36], the same approach was only used to control conventional quadrotors but wind disturbance was not considered, and the problem of coupling still exists.

In spite of the milestone recorded with the conventional quadrotor, its model structure still possess some limitations regarding the orientation angles (roll, pitch and yaw) and position (x, y, z) coupling because of insufficient inputs. Typically, the outputs are either the position and yaw angle for tracking purposes or orientation angle together with altitude for VTOL, hence making it incongruous for some particular tasks. In light of this, different modeling and control schemes have been employed to its structure so as to complement such deficiencies. In order to address the coupling flaw associated with the structure of conventional quadrotors, tilt-wing and tiltrotor quadrotors evolved in [37], [38] [39], [40], [41], [42], and [43], thereby improving the actuation capacity of the conventional quadrotor by introducing additional inputs.

2.2 Tiltrotor/Wing Quadrotor Modeling and Control

In [37], a tilt tri-rotor system was introduced to achieve airplane flight mode whereby adaptive control technique is used to tackle the issue of model uncertainties. In [38], the rotors of a quadrotor are placed on a tilt-wing with the aim of achieving a hovering and airplane flight mode. Here, an LQR controller was utilized to achieve this objective. In [39], a robust adaptive PID controller was introduced for the tilt-wing quadrotor proposed in [36] under wind disturbances from Dryden wind model. In [40], a tiltrotor quadrotor with eight inputs was used perform a “tilting on the spot” flight mode by introducing four additional inputs in a bid to decouple orientation angles and position. This was achieved

using an output feedback linearization control technique. In [41], a thrust tilting approach was also introduced for quadrotor with eight inputs. In [42], twelve input model was introduced to achieve different flight modes and to showcase fault tolerance capability using PID controllers. In [43], adaptive control technique was applied to a tilt-roll quadrotor structure with eight inputs. Here, a cascade PID was first used to test the quadrotor performance. Hitherto, additional inputs have only been successfully aimed at decoupling the quadrotor orientation either to achieve forward flight mode or hovering as the case may be. These types mission are particularly useful in applications requiring high maneuverability.

2.3 Wind Disturbance Rejection

External disturbances are inevitable and are sometimes referred to as constants in some research papers, for instance in conventional quadrotors, [44] and for a hexarotor structure in [45]. This may lead to misleading conclusions about the flight accuracy. However, atmospheric disturbances, particularly wind gust models, incorporated in the modelling dynamics reflects a more realistic approach. For conventional quadrotors, various wind modelling techniques have been investigated in [46], [47], [48], [49], [50] and [51]. In [46], a PID controller was used to reject wind disturbance derived from the Dryden wind modelling technique. In [47] ducted fans were used to generate wind gust in an experimental setup and a switching MPC controller was utilized to achieve some robustness against such disturbance. In [48] and [49], backstepping control was applied to control the conventional quadrotor under Dryden wind model. In [50] a decentralized PID neural network control was also demonstrated. In [51], a macro approach to wind

modeling was introduced to showcase the effect of wind disturbance on a quadrotor, but no control method was adopted.

Backstepping control have also been used in some other research works because of its simplicity. This is intuitive because the conventional quadrotor can now be directly driven by four available inputs. However, selecting the gains for backstepping controller gives commendable results but using optimization techniques are better. For instance, in [48], the backstepping controller was used to control the conventional quadrotor whereby the controller parameters are selected. In [49], for conventional quadrotor whereby the controller parameters gotten from Particle Swarm Optimization (PSO) was proven to produce better results when compared to Genetic Algorithm (GA) technique.

The effect of wind disturbance on a tiltrotor quadrotor (particularly that with twelve inputs) under various orientation flight modes is an important mission but yet to be investigated. However, the conventional quadrotor is incapable of completely achieving this objective because for instance, it cannot hover at a tilt angle on the spot. In this work, cascade control consisting nested PID controller and decentralized backstepping controllers are used to precisely controlling the tiltrotor quadrotor orientation and position individually under wind disturbance whereby a more robust optimization technique is used to derive the gains of the controllers.

2.4 Optimization Techniques

In [52], optimization techniques, Differential Evolution (DE), PSO and Evolutionary Algorithms (i.e GA), underwent a comparative study, over 34 widely used benchmark

problems. Also, in [53], DE, PSO, and GA were compared for hard clustering problems. In both cases, the results shows that Differential Evolution (DE) consistently outperforms PSO and GA. In [54], DE was also proven to surpass PSO when compared over twelve constraint nonlinear test functions. DE sets a more outstanding results in addition to its simplicity, robustness, convergence time and finds optimum values in almost every run. This is the motivation behind choosing the DE as the optimization technique to derive our controller parameters and the wind disturbance model used in this work exhibits some advantages over the regularly used Dryden wind model as would be discussed later.

CHAPTER 3

MODELLING

In this chapter, the kinematics and dynamics of both conventional and tilt-wing quadrotor shall be discussed.

3.1 Quadrotor Aerodynamics and Moments

In order to achieve a more realistic simulation, it is important to take the aerodynamics into considerations.

3.1.1 Thrust Force

Thrust force produced by each rotor is calculated using momentum theory. For hover condition the relationship is given by [6]:

$$T = 2\rho Av_i^2 \quad (1)$$

T = thrust; ρ = air density; v = induced air velocity; A = rotor area, for each rotor i .

3.1.2 Blade Element Theory

Detailed information about the design of rotors and its performance is given by blade element theory [6]. The forces acting on differential elements of the blade are calculated and then integrated over the entire propeller radius giving an estimation about the thrust, torque and power characteristics of the rotor.

Relation for thrust force, F_i and drag moment, T_{di} are obtained by integrating the lift and

drag along the length of the blade. The rotor thrust (F_i) and moments (T_{di}) are proportional to square of the rotor speed (w).

$$F_i = bw_i^2 \quad (2)$$

$$T_{di} = dw_i^2 \quad (3)$$

where $i = 1,2,3,4$ representing each rotor. The thrust and drag coefficients are given below:

$$b = C_T \rho A c^2$$

$$d = C_Q \rho A c^3$$

C_Q and C_T are drag and thrust moment constants and c is rotor radius and A is the area of the quadrotor.

The total thrust force produced by all four rotors is the sum of individual thrust produced by each rotor given by:

$$F = \sum_{i=1}^n F_i \quad ; n = 4 \quad (4)$$

3.1.3 Drag Forces and Moments

There is friction between the quadrotor body and air during movement, this creates a force acting on the body of the quad rotor resisting motion and is called the drag force, F_a . For small objects, air is approximately proportional to velocity. Increased velocity increases the drag force therefore there exist a direct proportionality relationship between

the drag force and the time derivative of the position vector \dot{r} , ($r = x, y, z$) of the quadrotor given by:

$$F_a = K_a \dot{r} \quad (5)$$

$K_a = [K_1 \ K_2 \ K_3]$. K_1 , K_2 and K_3 are the translational drag coefficients [23], [55].

Similarly, drag moments M_f due to air friction which is proportional to Euler rates $\Omega^T = [\varphi \ \theta \ \psi]$ and is given by:

$$M_f = K_f \dot{\Omega} \quad (6)$$

$K_f = [K_4 \ K_5 \ K_6]$. K_4 , K_5 and K_6 are the rotational drag coefficients [23], [55].

3.2 Quadrotor Kinematics

A quadrotor is a system whereby 6 coordinates are needed to fully describe the position and the orientation of the rotorcraft. These 6 coordinate points are acquired by attaching a frame to the body of the quadrotor and considering another frame. The fixed frame is known as the earth frame (E) as this frame tells about the position of rotorcraft whereas the body frame tells about its orientation with respect to the earth fixed frame. The body fixed frame is assumed to be situated at the center of gravity (CoG). It is assumed that all rotation is about the origin about a reference axis about the angle in which the rotation occurs. These rotations can be explained by the help of Euler's theorem which states that a rotation is always about a fixed point and axis passing through that point. The same applies to two frames that is the relation of orientations between two frames can be given by a rotation through an angle about a fixed point and a fixed axis. The fixed point in this

case is the common origin.

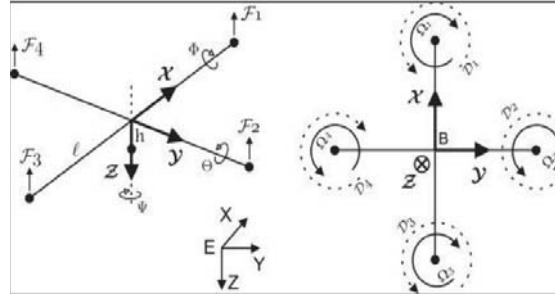


Figure 7 Quadrotor Coordinate System/ Free Body Diagram [6].

3.2.1 Rotation Matrix

A rotation matrix represent a rotation about an axis. For example if i, j, k are unit vectors in x, y, z direction and i', j', k' are rotated unit vectors in x', y', z' directions, the new coordinate is given as:

$$\begin{bmatrix} i' \\ j' \\ k' \end{bmatrix} = R \begin{bmatrix} i \\ j \\ k \end{bmatrix} \quad (7)$$

A rotation matrix is orthogonal i.e. its transpose and inverse are equal.

$$R = \begin{bmatrix} i'.i & i'.j & i'.k \\ j'.i & j'.j & j'.k \\ k'.i & k'.j & k'.k \end{bmatrix} \quad (8)$$

A rotation matrix exist for every rotation and thus the new coordinates can be given as:

$$R'' = R. R'$$

By the above, we can say that the total rotation is the product of rotation about individual axes. For roll angle ϕ (rotation about x axis), pitch angle θ (rotation about y axis) and yaw angle ψ (rotation about z axis).

$$R = R_x \cdot R_y \cdot R_z \quad (9)$$

where,

$$R_x = \begin{bmatrix} 1 & 0 & 0 \\ 0 & \cos\varphi & -\sin\varphi \\ 0 & \sin\varphi & \cos\varphi \end{bmatrix}; R_y = \begin{bmatrix} \cos\theta & 0 & \sin\theta \\ 0 & 1 & 0 \\ -\sin\theta & 0 & \cos\theta \end{bmatrix}$$

$$R_z = \begin{bmatrix} \cos\psi & -\sin\psi & 0 \\ \sin\psi & \cos\psi & 0 \\ 0 & 0 & 1 \end{bmatrix}$$

The complete rotation matrix thus becomes:

$$R = \begin{bmatrix} C\psi C\theta & C\psi S\theta S\varphi - S\psi C\varphi & C\psi S\theta C\varphi + S\psi S\varphi \\ S\psi S\theta & C\psi S\theta S\varphi + C\psi C\varphi & S\psi S\theta C\varphi - C\psi S\varphi \\ -S\theta & C\theta S\varphi & C\theta C\varphi \end{bmatrix} \quad (10)$$

The transformation of the vectors from the body fixed frame to the inertial frame is given by the rotation matrix R , where $C\theta$ denotes $\cos(\theta)$ and $S\theta$ denotes $\sin(\theta)$.

3.3 Quadrotor Dynamic Modelling

Dynamic modelling of a quadrotor can be obtained by two methods;

Newton- Euler.

Euler – Lagrange.

The Euler – Lagrange method is based on concept of total energy in a system while the Newton Euler method is based on balancing forces in the system. Newton Euler's method enables us to write the equations for each link or body separately (i.e for multi-body system) and the equations are solved numerically or recursively and it is suitable for model based control. On the other hand, Euler Lagrange considers the whole system as a

body and it is suitable for the study and analysis of dynamic properties and control schemes for a system. However, the Newton Euler in the end gives the same results as the Euler Lagrange through elimination of reaction forces and back substitution of expressions. The Newton Euler method is discussed below.

To model a conventional quadrotor below assumptions are taken into account;

- Input to the system; rotor speeds/Output; position and coordinates.
- Body frame origin and center of gravity are assumed to be coincident.
- Structure is assumed inflexible and symmetric.
- Propeller are assumed to be rigid (no blade flapping).

The three Euler angles for roll angle φ , pitch angle θ and yaw angle ψ together forms:

$$\Omega^T = [\varphi \ \theta \ \psi]$$

The position of the vehicle in the inertial frame also forms:

$$r^T = (x, y, z)$$

3.3.1 Dynamic Equations of Conventional Quadrotor

The differential equation that describes summation of forces acting on the quadrotor body is given by:

$$m \ddot{r} = mg \begin{bmatrix} 0 \\ 0 \\ 1 \end{bmatrix} - F_a + RF + D \quad (11)$$

Where, m is the mass of the quadrotor, F_a is the drag force, D is external disturbance given by;

$$D = \begin{bmatrix} d_1 \\ d_2 \\ d_3 \end{bmatrix} \quad (12)$$

d_1 , d_2 , and d_3 are the disturbances components of wind gust that will be discussed later.

R is the rotation matrix of the body frame and F is the total thrust force by all the rotors.

$$F = b \sum_{i=1}^4 w_i^2 = b(w_1^2 + w_2^2 + w_3^2 + w_4^2)$$

Let $u_1 = b(w_1^2 + w_2^2 + w_3^2 + w_4^2)$

$$F = Rb \sum_{i=1}^4 w_i^2 = Ru_1$$

$$= \begin{bmatrix} C\psi S\theta C\varphi + C\psi S\varphi \\ S\psi S\theta C\varphi - C\psi S\varphi \\ C\theta C\varphi \end{bmatrix} u_1$$

$$\ddot{r} = \begin{bmatrix} 0 \\ 0 \\ g \end{bmatrix} - K_a \dot{r} + \frac{b}{m} \begin{bmatrix} (C\psi S\theta C\varphi + C\psi S\varphi)u_1 \\ (S\psi S\theta C\varphi - C\psi S\varphi)u_1 \\ (C\theta C\varphi)u_1 \end{bmatrix}$$

$$\begin{bmatrix} \ddot{x} \\ \ddot{y} \\ \ddot{z} \end{bmatrix} = \begin{bmatrix} 0 \\ 0 \\ g \end{bmatrix} - K_a \begin{bmatrix} K_1 \dot{x} \\ K_2 \dot{y} \\ K_3 \dot{z} \end{bmatrix} + \begin{bmatrix} -\frac{u_1}{m} (C\psi S\theta C\varphi + C\psi S\varphi) \\ -\frac{u_1}{m} (S\psi S\theta C\varphi - C\psi S\varphi) \\ g - \frac{u_1}{m} (C\theta C\varphi) \end{bmatrix} + \begin{bmatrix} d_1 \\ d_2 \\ d_3 \end{bmatrix} \quad (13)$$

For the case of angular motion, it can be formulated as:

$$I\ddot{\Omega} = -(\dot{\Omega} \times I\dot{\Omega}) - M_g + M \quad (14)$$

With M as the torque applied to the vehicles body given by:

$$M = \begin{bmatrix} L b (w_2^2 - w_4^2) \\ L b (w_1^2 - w_3^2) \\ d (w_1^2 + w_3^2 - w_2^2 - w_4^2) \end{bmatrix} \quad (15)$$

where d is the drag factor and L is the length of the lever and with inertia matrix corresponding to the body reference frame:

$$I = \begin{bmatrix} I_x & 0 & 0 \\ 0 & I_y & 0 \\ 0 & 0 & I_z \end{bmatrix} \quad (16)$$

I_x , I_y and I_z are moment of inertia corresponding to each axes. The gyroscopic torques M_g , caused by rotations of the vehicle with rotating rotors are:

$$M_g = I_R \begin{bmatrix} \dot{\Omega} \times \begin{bmatrix} 0 \\ 0 \\ 1 \end{bmatrix} \end{bmatrix} \cdot [w_1 - w_2 + w_3 - w_4] \quad (17)$$

where w_i are the input variables.

A new input variables are denoted by:

$$\begin{aligned} u_1 &= b (w_1^2 + w_2^2 + w_3^2 + w_4^2) \\ u_2 &= b (w_2^2 - w_4^2) \\ u_3 &= b (w_1^2 - w_3^2) \\ u_4 &= b (w_1^2 + w_3^2 - w_2^2 - w_4^2) \end{aligned} \quad (18)$$

where, u_1 are the altitude control inputs and u_2 , u_3 and u_4 are the attitude control inputs.

The gyroscopic torques depend also on the rotational velocities of the rotor and hence on the vector:

$$\begin{aligned}
u^T &= [u_1, u_2, u_3, u_4] \\
g(u) &= w_1 - w_2 + w_3 - w_4
\end{aligned} \tag{19}$$

From Eq. 17,

$$M_g = I_R \begin{bmatrix} \dot{\Omega} \times \begin{bmatrix} 0 \\ 0 \\ 1 \end{bmatrix} \end{bmatrix} g(u)$$

where x is given by the skew matrix represented by the following example . For $v = [v_1 \ v_2 \ v_3]$ and $w = [w_1 \ w_2 \ w_3]$,

$$(v \times w) = \begin{bmatrix} 0 & -v_3 & v_2 \\ v_3 & 0 & -v_1 \\ -v_2 & v_1 & 0 \end{bmatrix} \begin{bmatrix} w_1 \\ w_2 \\ w_3 \end{bmatrix}$$

So,

$$\begin{aligned}
\dot{\Omega} \times \begin{bmatrix} 0 \\ 0 \\ 1 \end{bmatrix} &= [\dot{\theta} - \dot{\varphi} \ 0]^T \\
M_g &= I_R \begin{bmatrix} \theta \\ -\varphi \\ 0 \end{bmatrix} \times [(w_1 - w_2 + w_3 - w_4)] \\
M_g &= I_R \begin{bmatrix} \theta(w_1 - w_2 + w_3 - w_4) \\ -\varphi(w_1 - w_2 + w_3 - w_4) \\ 0 \end{bmatrix} \\
&= \begin{bmatrix} I_R \dot{\theta} g(u) \\ -I_R \dot{\varphi} g(u) \\ 0 \end{bmatrix}
\end{aligned}$$

$$I\dot{\Omega} = [I_x \dot{\varphi} \ I_y \dot{\theta} \ I_z \dot{\psi}]$$

$$\dot{\Omega} \times I\dot{\Omega} = [\dot{\varphi} \ \dot{\theta} \ \dot{\psi}] \times [I_x \dot{\varphi} \ I_y \dot{\theta} \ I_z \dot{\psi}]$$

$$= \begin{bmatrix} \dot{\phi}\dot{\psi} [I_y - I_z] \\ \dot{\psi}\dot{\theta} [I_x - I_z] \\ \dot{\phi}\dot{\theta} [I_y - I_x] \end{bmatrix}$$

$$I^{-1} = \begin{bmatrix} \frac{1}{I_x} & 0 & 0 \\ 0 & \frac{1}{I_y} & 0 \\ 0 & 0 & \frac{1}{I_z} \end{bmatrix}$$

$$I^{-1}[\dot{\Omega} \times I \dot{\Omega}] = \begin{bmatrix} \dot{\phi}\dot{\psi} \frac{[I_z - I_y]}{I_x} \\ \dot{\psi}\dot{\theta} \frac{[I_x - I_z]}{I_y} \\ \dot{\phi}\dot{\theta} \frac{[I_y - I_x]}{I_z} \end{bmatrix}$$

$$I^{-1} M = \begin{bmatrix} \frac{L}{I_x} u_2 & \frac{L}{I_y} u_3 & \frac{L}{I_z} u_4 \end{bmatrix}$$

Therefore,

$$\begin{bmatrix} \ddot{\phi} \\ \ddot{\theta} \\ \ddot{\psi} \end{bmatrix} = \begin{bmatrix} \dot{\theta}\dot{\psi} \frac{[I_z - I_y]}{I_x} - I_R \dot{\theta} g(u) + \frac{L}{I_x} u_2 \\ \dot{\phi}\dot{\psi} \frac{[I_x - I_z]}{I_y} + I_R \dot{\phi} g(u) + \frac{L}{I_y} u_3 \\ \dot{\phi}\dot{\theta} \frac{[I_y - I_x]}{I_z} + \frac{L}{I_z} u_4 \end{bmatrix} \quad (20)$$

In state variable form, the model can be written as:

$$X^T = [\dot{x}, \dot{y}, \dot{z}, \phi, \theta, \psi, \dot{\phi}, \dot{\theta}, \dot{\psi}]$$

(21)

$$X^T = [x_1, x_2, x_3, x_4, x_5, x_6, x_7, x_8, x_9]$$

$$\dot{X} = \begin{bmatrix} [Cx_4Sx_5Cx_6 + Sx_4Sx_6] - K_1x_1 + d_1 \\ [Cx_4Sx_5Sx_6 - Sx_4Cx_6] \frac{u_1}{m} - K_2x_2 + d_2 \\ g + (Cx_4Sx_5) \frac{u_1}{m} - K_3x_3 + d_3 \\ x_7 \\ x_8 \\ x_9 \\ x_8x_9I_1 - \frac{I_R}{I_x} [x_8 g(u)] - K_4x_7 + \frac{L}{I_x} u_2 \\ x_7x_9I_2 - \frac{I_R}{I_y} [x_7 g(u)] - K_5x_8 + \frac{L}{I_y} u_3 \\ x_7x_8I_3 + \frac{L}{I_z} u_4 - K_6x_9 \end{bmatrix} \quad (22)$$

with

$$I_1 = \frac{[I_y - I_z]}{I_x}, \quad I_2 = \frac{[I_z - I_x]}{I_y}, \quad I_3 = \frac{[I_x - I_y]}{I_z}$$

3.3.2 Dynamic Equations of Tiltrotor Quadrotor

The mathematical model of a quadrotor is essential for good controller design. The model considered in this work is a modified version of that represented in [40] and is shown in Fig. 8. However, a more pragmatic approach is used in the modelling of this work with the following assumptions;

- Translation dynamics is expressed with respect to a fixed world coordinate frame while, the rotational dynamic is expressed with respect to body fixed frame.
- Body frame origin and center of gravity are assumed to be coincident.
- Air friction and drag moment together with external wind forces are considered.

Structure is assumed inflexible and symmetric.

- Propeller are assumed to be rigid (no blade flapping).

- The rotors are located at points O_1 , O_2 , O_3 , and O_4 , tilted with respect to the fixed rotor points as shown in Fig 5.
- These rotor frames are taken parallel to the body fixed reference frame at the center of gravity.
- The translational and rotational dynamic equations are established according to Newton-Euler formation.

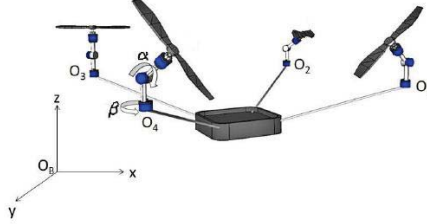


Figure 8 Quadrotor structure [40]

Let $R_{r_i}^B$ represent the orientation rotor axis O_i with respect to the fixed rotor body frame.

Since the fixed rotor frames are parallel to the body fixed frame at the CoG. Then, by denoting α_i , the rotational angle about y_i and β_i , the rotational axes about z_i as shown in above Fig. 8. Then the rotational matrix from the rotors-rotating frame to the fixed rotor frame is given by:

$$R_{r_i}^B = \begin{bmatrix} c\beta_i c\alpha_i & -s\beta_i & c\beta_i s\alpha_i \\ s\beta_i c\alpha_i & c\beta_i & s\beta_i s\alpha_i \\ -s\alpha_i & 0 & c\alpha_i \end{bmatrix} \quad (23)$$

Therefore, for each rotor the thrust, F_i is therefore given by:

$$F_i = \begin{bmatrix} c\beta_i c\alpha_i & -s\beta_i & c\beta_i s\alpha_i \\ s\beta_i c\alpha_i & c\beta_i & s\beta_i s\alpha_i \\ -s\alpha_i & 0 & c\alpha_i \end{bmatrix} \begin{bmatrix} 0 \\ 0 \\ bw_i^2 \end{bmatrix} \quad (24)$$

The resulting moments at the center of gravity by each rotor consists of the drag moment M_{iA} and moments generated by the thrust component M_{iB} given by;

$$M_i = M_{iA} + M_{iB} = \begin{bmatrix} c\beta_i c\alpha_i & -s\beta_i & c\beta_i s\alpha_i \\ s\beta_i c\alpha_i & c\beta_i & s\beta_i s\alpha_i \\ -s\alpha_i & 0 & c\alpha_i \end{bmatrix} \begin{bmatrix} 0 \\ 0 \\ d\omega_i^2 \cdot \bar{\omega}(i) \end{bmatrix} + r_i x F_i \quad (25)$$

where c denotes cosine and s denotes sine. $\bar{\omega} = [1, 1, -1, -1]$ accounts for the direction of rotation to each rotor (i.e. rotors 1 and 2 rotates counter clockwise, and rotors 3 and 4 rotates clockwise) and r_i represents the vector from CoG to the reference point of the rotors given by;

$$\begin{aligned} r_1 &= [l, 0, -h], r_2 = [0, l, -h], \\ r_3 &= [-l, 0, -h], r_4 = [0, -l, -h] \end{aligned} \quad (26)$$

l and h represents the horizontal and vertical displacements from the rotors to center of gravity respectively.

The translational dynamic equation established in the reference earth frame is given by:

$$m\ddot{r} = \begin{bmatrix} 0 \\ 0 \\ -mg \end{bmatrix} - F_a + F + D \quad (27)$$

where F_a represents the aerodynamic drag, F represents the thrust force and D may represent any disturbance and $[0 \ 0 \ mg]^T$ represents acceleration due to gravity:

$$m \begin{bmatrix} \ddot{x} \\ \ddot{y} \\ \ddot{z} \end{bmatrix} = \begin{bmatrix} 0 \\ 0 \\ -mg \end{bmatrix} - \begin{bmatrix} K_1 \dot{x} \\ K_2 \dot{y} \\ K_3 \dot{z} \end{bmatrix} + R \sum_{i=1}^4 F_i + \begin{bmatrix} d_1 \\ d_2 \\ d_3 \end{bmatrix} \quad (28)$$

As earlier shown, R is the body Euler transformation matrix with respect to the earth inertia frame.

The rotational dynamic established in the reference body frame B is given by:

$$\ddot{\Omega} = I^{-1}[(-\dot{\Omega} \times I \dot{\Omega}) - M_g - M_f + M + M_d] \quad (29)$$

where M_d represents a random disturbance moment, M_f is the drag/friction moments with K_4 , K_5 and K_6 representing the drag coefficients, and is given by;

$$M_f = \begin{bmatrix} K_4 \dot{\phi} \\ K_5 \dot{\theta} \\ K_6 \dot{\psi} \end{bmatrix} \quad (30)$$

$$M_d = \begin{bmatrix} m_{dp} \\ m_{dq} \\ m_{dr} \end{bmatrix} \quad (31)$$

I , the body inertia matrix and M_g the gyroscopic forces are respectively given by given by:

$$I = \begin{bmatrix} I_x & 0 & 0 \\ 0 & I_y & 0 \\ 0 & 0 & I_z \end{bmatrix} \quad (32)$$

$$M_g = I_R \sum_{i=1}^4 (\Omega \times \bar{\omega}_i) \delta(i) \quad (33)$$

I_R ; rotor inertia and

$$\bar{\omega}_i = \begin{bmatrix} c\beta_i \alpha_i & -s\beta_i & c\beta_i s\beta_i \\ s\beta_i c\alpha_i & c\beta_i & s\beta_i s\beta_i \\ -s\alpha_i & 0 & c\beta_i \end{bmatrix} \begin{bmatrix} 0 \\ 0 \\ \omega_i \end{bmatrix} \quad (34)$$

$$M = \sum_{i=1}^4 M_i \quad (35)$$

The equations of motion can be represented as:

$$\dot{X} = f(X, U) \quad (36)$$

$$X = [x, \dot{x}, y, \dot{y}, z, \dot{z}, \varphi, \dot{\varphi}, \theta, \dot{\theta}, \psi, \dot{\psi}] \quad (37)$$

$$U = [w_1, \alpha_1, \beta_1, w_2, \alpha_2, \beta_2, w_3, \alpha_3, \beta_3, w_4, \alpha_4, \beta_4] \quad (38)$$

and,

$$\dot{x} = \begin{pmatrix} \begin{matrix} x_2 \\ 1/m((cx_{11}cx_9)u_1 + (-sx_{11}cx_7 + cx_{11}sx_9sx_7)u_2 + (sx_{11}sx_7 + cx_{11}sx_9cx_7)u_3 - K_1x_2 + d_1) \end{matrix} \\ \begin{matrix} x_4 \\ 1/m((sx_{11}cx_9)u_1 + (cx_{11}cx_7 + sx_{11}sx_9sx_7)u_2 + (-cx_{11}sx_7 + sx_{11}sx_9cx_7)u_3 - K_2x_4 + d_2) \end{matrix} \\ \begin{matrix} x_6 \\ -g + 1/m((-sx_9)u_1 + (cx_9sx_7)u_2 + (cx_9cx_7)u_3 - K_3x_6 + d_3) \end{matrix} \\ \begin{matrix} x_8 \\ x_{10}x_{12}I_1 + 1/I_x(u_4 - I_R(x_{12}S_2 + x_{10}S_3) - K_4x_8 + m_{dp}) \end{matrix} \\ \begin{matrix} x_{10} \\ x_8x_{12}I_2 + 1/I_y(u_5 - I_R(x_{12}S_1 - x_8S_3) - K_5x_{10} + m_{dq}) \end{matrix} \\ \begin{matrix} x_{12} \\ x_8x_{10}I_3 + 1/I_z(u_6 - I_R(-x_{10}S_1 + x_8S_2) - K_6x_{12} + m_{dr}) \end{matrix} \end{pmatrix} \quad (39)$$

where

$$\begin{bmatrix} u_1 \\ u_2 \\ u_3 \end{bmatrix} = \begin{bmatrix} \sum_{i=1}^4 c\beta_i s\beta_i b w_i^2 \\ \sum_{i=1}^4 s\beta_i s\beta_i b w_i^2 \\ \sum_{i=1}^4 c\beta_i b w_i^2 \end{bmatrix} \quad (40)$$

$$\begin{bmatrix} u_4 \\ u_5 \\ u_6 \end{bmatrix} = \begin{bmatrix} \sum_{i=1}^4 c\beta_i s\alpha_i d\omega_i^2 \delta(i) - b\omega_1^2(-s\beta_1 s\alpha_1 h) - b\omega_2^2(-c\alpha_2 l - s\beta_2 s\alpha_2 h) - b\omega_3^2(-s\beta_3 s\alpha_3 h) - b\omega_4^2(-c\alpha_4 l - s\beta_4 s\alpha_4 h) \\ \sum_{i=1}^4 s\beta_i s\alpha_i d\omega_i^2 \delta(i) - b\omega_1^2(c\alpha_1 l + c\beta_1 s\alpha_1 h) - b\omega_2^2(c\beta_2 s\alpha_2 h) - b\omega_3^2(-c\alpha_3 l - c\beta_3 s\alpha_3 h) - b\omega_4^2(c\beta_4 s\alpha_4 h) \sum_{i=1}^4 s\beta_i s\alpha_i \omega_i \delta(i) \\ \sum_{i=1}^4 c\alpha_i d\omega_i^2 \delta(i) - b\omega_1^2(-s\beta_1 s\alpha_1 l) - b\omega_2^2(c\beta_2 s\alpha_2 l) - b\omega_3^2(s\beta_3 s\alpha_3 l) - b\omega_4^2(-c\beta_4 s\alpha_4 l) \end{bmatrix} \quad (41)$$

$$\begin{bmatrix} S_1 \\ S_2 \\ S_3 \end{bmatrix} = \begin{bmatrix} \sum_{i=1}^{i=4} c\beta_i s\alpha_i \omega_i \delta(i) \\ \sum_{i=1}^{i=4} s\beta_i s\alpha_i \omega_i \delta(i) \\ \sum_{i=1}^{i=4} c\alpha_i \omega_i \delta(i) \end{bmatrix} \quad (42)$$

Substituting α_i and β_i equal to zero, the dynamic equation of the quadrotor with tilt rotors becomes similar to that of conventional quadrotor.

CHAPTER 4

WIND GUST MODELLING

According to National Oceanic and Atmospheric Administration, wind gust is a sudden, brief increase in speed of the wind [where] the peak wind speed reaches at least 16 knots and the variation in wind speed between peaks and lulls is at least 9 knots. The most frequent poor weather condition is flight in turbulent atmosphere which is a major issue in aircraft design. The main effect of wind gusts is to cause a random fluctuation of helicopter's velocity [56].

In flight simulation there are two methods of representing wind gust.

a. Natural Wind gust

b. Modelling equations

Natural wind gust recorded from wind tunnels by the use of a set of electric fans although turbulent, it is passed through a pipe-system represented in Fig. 9 below, the wind flow becomes primarily laminar. The disturbance effect is measured experimentally by operating the helicopter in hovering mode and then applying the wind gust impulse generated. The maximum rate of attitude derivative is measured and the maximum acceleration corresponding to the maximum additive effect of the wind gust to the attitude is then computed. Alternatively, natural wind gust recorded from atmosphere can be utilized. This technique is more advantageous but tedious because it results from physical measurements and more accurately represents the wind gust.

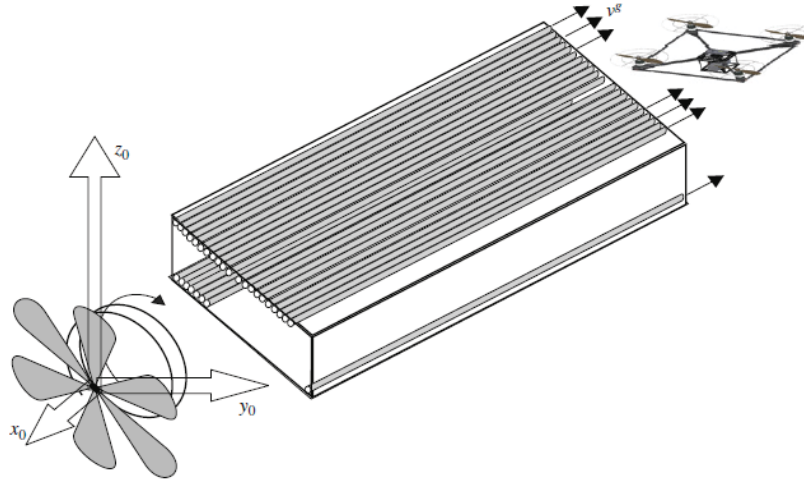


Figure 9 Artificial wind gust generation setup [45]

Modelling equation method defines wind gusts in terms of power spectral densities for the linear and angular velocity components parameterized by turbulence length scales and intensities [57]. A variety of models exist for gusts but the two methods namely Dryden and von Kármán models, are generally used for continuous gusts in flight dynamics applications. These approaches does not reflect on the variable component velocity of wind before and after the gust. However, a third approach called the “macro approach” for modelling also exists which takes other variables into account. These approaches are further discussed below.

4.1 Dryden Wind Gust Model

Dryden wind gust model is used to represent wind gust in the aviation industry and is accepted by the United States Department of Defense. This model is based on empirically measured power spectra of wind velocity in turbulent air. It assume that the turbulent gust is random, homogenous and isotropic. It uses band limited Gaussian white noise modified by shaping filters to approximate wind gust velocities in all three components of the body

reference frame.

The Dryden wind gust model from [58] is defined as the summation of sinusoidal excitation:

$$v_{\omega}(t) = v_w^0 + \sum_{i=1}^n a_i \sin(\Omega_i t + \varphi_i) \quad (43)$$

where

v_{ω} ; Time-dependent estimate of the wind vector given time t .

Ω_i ; Randomly selected frequencies with the values within the range of 0.1 to 1.5 rad/s.

φ_i ; Randomly selected phase shift.

n ; number of sinusoids.

a_i ; Amplitude of the sinusoid with magnitude given by: $a_i = \sqrt{\Delta\Omega_i \Phi(\Omega_i)}$.

$\Delta\Omega_i$; Frequency interval and $\Phi(\Omega_i)$ is power spectral density (PSD).

v_w^0 ; Ambient wind vector.

The PSD for the vertical and horizontal winds differ and are given by:

$$\Phi_h(\Omega) = \sigma_h^2 \frac{2L_h}{\pi} \frac{1}{1 + (L_h\Omega)^2} \quad (44)$$

$$\Phi_v(\Omega) = \sigma_v^2 \frac{L_v}{\pi} \frac{1 + 3(L_v\Omega)^2}{(1 + (L_v\Omega)^2)^2} \quad (45)$$

σ_h, σ_v ; represents the horizontal and vertical turbulence intensity.

L_h, L_v ; represents the horizontal and vertical length scales.

$$L_v = |z|, \sigma_v = 0.1w_{20}(\text{at } 20\text{ft altitude, } w_{20} \text{ is the wind speed in knots})$$

The following relation can be used to find L_h and σ_h ;

$$\frac{L_h}{L_v} = \frac{1}{(0.177 + 0.000823z)^{1.2}} \quad (46)$$

$$\frac{\sigma_h}{\sigma_v} = \frac{1}{(0.177 + 0.000823z)^{0.4}} \quad (47)$$

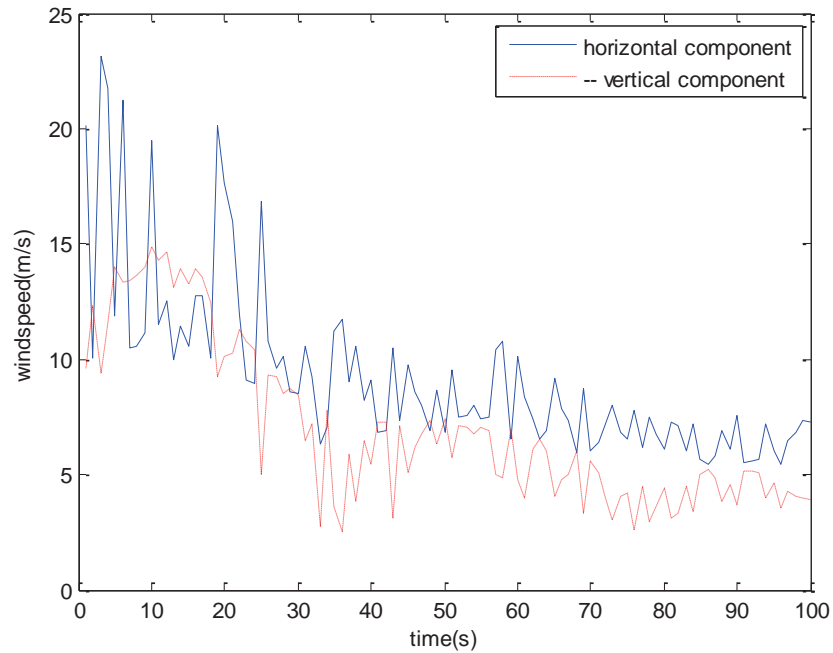


Figure 10 Wind velocity in inertial coordinate that results from the Dryden wind gust model developed in MATLAB.

4.2 Von Karman Wind Gust Model

This is also a mathematical model of wind gust. It is believed to capture continuous gusts better than the Dryden model [59]. The von Kármán wind turbulence model is

characterized by irrational power spectral densities, so filters can be designed that take white noise inputs and output stochastic processes with the approximated von Kármán gusts' power spectral densities.

This model is characterized by the power spectral densities for gusts three linear velocity components (u,v,w):

$$\Phi_u(\Omega) = \sigma_u^2 \frac{2L_u}{\pi} \frac{1}{(1 + (1.339L_u\Omega)^2)^{\frac{5}{6}}} \quad (48)$$

$$\Phi_v(\Omega) = \sigma_v^2 \frac{2L_v}{\pi} \frac{1 + (2.678L_v\Omega)^2}{(1 + (2.678L_v\Omega)^2)^{\frac{11}{6}}} \quad (49)$$

$$\Phi_w(\Omega) = \sigma_w^2 \frac{2L_w}{\pi} \frac{1 + (2.678L_w\Omega)^2}{(1 + (2.678L_w\Omega)^2)^{\frac{11}{6}}} \quad (50)$$

σ_i, L_i ; represents the turbulence intensity and scale length for the *i*th velocity component and spatial frequency (Ω).

The vehicle speed, V , through the gust field allows for conversion of these spectral densities into different types of frequencies.

$$\Omega = \frac{w_g}{V} \quad (51)$$

$$\Phi_i(\Omega) = V\Phi_i\left(\frac{w_g}{V}\right) \quad (52)$$

w_g in rad/time.

The angular velocity components (p, q, r) , defined as variation of the linear velocity components along the different vehicle axes,

$$p = \frac{\partial u}{\partial x} \quad (53)$$

$$q = \frac{\partial v}{\partial y} \quad (54)$$

$$r = -\frac{\partial w}{\partial z} \quad (55)$$

The power spectral densities for the angular velocity components are:

$$\Phi_p(w_g) = \frac{\sigma_{w_g}^2}{2VLw_g} \frac{0.8 (2.678L_v\Omega)^{\frac{1}{3}}}{1 + \left(\frac{4bw_g}{\pi V}\right)^2} \quad (56)$$

$$\Phi_q(w_g) = \frac{\pm\left(\frac{w_g}{V}\right)^2}{1 + \left(\frac{4bw_g}{\pi V}\right)^2} \Phi_w(w_g) \quad (57)$$

$$\Phi_r(w_g) = \frac{\mp\left(\frac{w_g}{V}\right)^2}{1 + \left(\frac{3bw_g}{\pi V}\right)^2} \Phi_v(w_g) \quad (58)$$

4.3 Macro Approach for Wind Gust Model

The wind gust modeling approach used in this work is based on [49]. This approach takes the following into consideration:

- The effect of wind velocity change
- Gust duration.
- Wind velocity change with respect to altitude.
- Wind direction change.

The wind force expression depending on the effective influence area on the quad rotor is also derived. However, this model is based on the finding in [54], that the effect of wind gust in small quadrotors are significantly correlated to the rate of increase or duration of a gust rather than the magnitude of the gust.

This macro modelling assumes that the whole quad rotor is connected to a point r , located at the origin of the body fixed frame. At any point in time the effect of wind felt at the different elements of the body have equal magnitude and direction as shown in Fig. 11.

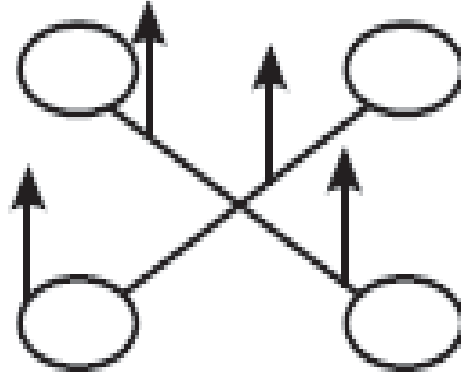


Figure 11 Effect of wind on the quadrotor body [49]

The model takes the form:

$$|V| = \begin{cases} V_{oi}, & t \leq t_{oi} \\ V_{oi} + \frac{|V_{mi} - V_{oi}|}{2} \left(1 - \cos \left(\frac{\pi(t - t_{oi})}{d_{ni} - t_{oi}} \right) \right), & t_{oi} < t \leq d_{ni}, & V_{mi} \geq V_{oi} \\ V_{oi} + \frac{|V_{mi} - V_{oi}|}{2} \left(\cos \left(\frac{\pi(t - t_{oi})}{d_{ni} - t_{oi}} \right) - 1 \right), & t_{oi} < t \leq d_{ni}, & V_{mi} < V_{oi} \\ V_{mi}, & t \leq t_m \end{cases} \quad (59)$$

where,

- t_m ; represents the maximum flight time.
- n ; represents a discrete random variable to determine the number of wind steps for t_m .
- V_{oi} ; represents the wind velocity before each step.
- t_{oi} ; represents a discrete random variable to determine each wind step start.
- d_{ni} ; represents a discrete random variable to determine each duration of gust.
- V_{mi} ; represents the gust magnitude.

Simulation example of the model given in [18], for $t_0 = [0; 9; 16; 19]$ s, $V_m = [1; 4.5; 0; 1]$ m/s, $d_n = [7; 5; 2; 5]$ s, $t_m = 25$ s and $V_0 = 0.5$ m/s is shown below,

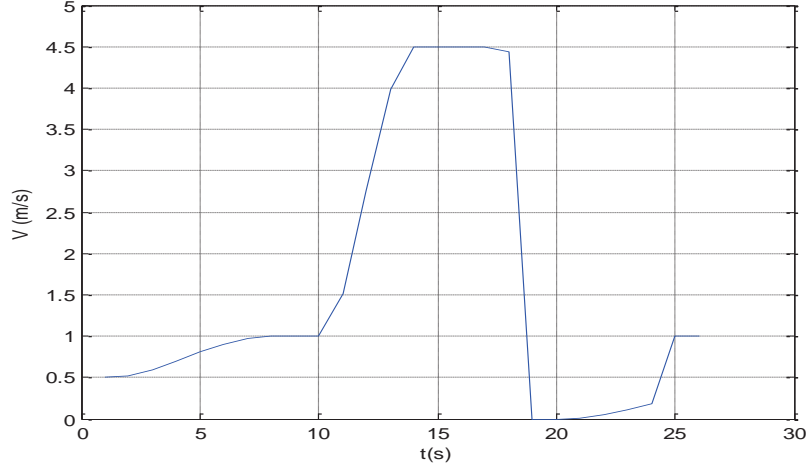


Figure 12 Simulation showing wind velocity before and after wind gust

However the following limitations applies when generating random values:

$$n \in \left[0, \frac{t_m}{10}\right]; d_i \in [0, t_{i+1} - t_i]; v_i \in [0, V_{max}];$$

$$\frac{|v_i - v_{i-1}|}{d_i} < a \quad (a: \text{restriction of the rate of step rise})$$

v_i ; represents a discrete random variable to determine each gust magnitude

Also, the point at which wind blows as a wind direction be the azimuth (Ψ_w), measured from the north through east.

Wind direction changes at each wind velocity step given by;

$$\Psi_{w(i+1)} = \Psi_{wi} \pm \Delta\Psi_{wi} \quad (60)$$

Where $\Delta\Psi_{wi}$ is the random value of change in wind direction

Since the wind velocity changes with altitude, the average wind velocity is determined by:

$$V_{cz} = V_{oz} \left(\frac{z}{z_o} \right)^p \quad (61)$$

where,

V_{cz} ; wind velocity at the altitude of z .

V_{oz} ; specified wind velocity at the altitude of z_o .

p ; energetic wind profile index.

The wind force is given by:

$$F_w = S_e A V_{cz}^2 \quad (62)$$

where,

S_e ; effective area influenced by the wind.

With reference to the influence force, it is decomposed into the following components for more appropriate or easier application:

$$\begin{aligned} F_{wx} &= S_e A V_{cz}^2 \cos(\Psi_w) \\ F_{wy} &= S_e A V_{cz}^2 \sin(\Psi_w) \end{aligned} \quad (63)$$

For simplicity, the quadrotor surface area is represented as a cylinder. So the surface area:

$$S_k = \mu 2\pi r h + \sigma 2\pi r^2 \quad (64)$$

The right hand representing the sum of lateral area and bases with μ, σ representing the fill factors here. Therefore if wind affects only half of the quadrotor the effective area will be given by:

$$\begin{aligned} S_{ex} &= \mu\pi r h \cos(\theta) + \sigma\pi r^2 \sin(\theta) \\ S_{ey} &= \mu\pi r h \cos(\varphi) + \sigma\pi r^2 \sin(\varphi) \end{aligned} \tag{65}$$

with θ and φ representing the pitch and yaw angles

CHAPTER 5

CASCADE CONTROL IMPLEMENTATION

Cascade control involves multiple cascaded loops for the purpose of controlling dependent variables provided the dynamics of the internal variable loops (secondary process) are faster than those of the outer variables loops (primary process). In general, the purpose of cascade control is to improve the performance of a single control loop when there is a disturbance that can affect a secondary variable that could compromise the performance of the primary variable of interest. Also, cascade control is used when the gain of the secondary process is nonlinear [57].

The controller methodology employed in this work is based on cascaded PID control loops.

5.1 PID Control

Proportional, Integral and Derivative control is arguably the most popularly used linear control design. Due to its versatility and availability of software implementation solutions, it is therefore commonly used for industrial solutions and research purposes [60].

The cascaded PID control loop as depicted in Fig. 13 below with the aim of cancelling wind disturbance while keeping the altitude and position as desired. This is because a PID controller is widely used and it exhibits a good robustness property. The inner PD controller approach (secondary loop) is used to control the position of the rotor axis, with

the aim of generating a force to cancel the effect of wind gust and for moving forward or sideways as the case may be. The primary PID controller (outer loop) is used to control the rotor speed according to error between the desired and actual altitude. The secondary (inner loop) utilizes the combination of the x, y desired and actual position to control the position and is also used to cancel wind gust effect. This is also stabilizes the attitude of the quadrotor.

We know that for conventional quadrotors, acceleration in the lateral or longitudinal direction is effected by tilting the quadrotor. For the tilt rotor quadrotor, only the tilt rotor axis are used for this purpose. Wind disturbance have the ability of moving the quadrotor against its path, thereby causing unwanted lateral or longitudinal movements. The concept of this work employs the PID controller to generate an equal amount of tilting against the wind direction so as to keep the quadrotor in its desired location.

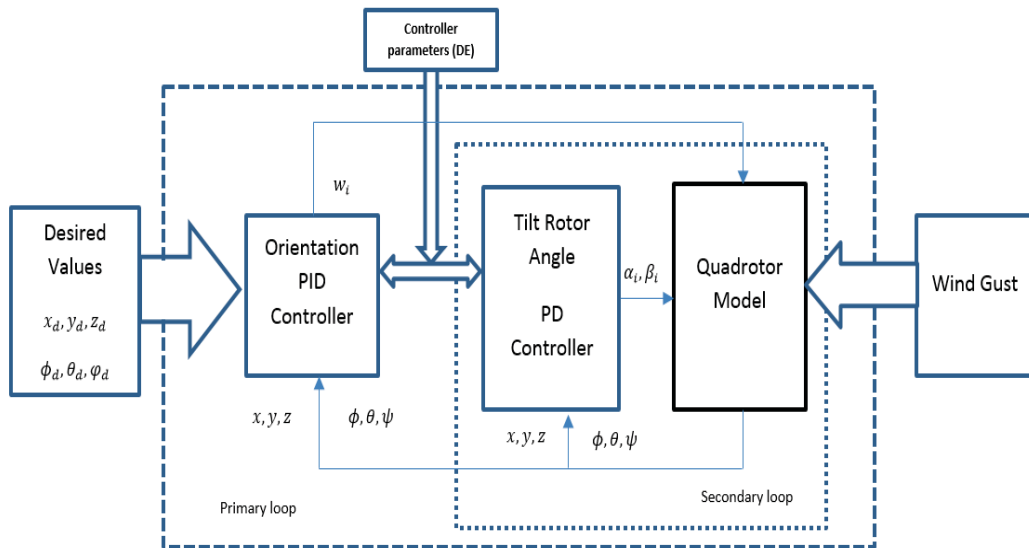


Figure 13 Cascade Control Block Diagram

5.1.1 Altitude Controller

For vertical takeoff and landing mission, the PID controller has the following structure

$$u = K_p(e) + K_i \sum_{i=1}^{t_f} (e) + K_d(e_{zi} - e_{zi-1}) \quad (66)$$

where $e = z_d - z$, K_p , K_i and K_d are the proportional, integral and derivative control coefficients and t_f is the simulation time. The parameters are derived from Differential Evolution (DE) optimization technique and would be described later:

Table 1 PID controller parameters for primary loop

Kp	Kd	Ki
50.0	1338.9	0.3365

5.1.2 Wind Force Cancellation Strategy

The concept of tilting the propeller axis generates a force in 3D. For rotors 1 and 3, β_i angles are set to zero and by controller action, α_i are allowed to tilt slightly to generate a force to cancel the effect of wind in the lateral (x) direction. Also, for rotors 2 and 4, β_i angles are set to 90 degrees so that α_i angles are used for the purpose of cancelling the wind force in the longitudinal (y) direction. The Figure 3 below depicts the concept which shows the variation of the α_i angles used to compensate the wind disturbance.

The PD controller represented by the following expression is used to control the orientation of the tilt axes and position;

$$\alpha_{1,3} = K_{p\alpha_{1,3}}e_x + K_{d\alpha_{1,3}}(e_{ix} - e_{(i-1)x}) \quad (67)$$

$$\alpha_{2,4} = K_{p\alpha_{2,4}}e_y + K_{d\alpha_{1,3}}(e_{iy} - e_{(i-1)y}) \quad (68)$$

where $e_r = r_d - r$, for $r = (x, y)$, in the earth frame. K_p and K_d are the proportional and derivative control gains are also derived from DE algorithm.

Table 2 PD controller parameters for the secondary loop

Kp	Kd
0.0226	2.9097

5.2 Controller Parameter Optimization by Differential Evolution

A significant evolution of optimization theory have emanated over time. A recent algorithm for evolutionary algorithm called the Differential Evolution (DE) was first introduced by Rainer Storn and Keneth Price in 1995 [50].

In brief, DE works in the following way; First, initialization and random selection of control parameters is done and then the objective function evaluated. Thereafter, the following processes will be executed so long as the stopping criteria is not met; For each individual in the population an offspring of controller parameters is created using the weighted difference of parent solutions. Finally, the fitter vector between the parent and offspring is passed on to the next iteration of the algorithm. Subsequently the controller parameters are passed on to the controller.

Fig.14 shows the flowchart for the process of DE; First, it starts, with (NP) initial population generated randomly between two bounds ($X_{j,max}, X_{j,min}$). Each solution (X) comprises of (D) elements which is the dimension of the problem (number of problem parameters needed to be optimized). Additional factors need to be defined, such as generation number or iteration (Ng), mutation factor (F) which control the convergence speed and crossover factor (CR) which plays role in the smoothness of the convergence and also ensures the diversity of the solutions in order not to be trapped in a local minimum during the optimization process. These are defined in table 3.

$$G^i = [X_1^i, X_2^i, \dots, \dots, X_{N_p}^i] \quad (69)$$

$$F \in [0,1], CR \in [0,1]$$

where i is the generation number, and each solution has (D) parameters which are the PID controller gains for this case.

$$X_n^i = [X_{n1}, X_{n2}, \dots, \dots, X_{nD}] \quad (70)$$

$$X_{i,j} = X_{j,min} + \text{random number}(X_{j,max} - X_{j,min})$$

In the next two steps, the fitness or objective function for each solution will be calculated, and according to it the best solution among the population will be nominated. The objective function is selected based on the Integral Square Error (ISE) given by:

$$IAE(z) = \int_0^{\infty} |e(z)| dt$$

$$\text{minimize } IAE(z)$$

$$x=(K_p, K_d, K_i, K_{p\alpha}, K_{d\alpha},)$$

Then the stopping criteria will be checked which may result in terminating or continuing to the next step. This step includes mutation and crossover processes which is the heart of

the differential evolution algorithm. Here, a variant vector solution V (offspring), is generated for each solution in the population by using the following formula:

$$V_i^{(G+1)} = X_i^{(G)} + F(X_{best}^{(G)} - X_i^{(G)}) + F(X_{r1}^{(G)} - X_{r2}^{(G)}) \quad (71)$$

where $X_{r1}^{(G)}, X_{r2}^{(G)}$ are randomly selected solution vectors from the current generation (different from each other and the corresponding X_i) and $X_{best}^{(G)}$ is the solution achieving best fitness function among the generation.

Then a trial solution will be generated by copying the parameters from the parent solution or the offspring solution based on randomly generated probability and the crossover factor. Fig. 15 illustrates the procedure of generating the trial solution, where a random probability number between $[0, 1]$ is generated and then compared to the crossover factor. If the random number is found to be larger than the crossover, then the trial solution will take the parameter from the parent and from the offspring otherwise. In one solution this procedure will be repeated (D) times until the trial solution is formed.

In the last step, there will be Np trial solutions corresponding to the original population. The fitness function will be calculated for them. The new generation will be formed by comparing the parent solution to the trial solution and takes the one which has the best fitness function as the member (new parent) for the new generation. The whole procedures will be repeated again and again until the stopping criteria is satisfied or the generation (iteration number) number is reached.

As long as the number of solutions and iterations gets larger, the possibility to reach the global minimum increases. Fig. 16 shows the plot of the convergence function.

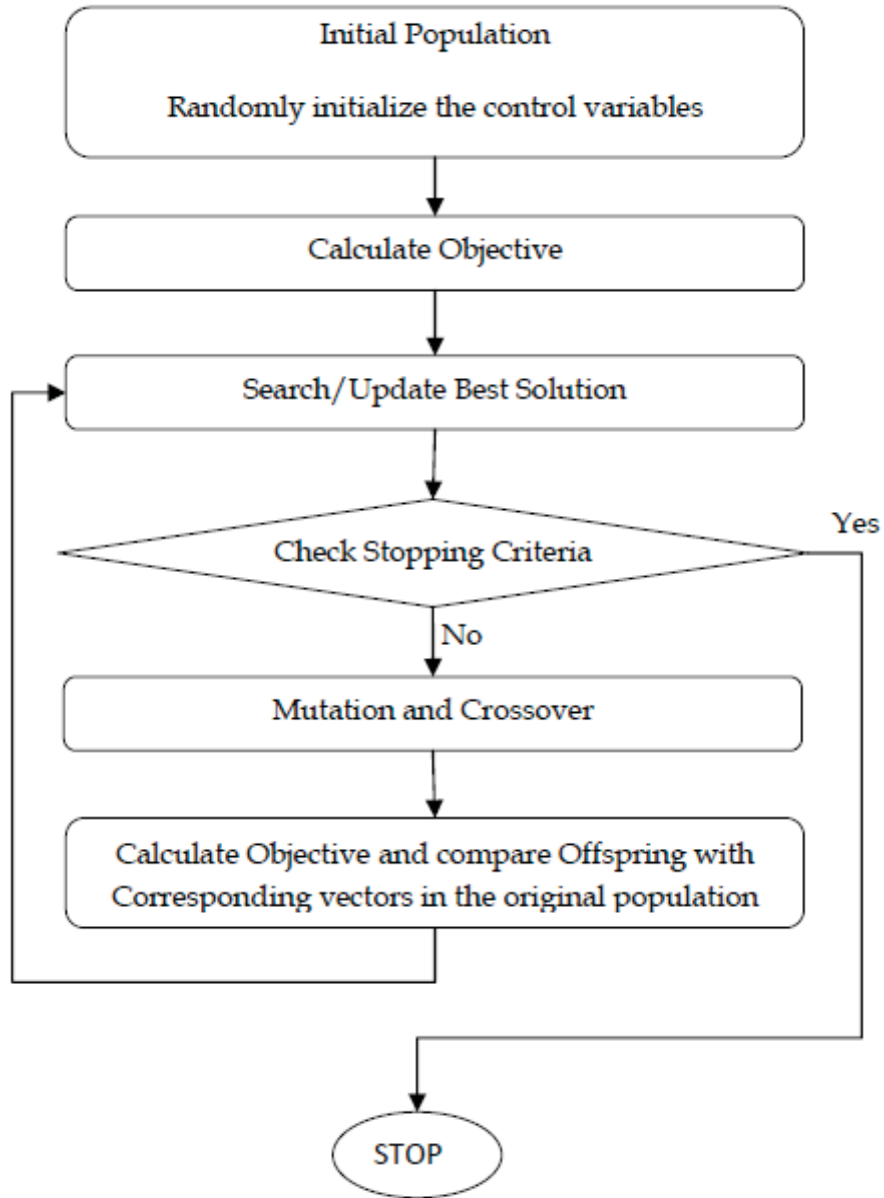


Figure 14 DE Flowchart (Vesterstro and Thomsen).

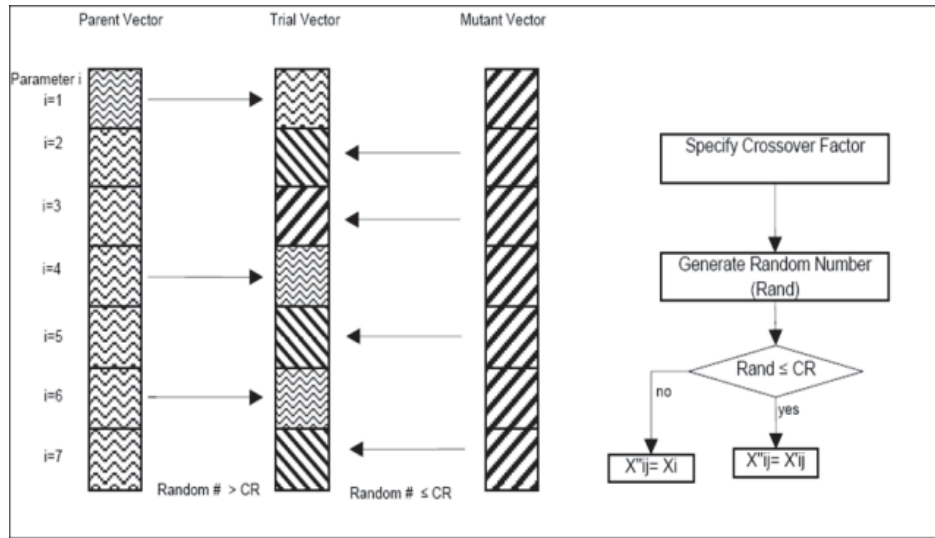


Figure 15 Crossover Procedure (Vesterstro and Thomsen).

Table 3 DE Algorithm Parameters

DE	
Cross over factor (CR)	0.5
Mutation factor (F)	0.5
Generation	50
Population size	25

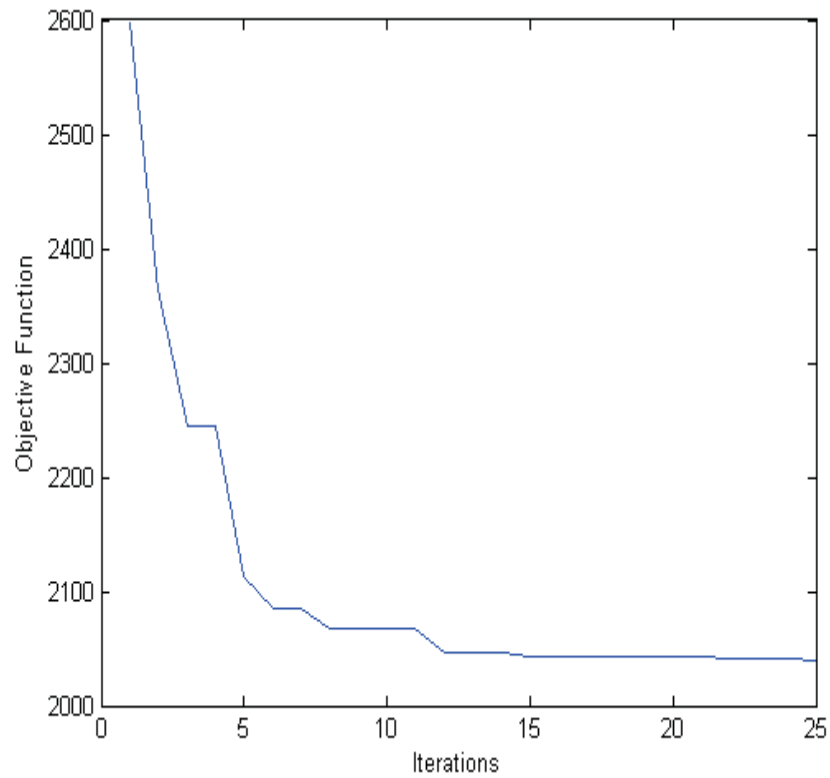


Figure 16 Convergence of DE algorithm

5.3 Simulation Results and Discussion

Simulation was carried out for a takeoff to an elevation of 50m with the parameters listed in the table below.

Table -4 Dynamic Parameters used for Cascade Control

Parameter	Definition	Value	Unit
g	Acceleration due to gravity	9.81	m/s ²
m	Mass	0.5	Kg
L, r, h	Arm length, radius, height	0.2	M
I _x = I _y	x, y inertia	4.85 x 10 ⁻³	kg.m ²
I _z	z inertia	8.81 x 10 ⁻³	kg.m ²
IR	Rotor inertia	3.36 x 10 ⁻⁵	kg.m ²

b	Trust factor	2.92×10^{-6}	kg.m
d	Drag factor	1.12×10^{-7}	kg.m ²
K1, K2,K3	Drag coefficients	0.01	Ns/m
K4, K5,K6	Drag coefficients	0.012	Ns/m
A	Rate of wind velocity	0.61	Nm ²

Fig. 17 depicts the 3D plot of the moving quadrotor without tilting its rotors while Fig. 18 shows the norm of the error between the x, y displacement which increases with increase in height. The error norm between x and y reaches up to 70 meters as shown. Fig. 19 of the position and altitude is given and the position error is shown. Fig. 20 shows the 3D plot when additional tilting inputs are used while Fig. 21 shows the norm of the error between the x, y displacement is now mitigated by the tilting effect. Figs. 22 and 23 represent the plots of the altitude and attitude. Fig. 22 shows that the quadrotor reaches the desired height of 50m and is able to hover around the desired position with some slight errors in the positions in x, y direction due to wind disturbance. Fig. 23 shows that the attitude angles are maintained zero. Fig. 24 shows how the tilt rotor angles are moving accordingly to distribute the force generated from the rotors to cancel the wind effect.

The simulation results clearly confirms that the concept of tilting the quadrotor motors can effectively mitigate the effect of wind disturbance.

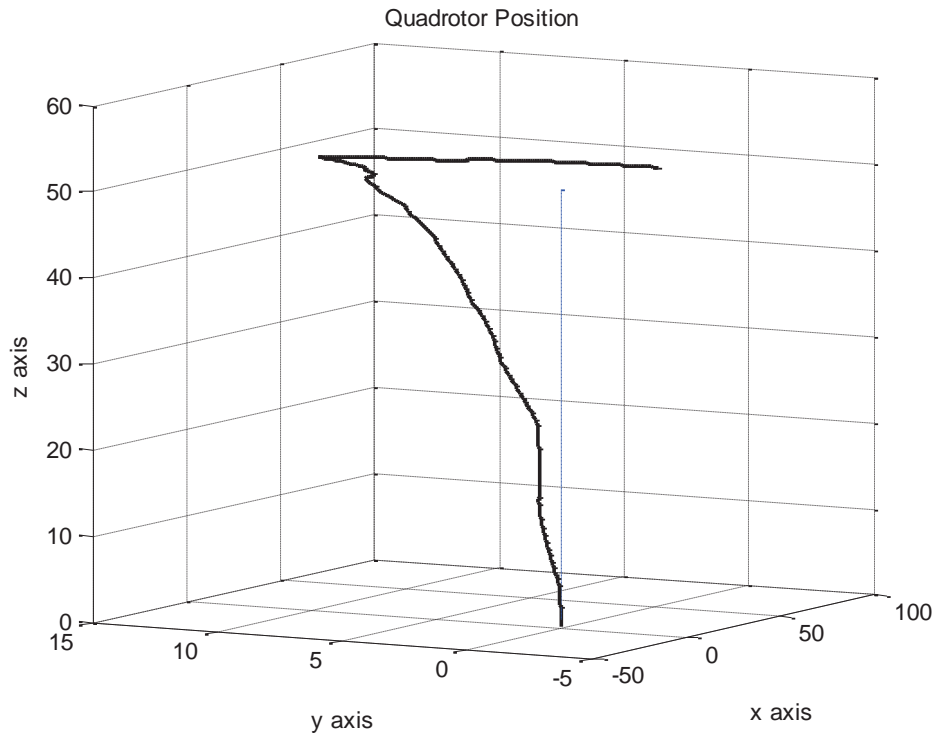


Figure 17 Position control without rotor tilting

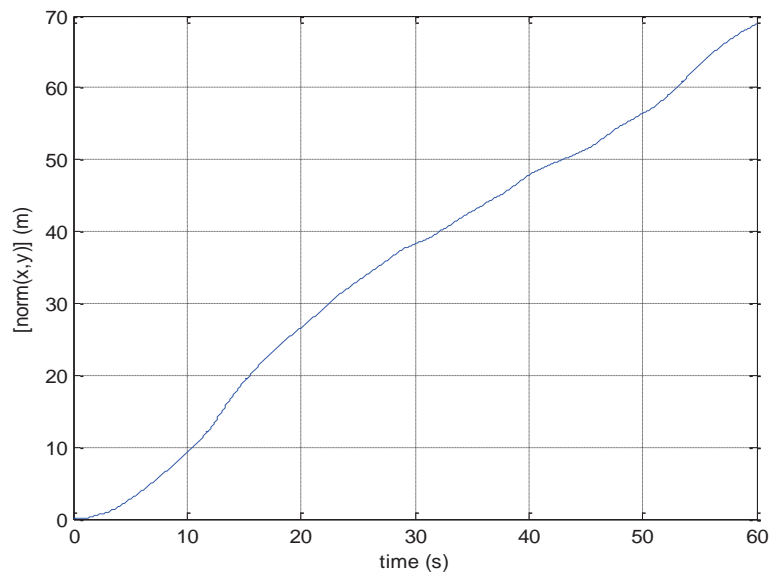


Figure 18 Error between x-y positions without tilting the rotors

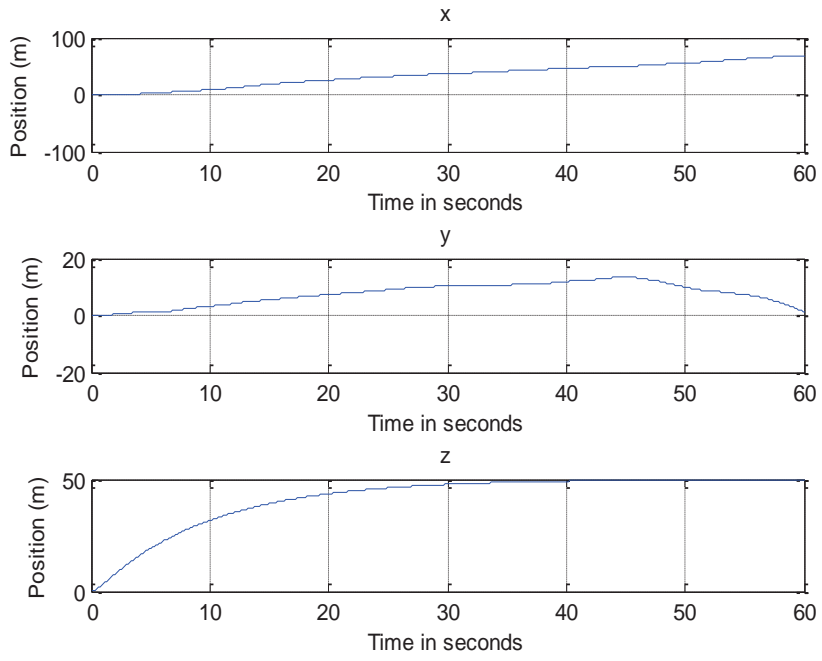


Figure 19 Quadrotor Altitude x, y, and z without rotor tilting

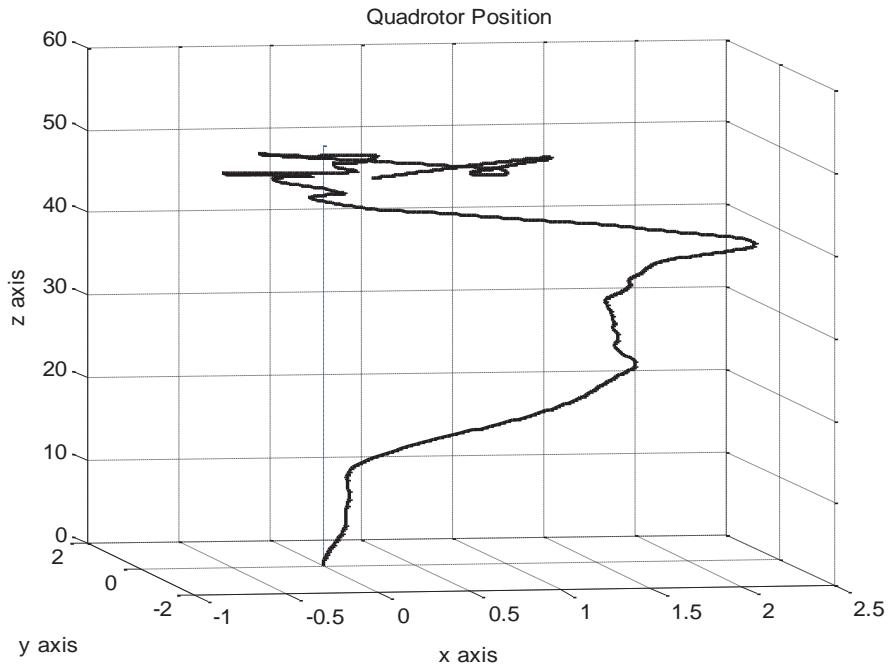


Figure 20 Quadrotor position with rotor tilting

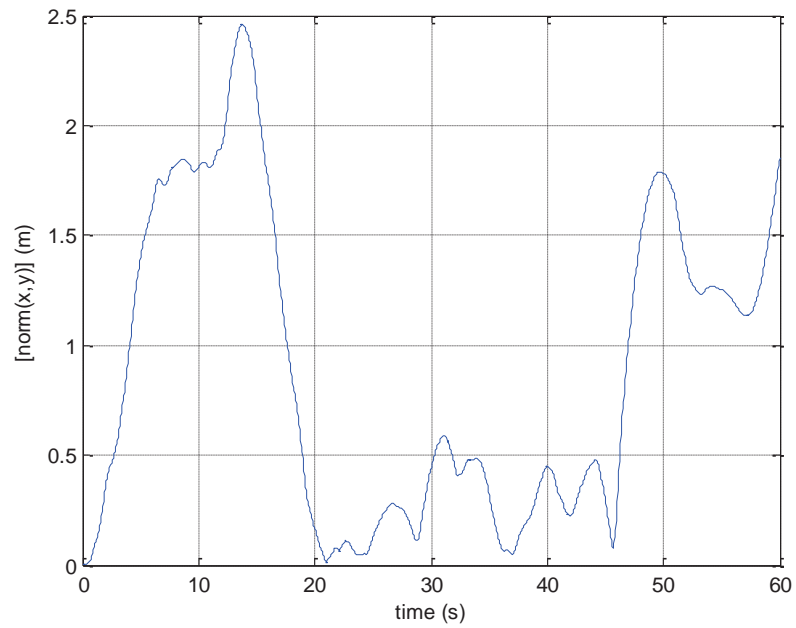


Figure 21 Error between x-y positions without tilting the rotors

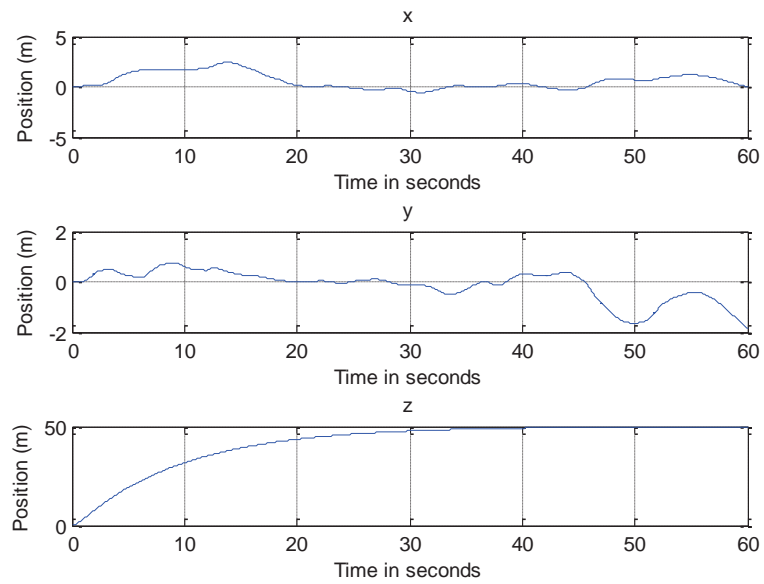


Figure 22 Quadrotor Altitude x, y, and z with rotor tilting

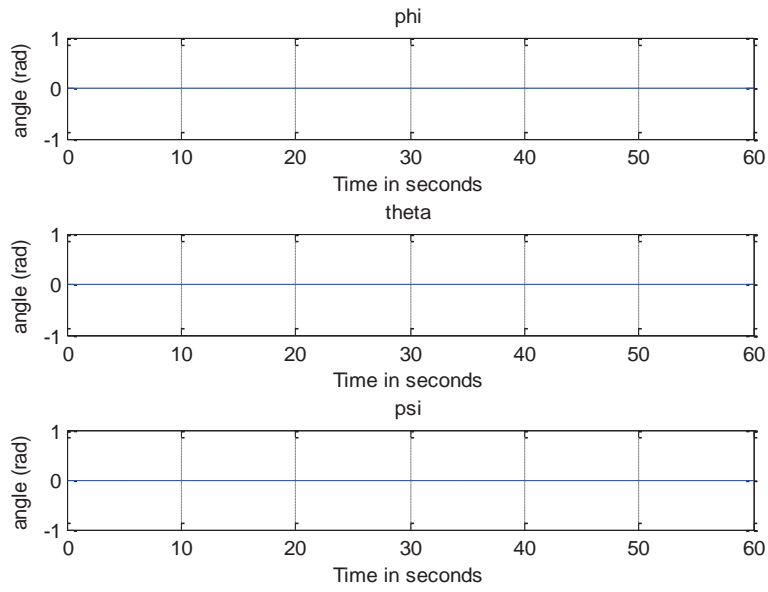


Figure 23 Quadrotor attitude ($\varphi \theta \psi$)

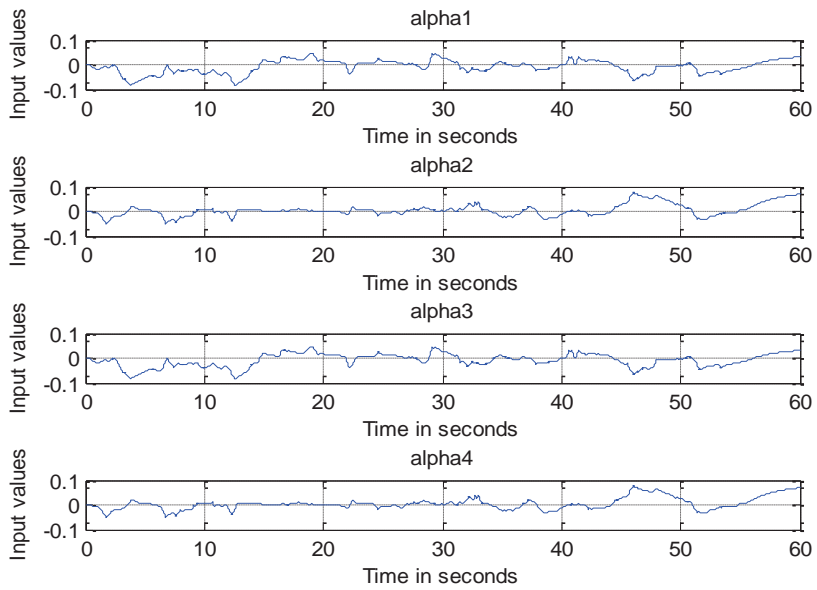


Figure 24 Plots of orientation axes, α_i

In order to showcase the capability of the performing multitask by using the tilting mechanism, the tiltrotor quadrotor is commanded to move forward at a speed of 0.5m/s after takeoff. Fig. 24 shows the 3D plot while Fig. 25 shows the lateral velocity.

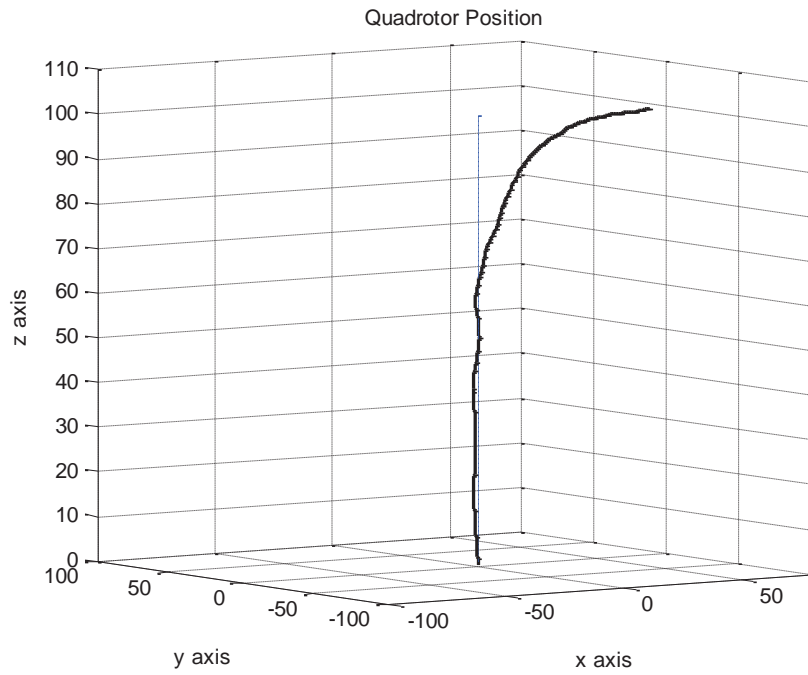


Figure 25 Multitasking Quadrotor

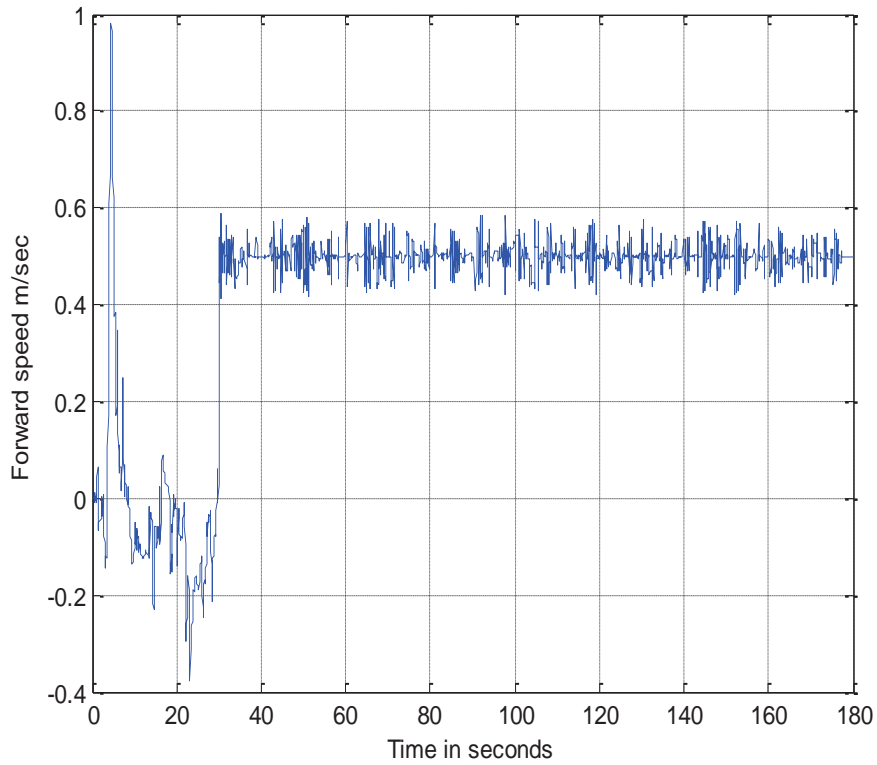


Figure 26 Forward speed of multitasking Quadrotor

The table 5 below shows the Mean Square Error (MSE), Maximum Absolute Error (MAE) and their corresponding confidence interval for ten randomly generated wind gust based on the macro approach. Confidence interval is used to show the effectiveness of the control method adopted by specifying a range of values for which there is high probability of not exceeding in most simulation run. A 95% confidence interval is chosen and the range of values (upper and lower bounds) are also given.

Table 5 Results of tiltrotor quadrotor under wind disturbance

With tilting			Without tilting	
	Mean Square Error [x, y]	Maximum Absolute Error [x, y]m	Mean Square Error [x, y]	Maximum Absolute Error [x, y]m
1	[0.54, 0.30]	[1.91,1.40]	[34.44,7.61]	[68.83,1.28]
2	[0.60,0.50]	[1.83,1.37]	[40.19,4.01]	[88.18,1.45]
3	[0.42,0.53]	[0.91,1.35]	[15.64,8.05]	[35.22,33.41]
4	[0.54,0.48]	[1.30,1.30]	[15.27,10.80]	[36.94,7.97]
5	[0.44,0.31]	[1.26,1.29]	[27.54,13.42]	[52.59,32.85]
6	[0.38,0.88]	[1.47,1.90]	[11.77,40.89]	[28.45,109.7]
7	[0.36,0.43]	[2.20,2.42]	[12.67,3.32]	[34.30,8.23]
8	[0.49,0.63]	[1.31,3.12]	[5.63,32.54]	[11.67,91.59]
9	[0.65,0.68]	[2.10,1.86]	[46.41,27.47]	[108.79,42.27]
10	[0.31,0.39]	[0.91,1.27]	[2.57,4.76]	[6.00,15.73]
95% Confidence Interval				
Upper	[0.54,0.62]	[1.81,2.11]	[30.52,23.60]	[67.44,57.93]
Lower	[0.40,0.40]	[1.23,1.34]	[11.91,6.98]	[26.75,10.96]

CHAPTER 6

DECENTRALIZED BACKSTEPPING CONTROL

IMPLEMENTATION

6.1 Decentralized Control

Theoretical framework of systems deals with how to decompose a given control problem into manageable sub problems that are weakly related to each other and can be solved independently. Therefore, the overall system is no longer controlled by a single but multiple independent controllers that together represents a decentralized controller. These controllers are designed in different design steps by means of models that describe only the relevant part of the plant. Therefore, the controllers are only based on an incomplete knowledge of the plant [33].

For the tiltrotor quadrotor a multi-controller structure would be employed to cope with the issue of its dynamic complexity by:

Decomposition - Coordination; a group of six subsystems is generated from the tiltrotor quadrotor.

Decentralization; the decentralization procedure adopted is outlined in [35] for solving the problem of inverted pendulum and [36] for the conventional quadrotor as earlier mentioned in chapter two.

6.1.1 Model Presentation

Consider the mathematical model of the quadrotor which can be re-written as:

$$\dot{X} = f(x) + g(x)u + f(t)$$

where,

$$f(x) = \begin{pmatrix} x_2 \\ -K_1 x_2 \\ x_4 \\ -K_2 x_4 \\ x_6 \\ -K_3 x_6 - g \\ x_8 \\ -K_4 x_8 + x_{10} x_{12} I_1 \\ x_{10} \\ -K_5 x_{10} + x_8 x_{12} I_2 \\ x_{12} \\ -K_6 x_{12} + x_{10} x_8 I_3 \end{pmatrix} \quad (72)$$

$$g(x) = \begin{pmatrix} 0 & 0 & 0 & 0 & 0 & 0 \\ 1/m(cx_{11}cx_9) & 1/m(-sx_{11}cx_7 + cx_{11}sx_9sx_7) & 1/m(sx_{11}sx_7 + cx_{11}sx_9cx_7) & 0 & 0 & 0 \\ 0 & 0 & 0 & 0 & 0 & 0 \\ 1/m(sx_{11}cx_9) & 1/m(cx_{11}cx_7 + sx_{11}sx_9sx_7) & 1/m(-cx_{11}sx_7 + sx_{11}sx_9cx_7) & 0 & 0 & 0 \\ 0 & 0 & 0 & 0 & 0 & 0 \\ 1/m(-sx_9) & 1/m(cx_9sx_7) & 1/m(cx_9cx_7) & 0 & 0 & 0 \\ 0 & 0 & 0 & 0 & 0 & 0 \\ 0 & 0 & 0 & 1/I_x & 0 & 0 \\ 0 & 0 & 0 & 0 & 0 & 0 \\ 0 & 0 & 0 & 0 & 1/I_y & 0 \\ 0 & 0 & 0 & 0 & 0 & 0 \\ 0 & 0 & 0 & 0 & 0 & 1/I_z \end{pmatrix} \quad (73)$$

$$L(t) = \begin{pmatrix} 0 \\ 0 \\ 0 \\ 0 \\ 0 \\ 0 \\ (-\frac{I_R}{I_x})(x_{12}S_2 + x_{10}S_3) \\ 0 \\ (-\frac{I_R}{I_y})(x_{12}S_1 - x_8S_3) \\ 0 \\ (-\frac{I_R}{I_z})(-x_{10}S_1 + x_8S_2) \end{pmatrix} \quad (74)$$

$$\begin{aligned} u_a &= (1/m)(sx_{11}sx_7 + cx_{11}sx_9cx_7); u_b = (1/m)(-cx_{11}sx_7 + sx_{11}sx_9cx_7); \\ u_c &= (1/m)(cx_9cx_7); \\ u_d &= (1/m)(-sx_{11}cx_7 + cx_{11}sx_9sx_7); u_e = (1/m)(cx_{11}cx_7 + sx_{11}sx_9sx_7); \\ u_f &= (1/m)(cx_9sx_7); \\ u_g &= (1/m)(cx_{11}cx_9); u_h = (sx_{11}cx_9) \text{ and } u_i = (1/m)(-sx_9) \end{aligned} \quad (75)$$

$L(t)$ are neglected because the rotor inertia I_R is negligibly small compared to the dynamics of the quadrotor [4]. This will make $f(t) = 0$. Transforming into m subsystems will be given in the following steps.

6.1.2 Model Decomposition - Coordination

Consider a class of nonlinear MIMO system [35]:

$$\begin{aligned} \dot{x} &= f(x) + g(x)u \\ y &= h(x) \end{aligned} \quad (76)$$

where $x \in R^n$ is the state and $u \in R^m$ is the control input. Let the system Eq. 76 be subdivided into m subsystems $\Sigma_1, \Sigma_2, \dots, \Sigma_m$ with interactions block such that $y_i = h_i(x_i), i = 1, 2, \dots, m$ with $x = [x_1, x_2, \dots, x_m], x_i \in R^{v_i}, 1 \leq i \leq m$ and $\sum_{i=1}^m v_i = n$. Also, the control signal u is divided into m vectors as:

$$w_1 = \begin{pmatrix} u_1 \\ 0 \\ \vdots \\ 0 \end{pmatrix}, w_2 = \begin{pmatrix} 0 \\ u_2 \\ \vdots \\ 0 \end{pmatrix}, w_m = \begin{pmatrix} 0 \\ 0 \\ \vdots \\ u_m \end{pmatrix} \quad (77)$$

With $w_i \in R^m$ and $\sum_{i=1}^m w_i = u$. Assuming that the functions $f(x)$ and $g(x)$ can be decomposed accordingly as:

$$\Sigma_{si}, \quad \begin{aligned} \dot{x}_i &= f_{vi}(x) + g_{vi}(x)u \\ y_i &= h_i(x), \end{aligned} \quad \forall 1 \leq i \leq m \quad (78)$$

One more decomposition of $f_{vi}(x)$ and $g_{vi}(x)$ as follows:

$$\begin{aligned} f_{vi}(x) &= \psi_{vi1}(x) + \psi_{vi2}(x) \\ g_{vi}(x) &= \varphi_{vi1}(x) + \varphi_{vi2}(x), \end{aligned} \quad \forall 1 \leq i \leq m \quad (79)$$

where $\psi_{vi1}(x)$ and $\varphi_{vi1}(x)$ depend on x_i only. Then Σ_{si} can be transformed into:

$$\dot{x}_i = [\psi_{vi1}(x) + \psi_{vi2}(x)] + [\varphi_{vi1}(x) + \varphi_{vi2}(x)]u \quad (80)$$

$$= \psi_{vi1}(x) + \varphi_{vi1}(x)w_i + \left[\psi_{vi2}(x) + \varphi_{vi2}(x)w_i + \sum_{\substack{j=i \\ j \neq i}}^m g_{vi}(x)w_j \right]$$

$$y_i = h_i(x), \quad \forall 1 \leq i \leq m$$

Define,

$$F_i(x) \Delta_i(x, u, t) = \left[\psi_{vi2}(x) + \varphi_{vi2}(x)w_i + \sum_{\substack{j=1 \\ j \neq 1}}^m g_{vi}(x)w_j \right] \quad \forall 1 \leq i \leq m \quad (81)$$

where $F_i(x)$ depends only on x_i and $\Delta_i(x, u, t) \in R^{vi}$ contains all interactions and plant parameters. Then the global system, is transformed into:

$$\dot{x}_i = \psi_{vi1}(x_i) + \psi_{vi2}(x_i)w_i + F_i(x) \Delta_i(x, u, t)$$

$$y_i = h_i(x), \quad \forall 1 \leq i \leq m$$

where $F_i(x) \Delta_i(x, u, t)$ is considered the uncertainty term. However, the effect of the uncertainty term is left for future investigation in this work. Decomposing $f(x)$ in the tiltrotor quadrotor

$$f(x) = \begin{pmatrix} f_{v1} \\ f_{v2} \\ f_{v3} \\ f_{v4} \end{pmatrix} = \begin{pmatrix} \psi_{v11} + \psi_{v12} \\ \psi_{v21} + \psi_{v22} \\ \psi_{v31} + \psi_{v32} \\ \psi_{v41} + \psi_{v42} \end{pmatrix} \quad (82)$$

$$\begin{aligned}\psi_{v11} &= \begin{pmatrix} x_2 \\ -K_1 x_2 \\ x_4 \\ -K_2 x_4 \\ x_6 \\ -K_3 x_6 \end{pmatrix}; \psi_{v12} = \begin{pmatrix} 0 \\ 0 \\ 0 \\ 0 \\ 0 \\ -g \end{pmatrix} \\ \psi_{v21} &= \begin{pmatrix} x_8 \\ -K_4 x_8 \end{pmatrix}; \psi_{v22} = \begin{pmatrix} 0 \\ x_{11} x_{12} I_1 \end{pmatrix} \\ \psi_{v31} &= \begin{pmatrix} x_{10} \\ -K_5 x_{10} \end{pmatrix}; \psi_{v32} = \begin{pmatrix} 0 \\ x_{10} x_{12} I_2 \end{pmatrix} \\ \psi_{v41} &= \begin{pmatrix} x_{12} \\ -K_6 x_{12} \end{pmatrix}; \psi_{v42} = \begin{pmatrix} 0 \\ x_{10} x_{11} I_3 \end{pmatrix}\end{aligned}$$

Decomposing $g(x)$

$$g(x) = \begin{pmatrix} g_{v1} \\ g_{v2} \\ g_{v3} \\ g_{v4} \end{pmatrix} = \begin{pmatrix} \phi_{v11} + \phi_{v12} \\ \phi_{v21} + \phi_{v22} \\ \phi_{v31} + \phi_{v32} \\ \phi_{v41} + \phi_{v42} \end{pmatrix} \quad (83)$$

$$\phi_{v11} = \begin{pmatrix} 0 & 0 & 0 & 0 & 0 & 0 \\ (u_g) & (u_d) & (u_a) & 0 & 0 & 0 \\ 0 & 0 & 0 & 0 & 0 & 0 \\ (u_h) & (u_e) & (u_b) & 0 & 0 & 0 \\ 0 & 0 & 0 & 0 & 0 & 0 \\ (u_i) & (u_f) & (u_c) & 0 & 0 & 0 \end{pmatrix}$$

$u_a, u_b, u_c, u_d, u_e, u_f, u_g, u_h$ and u_i are given in Eq. 75.

$$\begin{aligned}\phi_{v12} &= 0_{6 \times 6} \\ \phi_{v21} &= \begin{pmatrix} 0 & 0 & 0 & 0 & 0 & 0 \\ 0 & 0 & 0 & 1/I_x & 0 & 0 \end{pmatrix}; \phi_{v22} = 0_{6 \times 2} \\ \phi_{v31} &= \begin{pmatrix} 0 & 0 & 0 & 0 & 0 & 0 \\ 0 & 0 & 0 & 0 & 1/I_y & 0 \end{pmatrix}; \phi_{v32} = 0_{6 \times 2} \\ \phi_{v41} &= \begin{pmatrix} 0 & 0 & 0 & 0 & 0 & 0 \\ 0 & 0 & 0 & 0 & 0 & 1/I_z \end{pmatrix}; \phi_{v42} = 0_{6 \times 2}\end{aligned}$$

$$w_1 = \begin{pmatrix} u_1 \\ 0 \\ 0 \\ 0 \\ 0 \\ 0 \end{pmatrix}; w_2 = \begin{pmatrix} 0 \\ u_2 \\ 0 \\ 0 \\ 0 \\ 0 \end{pmatrix}; w_3 = \begin{pmatrix} 0 \\ 0 \\ u_3 \\ 0 \\ 0 \\ 0 \end{pmatrix}; w_4 = \begin{pmatrix} 0 \\ 0 \\ 0 \\ u_4 \\ 0 \\ 0 \end{pmatrix}; w_5 = \begin{pmatrix} 0 \\ 0 \\ 0 \\ 0 \\ u_5 \\ 0 \end{pmatrix}; w_6 = \begin{pmatrix} 0 \\ 0 \\ 0 \\ 0 \\ 0 \\ u_6 \end{pmatrix}$$

Therefore, S_1 can be written as;

$$\begin{aligned} \tilde{x}_1 = & \begin{pmatrix} x_2 \\ -K_1 x_2 \\ x_4 \\ -K_2 x_4 \\ x_6 \\ -K_3 x_6 \end{pmatrix} + \begin{pmatrix} 0 & 0 & 0 & 0 & 0 & 0 \\ (u_g) & 0 & 0 & 0 & 0 & 0 \\ 0 & 0 & 0 & 0 & 0 & 0 \\ (u_h) & 0 & 0 & 0 & 0 & 0 \\ 0 & 0 & 0 & 0 & 0 & 0 \\ (u_i) & 0 & 0 & 0 & 0 & 0 \end{pmatrix} w_1 + \begin{pmatrix} 0 & 0 & 0 & 0 & 0 & 0 \\ 0 & u_d & 0 & 0 & 0 & 0 \\ 0 & 0 & 0 & 0 & 0 & 0 \\ 0 & u_e & 0 & 0 & 0 & 0 \\ 0 & 0 & 0 & 0 & 0 & 0 \\ -g & u_f & 0 & 0 & 0 & 0 \end{pmatrix} \begin{pmatrix} 1 \\ u_2 \\ 0 \\ 0 \\ 0 \\ 0 \end{pmatrix} \\ & + \begin{pmatrix} 0 & 0 & 0 & 0 & 0 & 0 \\ 0 & 0 & u_a & 0 & 0 & 0 \\ 0 & 0 & 0 & 0 & 0 & 0 \\ 0 & 0 & u_b & 0 & 0 & 0 \\ 0 & 0 & 0 & 0 & 0 & 0 \\ 0 & 0 & u_c & 0 & 0 & 0 \end{pmatrix} w_3 \end{aligned} \quad (84)$$

$$S_{11}: \tilde{x}_{11} = \begin{pmatrix} x_2 \\ -K_1 x_2 \end{pmatrix} + \begin{pmatrix} 0 & 0 & 0 & 0 & 0 & 0 \\ u_g & 0 & 0 & 0 & 0 & 0 \end{pmatrix} w_1 + \begin{pmatrix} 0 & 0 & 0 & 0 & 0 & 0 \\ 0 & u_d & 0 & 0 & 0 & 0 \end{pmatrix} \begin{pmatrix} 1 \\ u_2 \\ 0 \\ 0 \\ 0 \\ 0 \end{pmatrix} + \begin{pmatrix} 0 & 0 & 0 & 0 & 0 & 0 \\ 0 & 0 & u_a & 0 & 0 & 0 \end{pmatrix} w_3 \quad (85)$$

$$S_{12}: \tilde{x}_{12} = \begin{pmatrix} x_4 \\ -K_2 x_4 \end{pmatrix} + \begin{pmatrix} 0 & 0 & 0 & 0 & 0 & 0 \\ 0 & u_e & 0 & 0 & 0 & 0 \end{pmatrix} \begin{pmatrix} 1 \\ u_2 \\ 0 \\ 0 \\ 0 \\ 0 \end{pmatrix} + \begin{pmatrix} 0 & 0 & 0 & 0 & 0 & 0 \\ u_h & 0 & 0 & 0 & 0 & 0 \end{pmatrix} w_1 + \begin{pmatrix} 0 & 0 & 0 & 0 & 0 & 0 \\ 0 & 0 & u_b & 0 & 0 & 0 \end{pmatrix} w_3 \quad (86)$$

$$\begin{aligned}
S_{13}; \tilde{x}_{13} = & \begin{pmatrix} x_6 \\ -K_3 x_6 \end{pmatrix} + \begin{pmatrix} 0 & 0 & 0 & 0 & 0 & 0 \\ 0 & 0 & u_c & 0 & 0 & 0 \end{pmatrix} w_3 + \begin{pmatrix} 0 & 0 & 0 & 0 & 0 & 0 \\ u_i & 0 & 0 & 0 & 0 & 0 \end{pmatrix} w_1 \\
& + \begin{pmatrix} 0 & 0 & 0 & 0 & 0 & 0 \\ -g & u_f & 0 & 0 & 0 & 0 \end{pmatrix} \begin{pmatrix} 1 \\ u_2 \\ 0 \\ 0 \\ 0 \\ 0 \end{pmatrix}
\end{aligned} \tag{87}$$

Similarly, S_2, S_3, S_4

$$S_2; \tilde{x}_2 = \begin{pmatrix} x_8 \\ -K_4 x_8 \end{pmatrix} + \begin{pmatrix} 0 & 0 & 0 & 0 & 0 & 0 \\ 0 & 0 & 0 & 1/I_x & 0 & 0 \end{pmatrix} w_4 + \begin{pmatrix} 0 \\ x_{11} x_{12} I_1 \end{pmatrix} + \begin{pmatrix} 0 & 0 & 0 & 0 & 0 & 0 \\ 0 & 0 & 0 & 0 & 0 & 0 \end{pmatrix} w_4 \tag{88}$$

$$S_3; \tilde{x}_3 = \begin{pmatrix} x_{10} \\ -K_5 x_{10} \end{pmatrix} + \begin{pmatrix} 0 & 0 & 0 & 0 & 0 & 0 \\ 0 & 0 & 0 & 0 & 1/I_y & 0 \end{pmatrix} w_5 + \begin{pmatrix} 0 \\ x_{10} x_{12} I_2 \end{pmatrix} + \begin{pmatrix} 0 & 0 & 0 & 0 & 0 & 0 \\ 0 & 0 & 0 & 0 & 0 & 0 \end{pmatrix} w_5 \tag{89}$$

$$S_4; \tilde{x}_4 = \begin{pmatrix} x_{12} \\ -K_6 x_{12} \end{pmatrix} + \begin{pmatrix} 0 & 0 & 0 & 0 & 0 & 0 \\ 0 & 0 & 0 & 0 & 0 & 1/I_z \end{pmatrix} w_6 + \begin{pmatrix} 0 \\ x_{10} x_{11} I_3 \end{pmatrix} + \begin{pmatrix} 0 & 0 & 0 & 0 & 0 & 0 \\ 0 & 0 & 0 & 0 & 0 & 0 \end{pmatrix} w_6 \tag{90}$$

6.1.3 Backstepping Control

Consider the system [17],

$$\begin{aligned}
\dot{x} &= f(x) + g(x)\xi \\
\dot{\xi} &= u
\end{aligned} \tag{91}$$

where $[x^T, \xi]^T \in R^{n+1}$ is the state and $x \in R^n$ is the control input. The functions $f: D \rightarrow R^n$ and $g: D \rightarrow R^n$ are smooth in a domain $D \subset R^n$ that contains $x = 0$ and $f(0) = 0$. We want to design a state feedback control law to stabilize the origin ($x = 0, \xi = 0$). We assume that both f and g are known. Suppose the Eq. 91 above can be stabilized by a smooth state feedback control law $\xi = \phi(x)$ with $\phi(0) = 0$; that is, the

origin of

$$\dot{x} = f(x) + g(x)\phi(x) \quad (92)$$

is asymptotically stable. Suppose further that we know a (smooth, positive definite) Lyapunov function $V(x)$ that satisfies the inequality

$$\frac{\partial V(x)}{\partial x} [f(x) + g(x)\phi(x)] \leq -W(x) \quad \forall x \in D \quad (93)$$

where $W(x)$ is positive definite. By adding and subtracting $g(x)\phi(x)$ on the right side of Eq. 91 we obtain the equivalent representation

$$\begin{aligned} \dot{x} &= [f(x) + g(x)\phi(x)] + g(x) [\xi - \phi(x)] \\ \dot{\xi} &= u \end{aligned}$$

The change of variables

$$z = \xi - \phi(x)$$

results in the system:

$$\begin{aligned} \dot{x} &= [f(x) + g(x)\phi(x)] + g(x)z \\ z &= u - \dot{\phi} \end{aligned} \quad (94)$$

is viewed as backstepping $-\phi(x)$ through an integrator. Since f , g and ϕ are known, the derivative $\dot{\phi}$ can be computed by using the expression:

$$\dot{\phi} = \frac{\partial \phi}{\partial x} [f(x) + g(x)\xi]$$

Taking $v = u - \dot{\phi}$ reduces the system to the cascade connection

$$\dot{x} = [f(x) + g(x)\phi(x)] + g(x)z \quad (95)$$

$$\dot{z} = v$$

This is similar to Eq. 91 except that we now have an asymptotically stable origin when the input is zero.

6.2 Decentralized Backstepping Control of Tiltrotor Quadrotor

Following [36], each subsystem is in the form:

$$S_i : \dot{x}_i = \psi_{vi1}(x) + \varphi_{vi1}(x)w_i + F_i(x) \Delta_i(x, u, t), i = 1, 2, 3, 4 \quad (96)$$

where $F_i(x)$ depends only on x_i and $\Delta_i(x, u, t) \in R^{vi}$ contains all interactions and plant parameters. Then each subsystem is treated separately without the uncertainty term to generate control inputs using backstepping method.

For S_2 :

$$S_2; \tilde{x}_2 = \begin{pmatrix} x_8 \\ -K_4 x_8 \end{pmatrix} + \begin{pmatrix} 0 & 0 & 0 & 0 & 0 & 0 \\ 0 & 0 & 0 & 1/I_x & 0 & 0 \end{pmatrix} w_4 + \begin{pmatrix} 0 \\ x_{11} x_{12} I_1 \end{pmatrix} + \begin{pmatrix} 0 & 0 & 0 & 0 & 0 & 0 \\ 0 & 0 & 0 & 0 & 0 & 0 \end{pmatrix} w_4$$

Without the uncertainty term, S_2 represents the roll angle subsystem which is now in a strict feedback form:

$$\tilde{x}_2 = \begin{pmatrix} x_8 \\ -K_4 x_8 \end{pmatrix} + \begin{pmatrix} 0 & 0 & 0 & 0 & 0 & 0 \\ 0 & 0 & 0 & 1/I_x & 0 & 0 \end{pmatrix} w_4$$

Extracting those gives:

$$\dot{x}_7 = x_8$$

$$\dot{x}_8 = -K_4 x_8 + u_4(1/I_x)$$

To achieve a change of state, we add and subtract u_{x7} ; where u_{x7} is a function of x_7 .

Thus we have:

$$\begin{aligned}\dot{x}_7 &= x_8 + u_{x7} - u_{x7} = u_{x7} + (x_8 - u_{x7}) \\ &= u_{x7} + e_2\end{aligned}\tag{97}$$

So that,

$$\dot{e}_2 = \dot{x}_8 - \dot{u}_{x7} = -K_4 x_8 + u_4(1/I_x) - \dot{u}_{x7} = v_2$$

Define the Lyapunov function $V(x_7, e_2)$:

$$V = \frac{1}{2}(x_7 - x_7^d)^2 + \frac{1}{2}e_2^2\tag{98}$$

The time derivative:

$$\begin{aligned}\dot{V} &= (x_7 - x_7^d)\dot{x}_7 + e_2\dot{e}_2 \\ &= (x_7 - x_7^d)(u_{x7} + e_2) + e_2v_2 \\ &= (x_7 - x_7^d)(u_{x7}) + e_2(x_7 - x_7^d + v_2);\end{aligned}$$

To ensure \dot{V} is negative definite in order to guarantee stability:

$$u_{x7} = -k_{21}(x_7 - x_7^d)$$

and

$$v_2 = -k_{22}e_2 - (x_7 - x_7^d); k_{21}, k_{22} > 0$$

Therefore,

$$\dot{V} = -k_{21}(x_7 - x_7^d)^2 + e_2[(x_7 - x_7^d) - k_{22}e_2 - (x_7 - x_7^d)]$$

Hence,

$$\dot{V} = -k_{21}e^2 - k_{22}e_2^2 < 0$$

This gives,

$$u_4 = I_x(K_4 x_8 + \dot{u}_{x7} + v_2)$$

$$u_4 = I_x(K_4x_8 + \dot{u}_{x7} + (-k_{22}e_2 - (x_7 - x_7^d)))$$

But, $\dot{u}_{x7} = -k_{21}\dot{x}_7 = -k_{21}x_8$ and $e_2 = \dot{x}_7 - u_{x7} = x_8 + k_{21}(x_7 - x_7^d)$

Therefore,

$$\begin{aligned} u_4 &= I_x(K_4x_8 - k_{21}x_8 + (-k_{22}(x_8 + k_{21}(x_7 - x_7^d)) - (x_7 - x_7^d))) \\ u_4 &= I_x((K_4 - k_{21} - k_{22})x_8 + (-k_{22}k_{21} - 1)(x_7 - x_7^d)) \end{aligned} \quad (99)$$

Similarly two other inputs are generated from S_3 and S_4 for pitch and yaw respectively:

$$u_5 = I_y((K_5 - k_{31} - k_{32})x_{10} + (-k_{32}k_{31} - 1)(x_9 - x_9^d)) \quad (100)$$

$$u_6 = I_z((K_6 - k_{41} - k_{42})x_{12} + (-k_{42}k_{41} - 1)(x_{11} - x_{11}^d)) \quad (101)$$

From subsystem S_1 ; S_{11}, S_{12} and S_{13} were formed. These subsystems were used to generate three inputs; u_1 , u_2 and u_3 ;

For instance; Backstepping control is applied to S_{13} as follows:

$$S_{13}; \tilde{x}_{11} = \begin{pmatrix} x_2 \\ -K_1x_2 \end{pmatrix} + \begin{pmatrix} 0 \\ u_g u_1 \end{pmatrix}$$

$$\dot{x}_1 = x_2$$

$$\dot{x}_2 = -K_1x_2 + u_g u_1$$

Again, to achieve a change of state, we add and subtract u_{x1} ; where u_{x1} is a function of x_1 we have:

$$\dot{x}_1 = x_2 + u_{x1} - u_{x1} = u_{x1} + (x_2 - u_{x1}) \quad (102)$$

$$= u_{x_1} + e_1;$$

So that,

$$\dot{e}_1 = \dot{x}_2 - \dot{u}_{x_1} = -K_1 x_2 + u_g u_1 - \dot{u}_{x_1} = v_1$$

The Lyapunov function is similar as previously defined so,

To ensure V is negative definite:

$$u_{x_1} = -k_{11}(x_1 - x_1^d)$$

And

$$v_1 = -k_{12}e_1 - (x_1 - x_1^d); k_{11}, k_{12} > 0$$

From

$$v_1 = -K_1 x_2 + (1/m)u_g u_1 - \dot{u}_{x_1}$$

$$u_1 = (m/u_g)(v_1 + K_1 x_2 + \dot{u}_{x_1})$$

But,

$$\dot{u}_{x_1} = -k_{11}\dot{x}_1 = -k_{11}x_2 \text{ and } e_1 = \dot{x}_1 - u_{x_1} = x_2 + k_{11}(x_1 - x_1^d)$$

$$v_1 = -k_{12}(x_2 + k_{11}(x_1 - x_1^d)) - (x_1 - x_1^d)$$

$$u_1 = (1/u_g)(-k_{12}(x_2 + k_{11}(x_1 - x_1^d)) - (x_1 - x_1^d) + K_1 x_2 - k_{11}x_2)$$

$$u_1 = (1/u_g)((-k_{12}k_{11} - 1)(x_1 - x_1^d) + (K_1 - k_{11} - k_{12})x_2) \quad (103)$$

Similarly, from S_{12} and S_{13} we have:

$$u_2 = (1/u_e)((-k_{62}k_{61} - 1)(x_3 - x_3^d) + (K_2 - k_{61} - k_{62})x_4) \quad (104)$$

$$u_3 = (1/u_c)((-k_{72}k_{71} - 1)(x_5 - x_5^d) + (K_3 - k_{71} - k_{72})x_6) \quad (105)$$

The Fig. 27 below shows the structure of the decentralized-backstepping system.

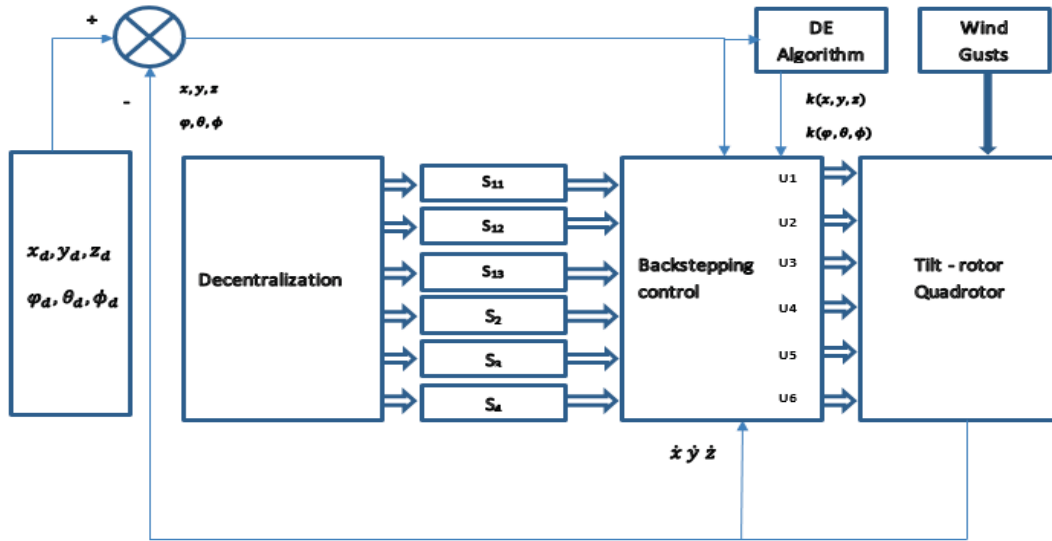


Figure 27 Block diagram of decentralized backstepping control

6.3 Simulation Results and Discussion

Fig. 28 shows that the objective function from DE algorithm converges after eight iterations.

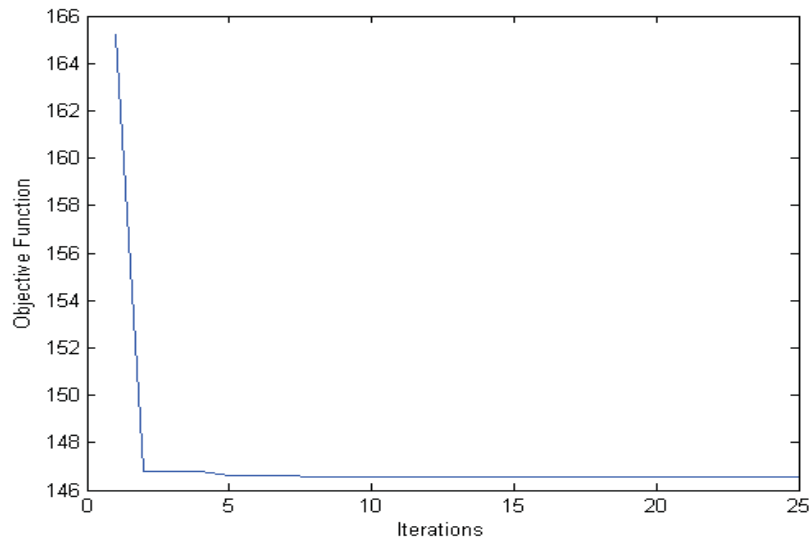


Figure 28 Convergence of DE algorithm for Decentralized Control gains

The control and dynamic parameters used are given in the table 6:

Table 6 Parameters used for Decentralized Backstepping control

Parameter	Definition	Value	Unit
g	Acceleration due to gravity	9.81	m/s ²
m	Mass	0.5	Kg
r, h	radius, height	0.2	m
$I_x = I_y$	x, y inertia	4.85×10^{-3}	kg.m ²
I_z	z inertia	8.81×10^{-3}	kg.m ²
I_R	Rotor inertia	3.36×10^{-5}	kg.m ²
b	Trust factor	2.92×10^{-6}	kg.m
d	Drag factor	1.12×10^{-7}	kg.m ²
K_1, K_2, K_3	Drag coefficients	0.01	Ns/m
K_4, K_5, K_6	Drag coefficients	0.012	Ns/m
A	Rate of wind velocity	0.61	Nm ²
μ, σ	Fill factors	0.2, 0.4	M
$k_{ij}; i = 1:6, j = 1$	Controller gains	35.1197, 33.3426, 38.8252, 14.2395, 40.6587, 24.4382	-
$k_{ij}; i = 1:7, j = 2$	Controller gains	0.0684, 0.0114, 2.0, 0.0262, 0.0262, 0.01	-

1. Elevation to [0,0,50]m under wind gust

Quadrotor commanded move to the following coordinate [0,0,50]m. Below results Fig. 29, shows that the target height is reached and the tiltrotor quadrotor is able to hover at 50m. Fig. 30 depicts the 3D plot which shows a location tracking of the coordinate with a negligibly small error. Fig. 31 and Fig. 32 shows the elevation and altitude and their corresponding velocities respectively. As earlier mentioned, wind gust is seen to cause random fluctuation in the velocities. Fig. 33 and Fig. 34 shows that the orientation and their rates respectively are not affected.

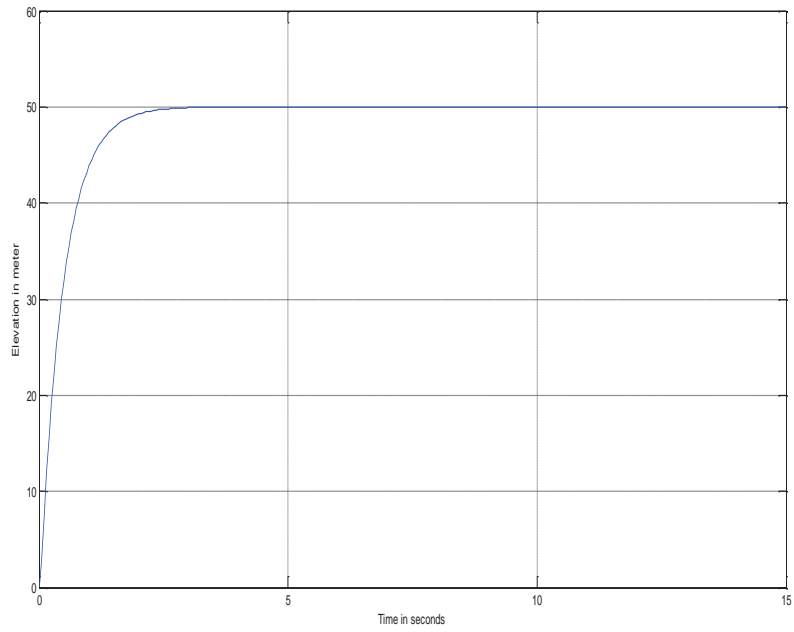


Figure 29 Elevation to [0,0,50]m under wind gust

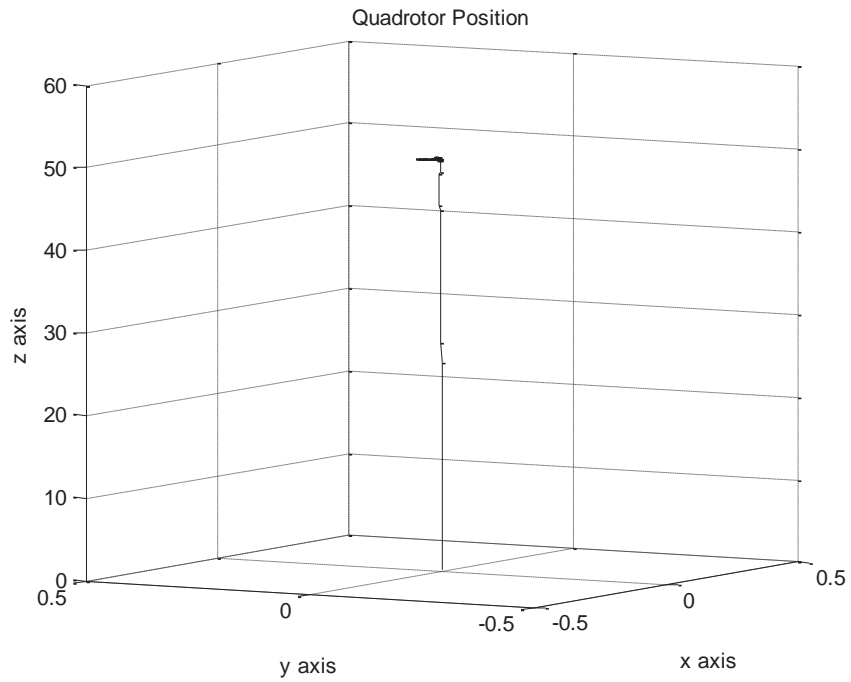


Figure 30 3D plot of Elevation to [0,0,50]m under wind gust

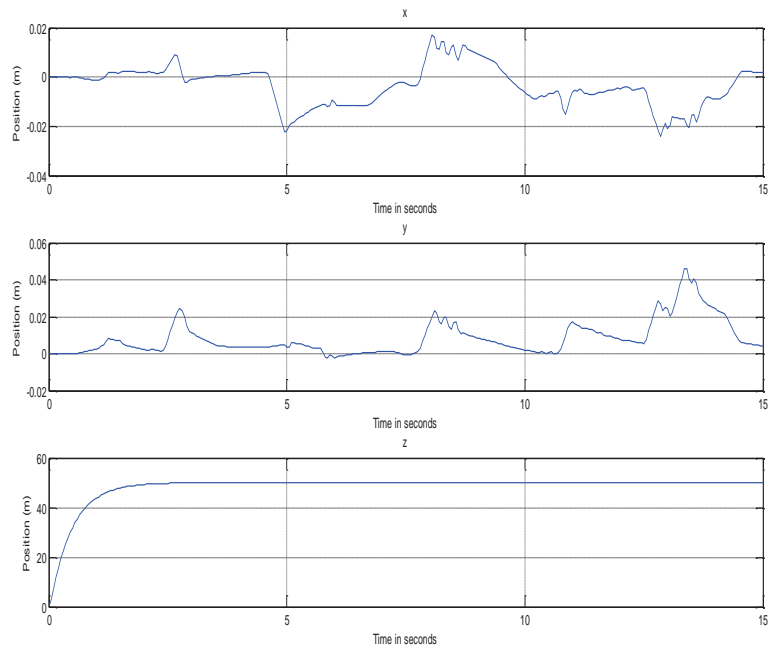


Figure 31 Position plots of elevation to [0,0,50]m under wind gust

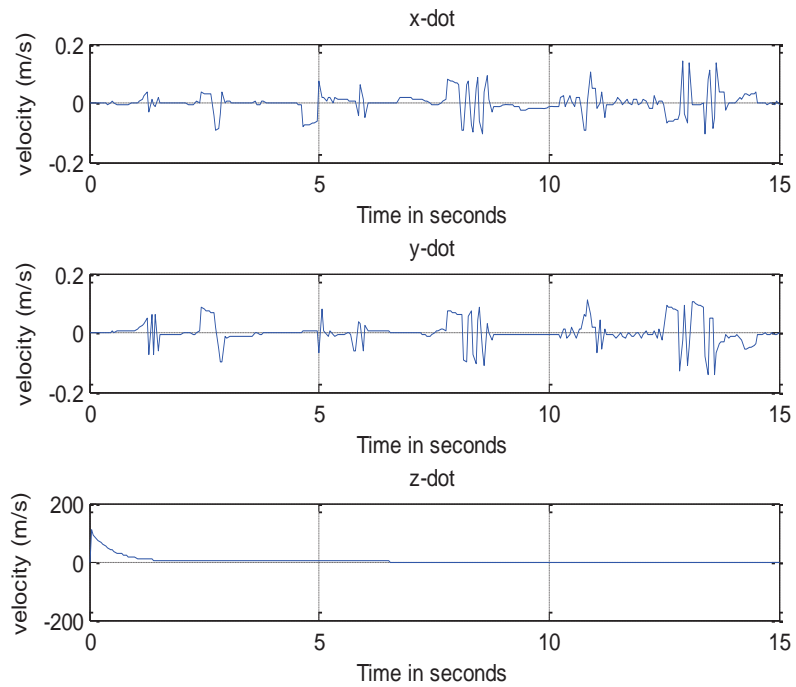


Figure 32 Velocity plots of elevation to [0,0,50]m under wind gust

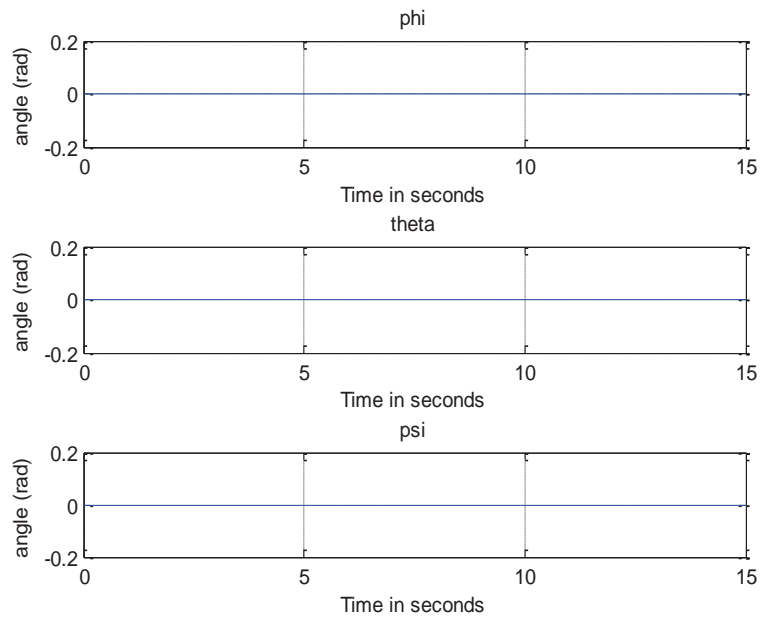


Figure 33 Orientation angles plots of elevation to [0,0,50]m under wind gust

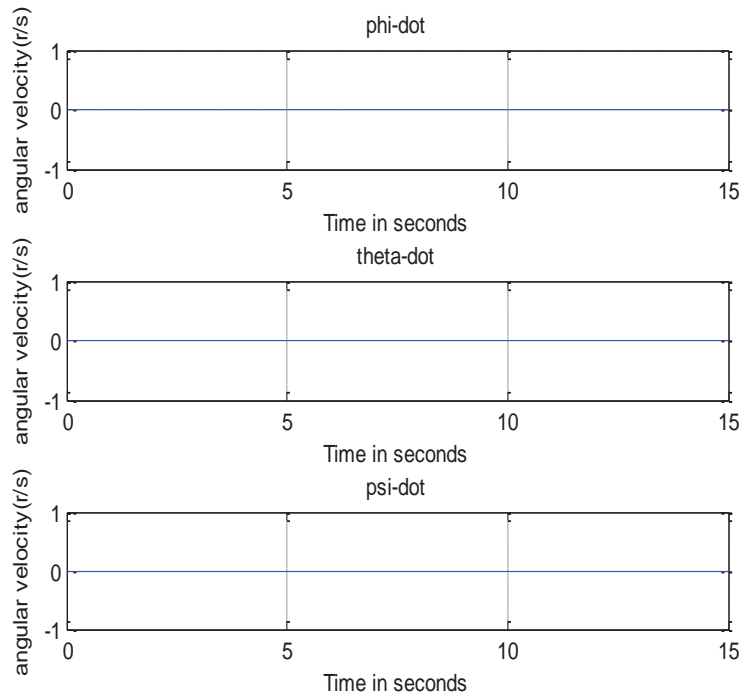


Figure 34 Angular rates of elevation to [0,0,50]m under wind gust

The table 7 shows the Mean Square Error (MSE), Maximum Absolute Error (MAE) and their corresponding confidence interval for ten randomly generated wind gust based on the macro approach. Here also, a 95% confidence interval is given.

In all simulations, the decentralized backstepping controller by far, shows more robustness against wind disturbance as compared to the cascade control.

Table 7 Results comparison between Cascade Control and Decentralized Backstepping Control under wind disturbance

Decentralized backstepping Control			Cascade Control	
	Mean Square Error [x, y]	Maximum Absolute Error [x, y]	Mean Square Error [x, y]	Maximum Absolute Error [x, y]
1	[0.0072,0.0061]	[0.0322,0.0310]	[0.54, 0.30]	[1.91,1.40]
2	[0.0067,0.0070]	[0.032,0.0415]	[0.60,0.50]	[1.83,1.37]
3	[0.0071,0.0074]	[0.0305,0.0280]	[0.42,0.53]	[0.91,1.35]
4	[0.0057,0.0067]	[0.0319,0.0345]	[0.54,0.48]	[1.30,1.30]
5	[0.0037,0.0051]	[0.0298,0.0277]	[0.44,0.31]	[1.26,1.29]
6	[0.007,0.0081]	[0.0325,0.031]	[0.38,0.88]	[1.47,1.90]
7	[0.007,0.0081]	[0.0325,0.031]	[0.36,0.43]	[2.20,2.42]
8	[0.007,0.0077]	[0.0363,0.069]	[0.49,0.63]	[1.31,3.12]
9	[0.0068,0.0073]	[0.0352,0.0393]	[0.65,0.68]	[2.10,1.86]
10	[0.0049,0.0058]	[0.0314,0.0314]	[0.31,0.39]	[0.91,1.27]
95% Confidence Interval				
Upper	[0.007,0.008]	[0.034,0.044]	[0.54,0.62]	[1.81,2.11]
Lower	[0.006,0.006]	[0.031,0.029]	[0.40,0.40]	[1.23,1.34]

2. Elevation to [10,10,50]m under wind disturbance

Quadrotor commanded move to the following coordinate [10,10,50]m. Below results Fig. 35, shows that the target is reached and hovering is achieved. Fig. 36 and 37 depicts the 3D plot and collapsed view respectively, which shows a precise location tracking of the coordinates. Fig. 38 and Fig. 39 shows the elevation and altitude and their corresponding velocities respectively. Fig. 40 and Fig. 41 shows that the attitude and velocities respectively are not affected.

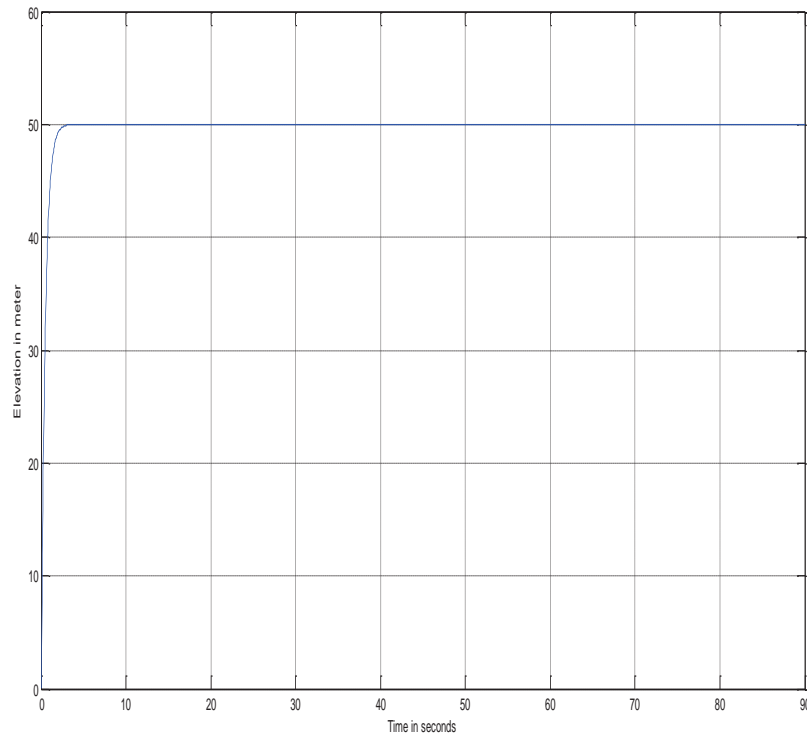


Figure 35 Elevation to height of 50m

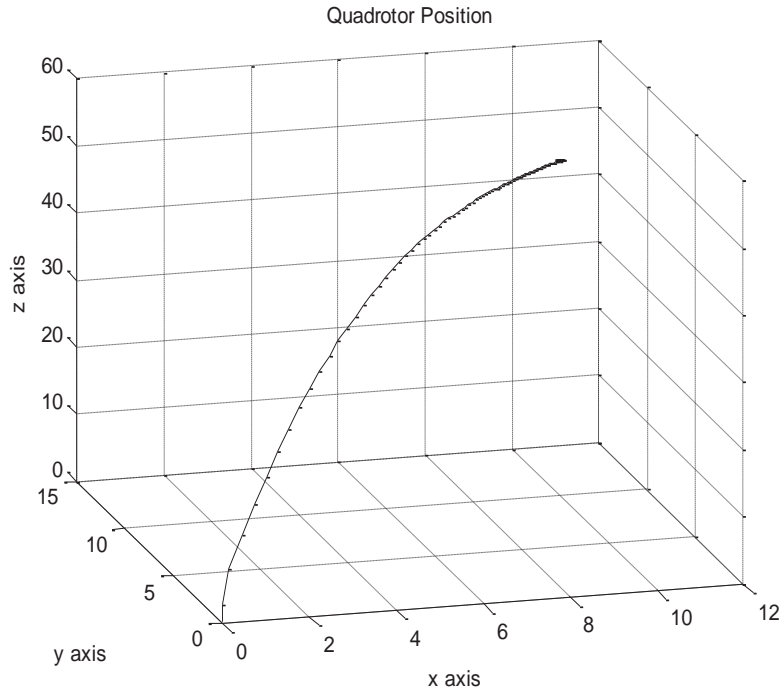


Figure 36 3D plot of target [10,10,50]m

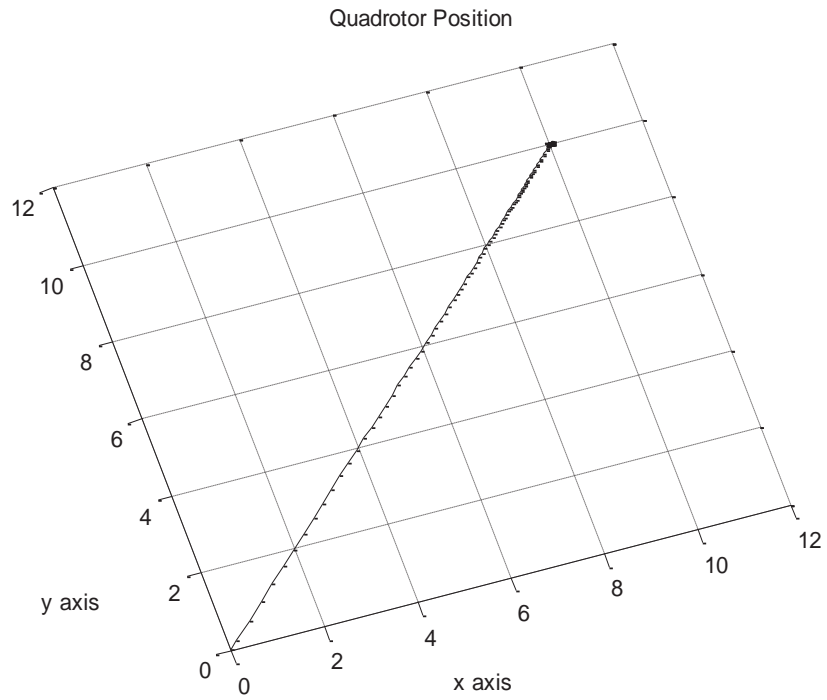


Figure 37 Collapsed View of 3D plot

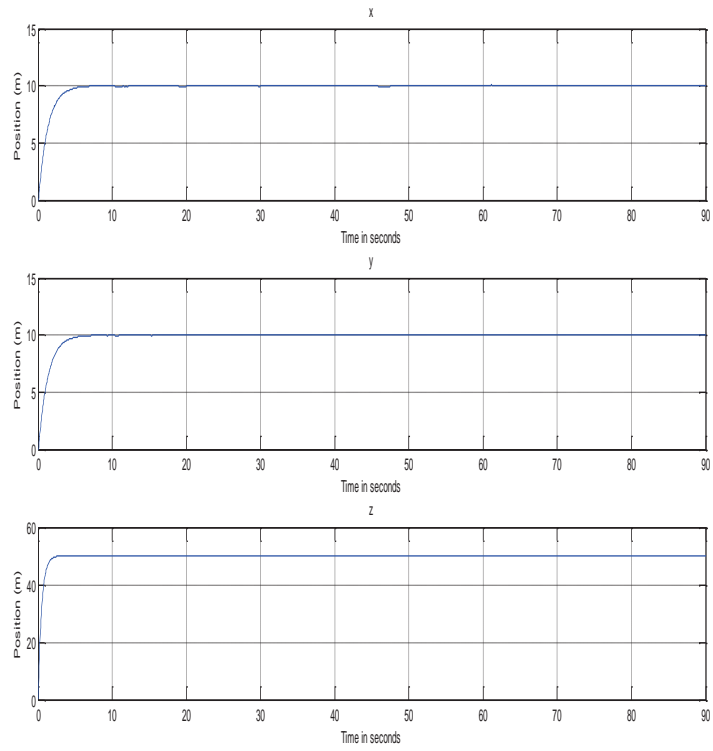


Figure 38 Plots of positions, x , y , and z for the coordinate $[10,10,50]$ m

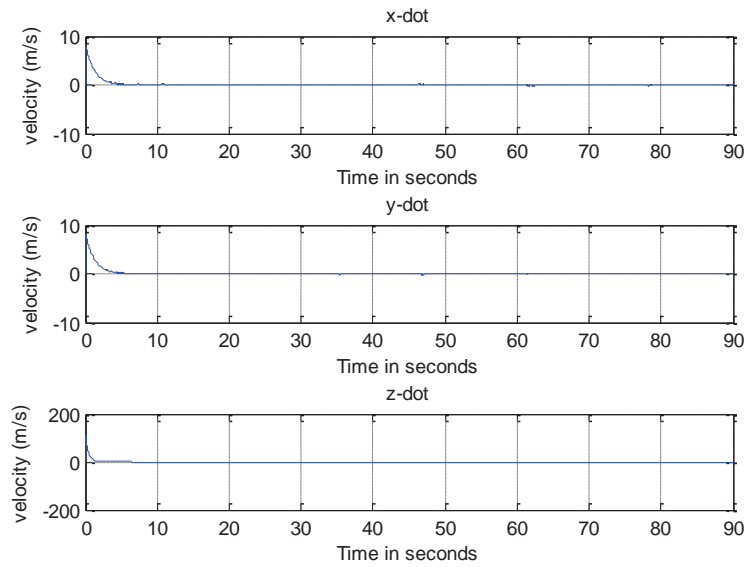


Figure 39 Velocities of x , y , z for the coordinate $[10,10,50]$ m

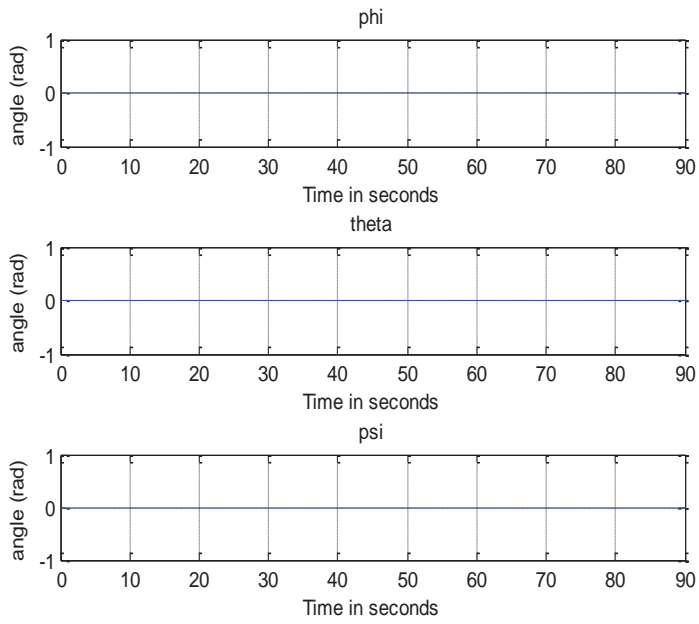


Figure 40 Orientation plots for the coordinate [10,10,50]m

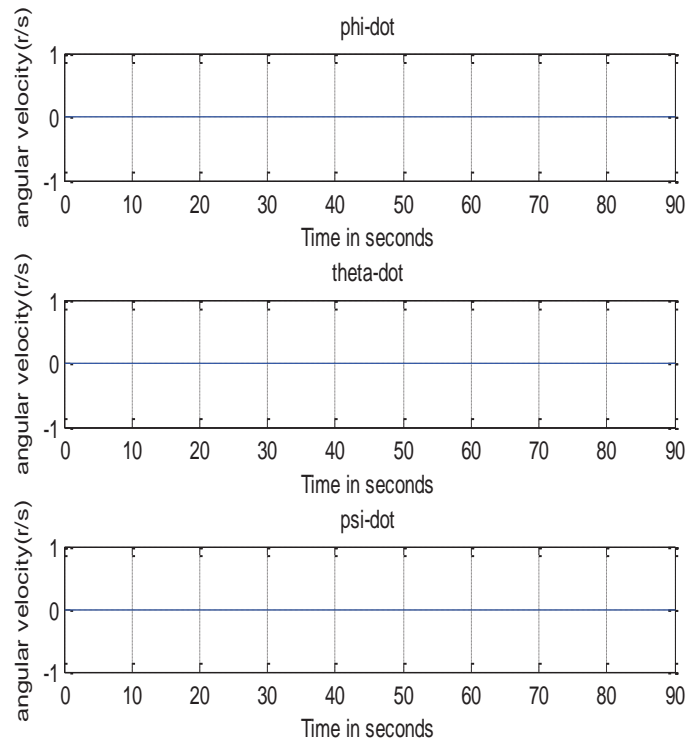


Figure 41 Plots of velocities, phi, theta and psi, for the coordinate [10,10,50]m

3. Elevation and thrust forward under wind disturbance

In Fig. 42 shows the elevation position of the command to take off vertically and then thrust further in x direction to a height of [10,0,50]m. In Figs. 43 and 44, the 3D plots is shown. Here, the controller is able to track the coordinate under wind disturbance with a negligible error due to wind. Fig. 45 which depicts the coordinates of the quadrotor moving in the x direction with a slight error in the y position as shown due to wind gust disturbance. Fig. 46 shows some fluctuation in the velocities due to effect of wind disturbance. Fig. 47 and Fig. 48 shows the angles are unaffected under wind disturbance. This shows the capability of the quadrotor itself to move towards a certain direction without compromising the attitude under wind disturbance.

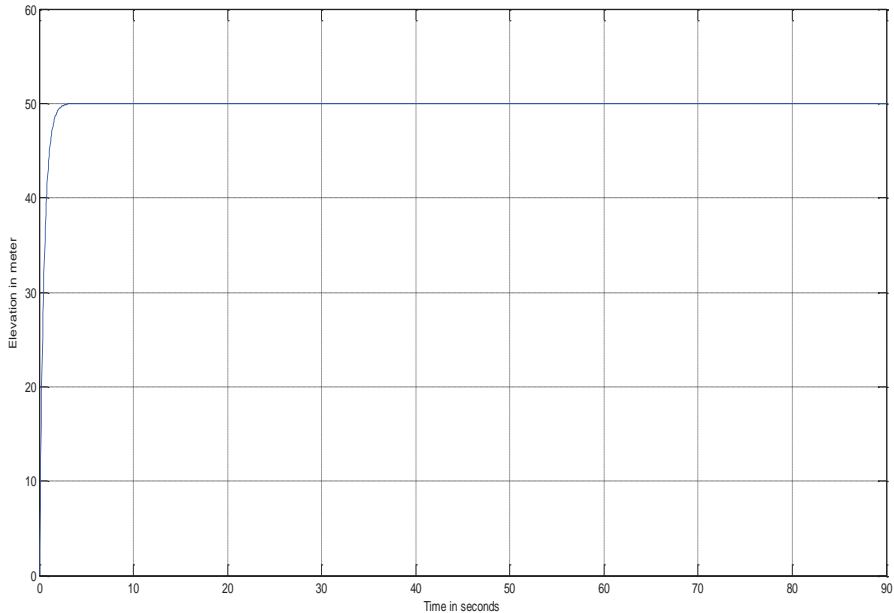


Figure 42 Position of elevation and thrust further to a [10,0,50]m location under wind gust

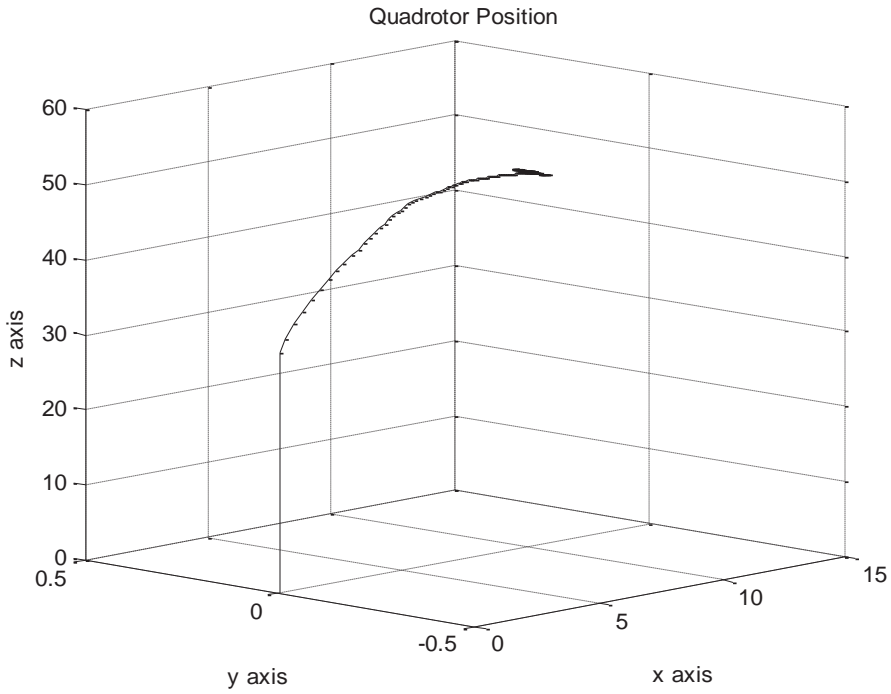


Figure 43 3D plot of Quadrotor position for elevation and thrust further to a [10,0,50]m location under wind gust

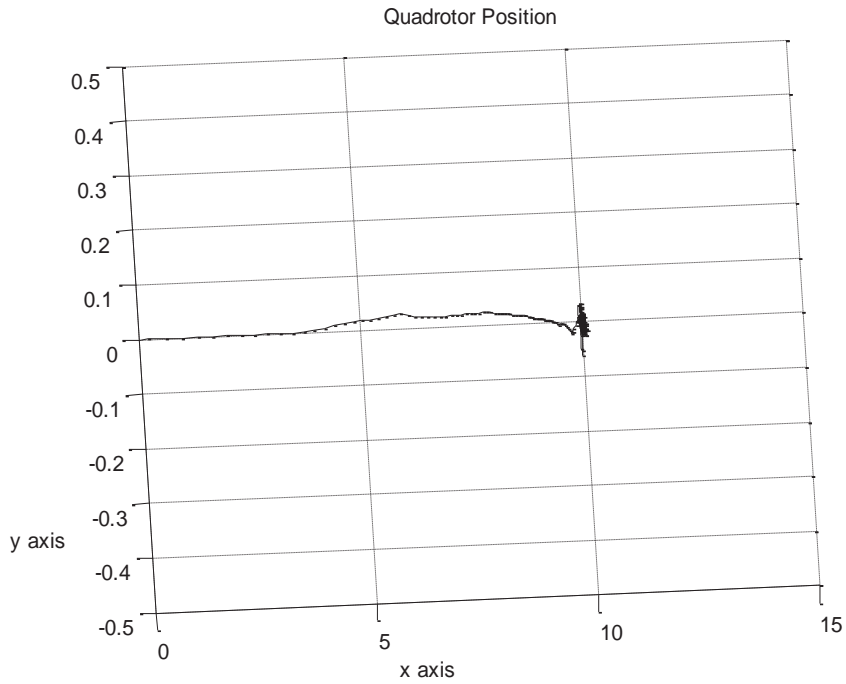


Figure 44 Collapsed view for elevation and thrust further to a [10,0,50]m location under wind gust

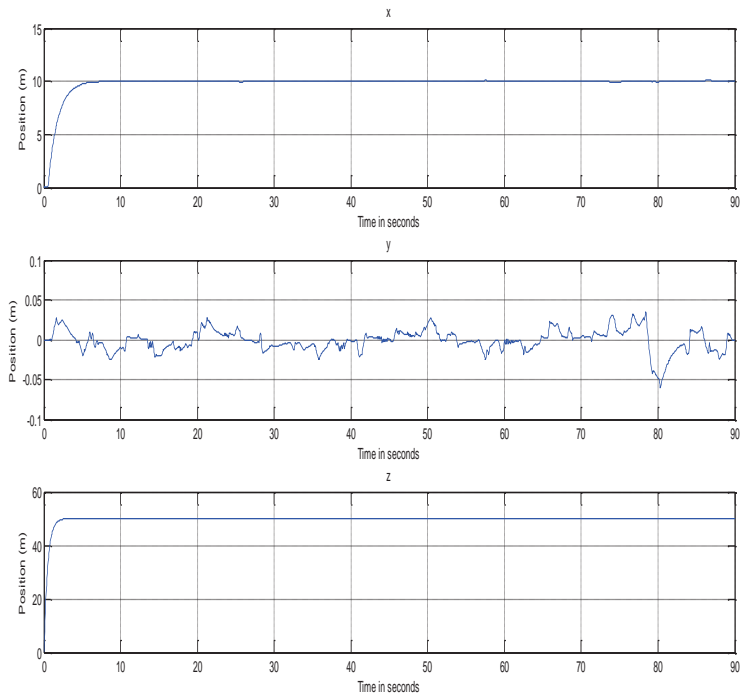


Figure 45 x, y and z position for elevation and thrust further to a [10,0,50]m location under wind gust

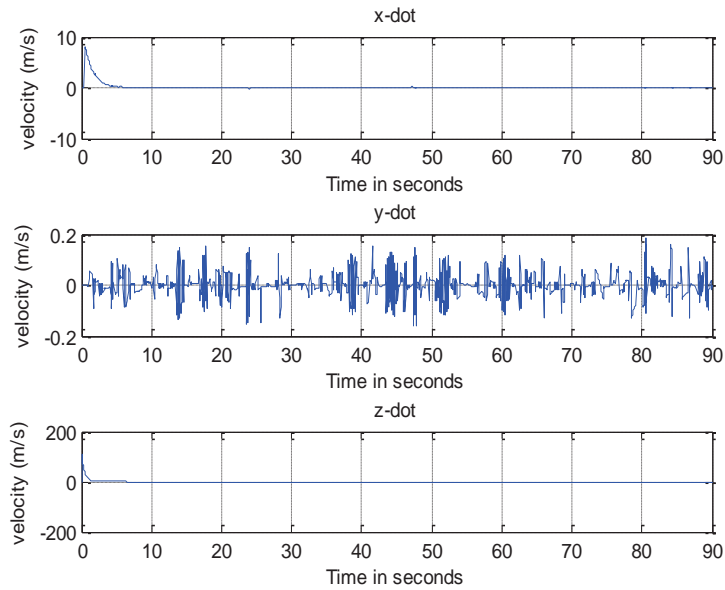


Figure 46 Velocities for elevation and thrust further to a [10,0,50]m location under wind gust

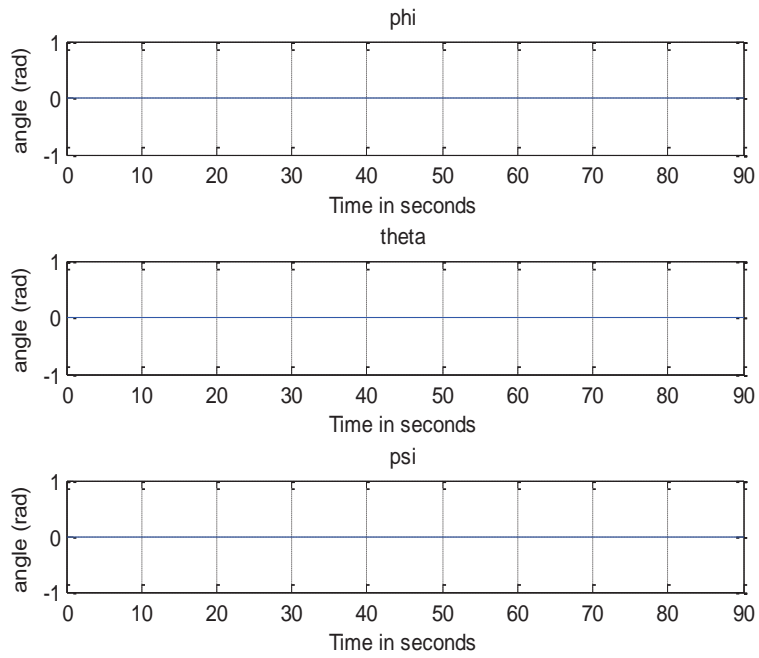


Figure 47 Orientation angles for elevation and thrust further to a [10,0,50]m location under wind gust

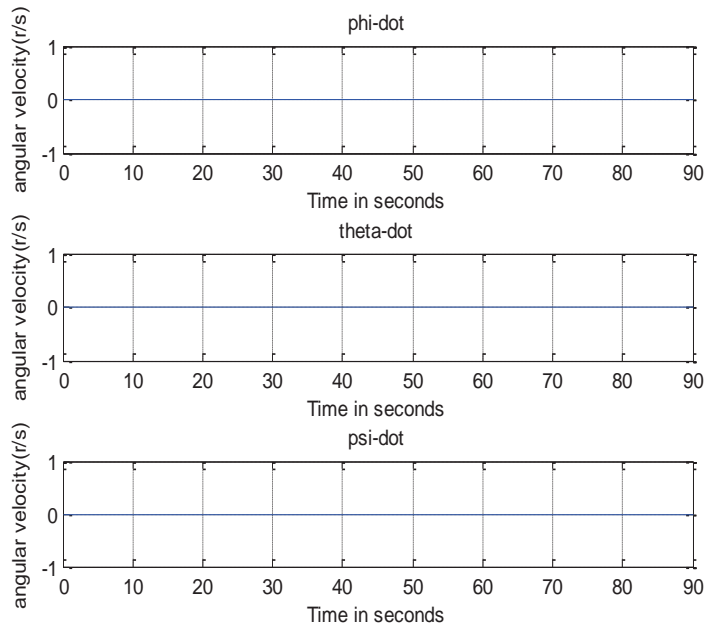


Figure 48 Angular velocities for elevation and thrust further to a [10,0,50]m location under wind gust

- Elevation hover to [10,10,50]m, move laterally and hover at an angle ($\pi/6$ rad).

In Fig. 49 the quadrotor is commanded to go and hover at [10,10,50]m and then move to another location at an angle. Here, there is some slight error in the height above the hovering point at the time the command was issued to tilt. This illustrates the capability of the controller to immediately keep track of the command. However this command also showcases the capability of the quadrotor. Figs. 50 and 51 shows the 3D plot. Figs. 52 and 53 shows the position and velocity transitions. Fig. 54 and Fig. 55 shows the orientation angles and their rates as well.

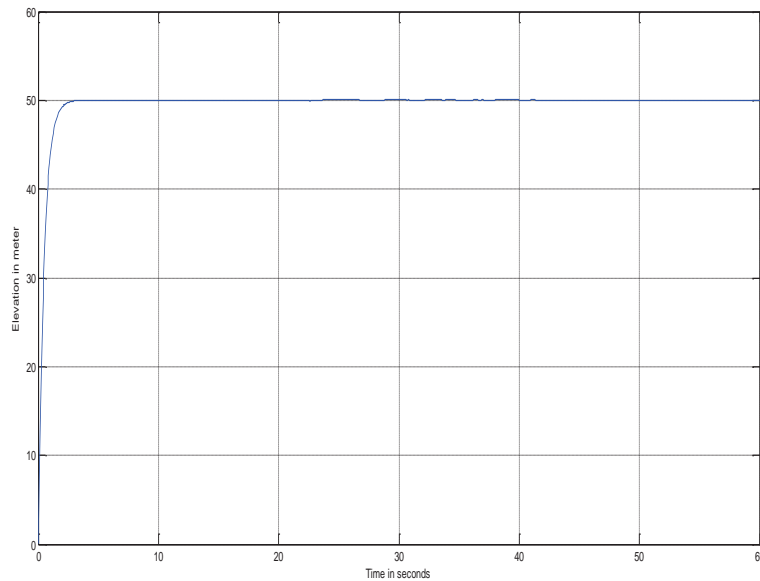


Figure 49 Height position for elevation, hovering and moving at an angle and then hover at an angle

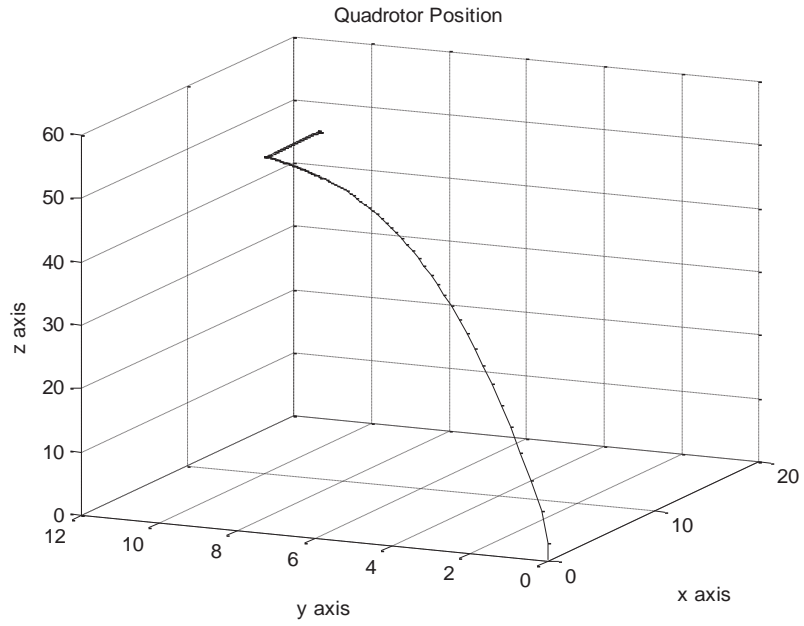


Figure 50 3D plot for elevation, hovering and moving at an angle and then hover at an angle

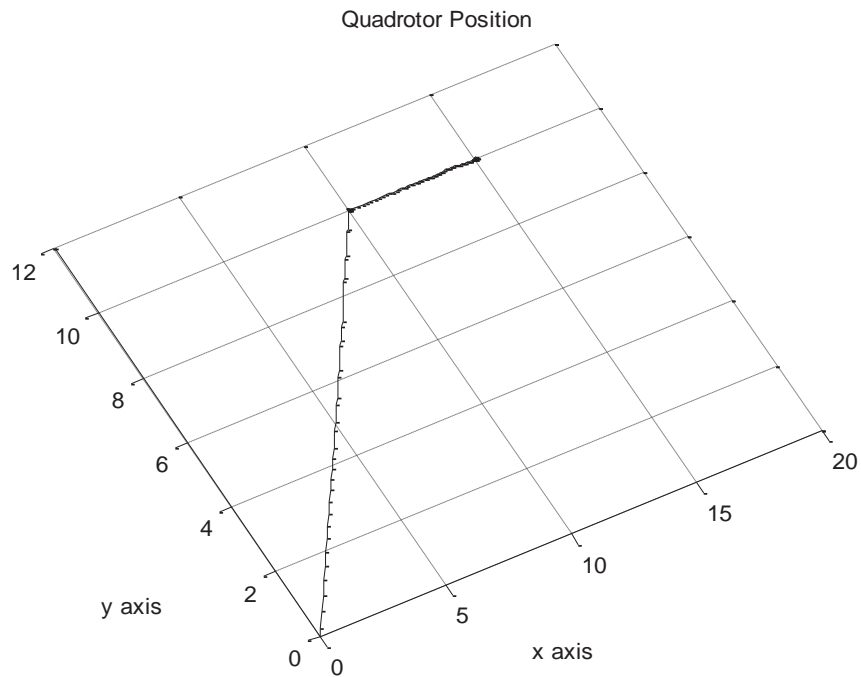


Figure 51 Collapsed 3D plot for elevation, hovering and moving at an angle and then hover at an angle

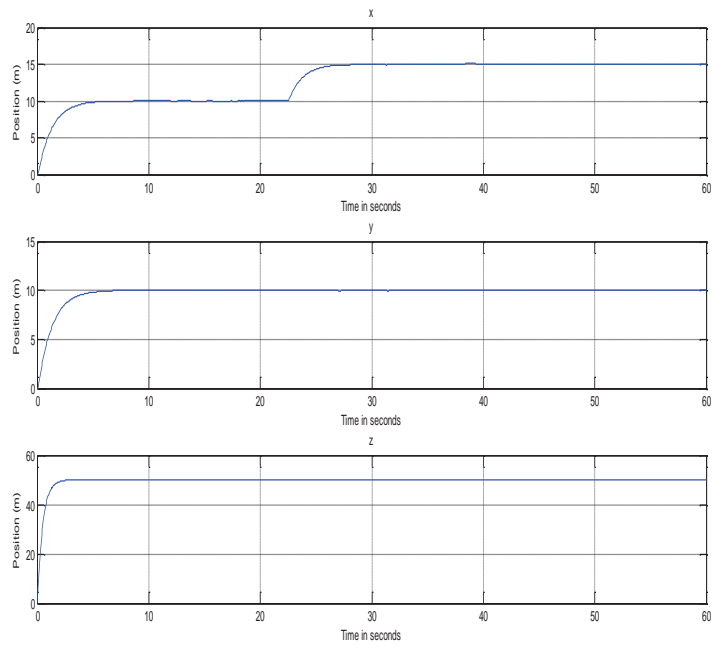


Figure 52 x, y and z position for elevation, hovering and moving at an angle and then hover at an angle

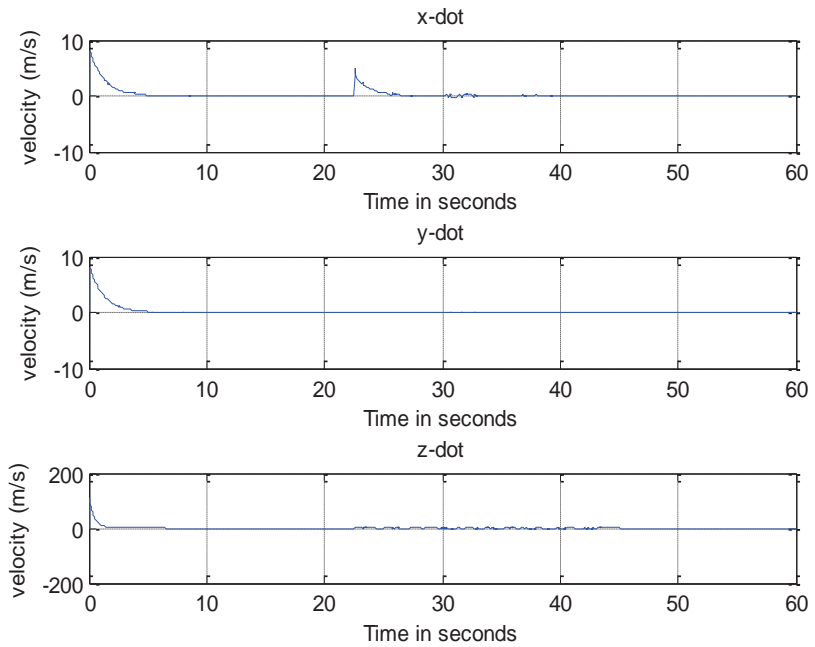


Figure 53 Velocities for elevation, hovering and moving at an angle and then hover at an angle

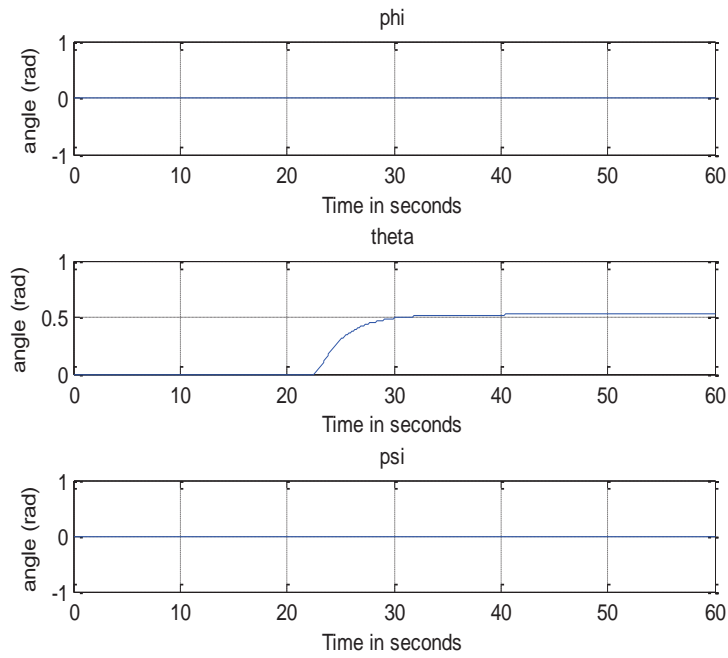


Figure 54 Orientation angles for elevation, hovering and moving laterally at an angle and then hover at an angle ($\pi/6$ rad)

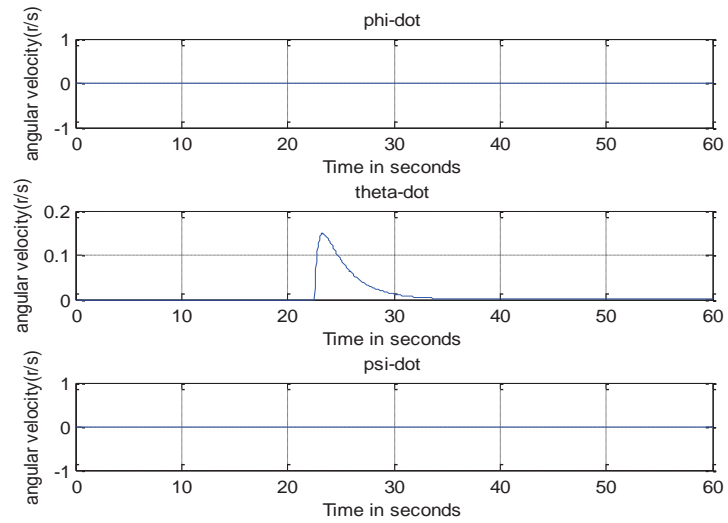


Figure 55 Angular velocities for elevation, hovering and moving at an angle ($\pi/6$ rad) and then hover at an angle

CHAPTER 7

CONCLUSION AND RECOMMENDATION

In this work, successful implementation of control strategies on a tiltrotor quadrotor under wind disturbances was achieved. In summary, the modelling equation for the tiltrotor quadrotor was first modified to incorporate wind gust derived from a macro approach found in the literature. Then, two control strategies namely, Cascade Control and Decentralized Backstepping Control were developed. The controller parameters are optimized using a heuristic technique known as the Differential Evolution (DE). Finally, simulation was carried out in MATLAB environment to test the effectiveness of both controllers.

A cascade control methodology which involved nested PID loops was adopted to control the tiltrotor quadrotor so as to cancel disturbances with additional inputs PID controllers. The wind model is derived from an approach which takes into account the wind velocity change, the wind gust step change, the variation of wind velocity with increase in height and the changes in wind direction. Simulation results demonstrated that the additional inputs of the tiltrotor quadrotor effectively mitigated wind disturbance while attaining the desired trajectory.

A decentralized backstepping control approach was also successfully demonstrated on the tiltrotor quadrotor under wind disturbance. A decentralization method is applied to the quadrotor dynamic to decouple the system into six subsystems. Then, a backstepping controller based on Lyapunov theory is used to achieve six control inputs capable of

controlling the six orientation and positions independently under wind disturbance.

Tuning of the controller parameters by DE was based on the minimization of the objective function which was the Integral Absolute Error (IAE). Simulation results from the decentralized backstepping control technique exhibited more robustness to wind disturbance when compared to those of the cascade control.

In the development of the decentralized backstepping control scheme, the inertia of the rotor is neglected due its minute value and the effect of the uncertainty term in each subsystem is left for future investigation.

Another suggestion for future work will include development of more controllers such as Feedback Linearization Control, Sliding Mode Control and Adaptive Control, building a prototype of the tiltrotor quadrotor and testing the performance experimentally. However, the effect of blade flapping would be considered and an adaptive technique would be used to account for parametric uncertainties.

References

- [1] Jaimes, Aldo, Srinath Kota, and Jose Gomez. "An Approach to Surveillance an Area Using Swarm of Fixed Wing and Quad-rotor Unmanned Aerial Vehicles UAV (s)". In System of Systems Engineering, 2008. SoSE'08. IEEE International Conference on, pp. 1-6. IEEE, 2008.
- [2] Yang, Hong Chul, Rami AbouSleiman, B. Sababaha, Ermal Gjoni, Daniel Korff, and O. Rawashded. "Implementation of an Autonomous Surveillance Quadrotor System". In AIAA Infotech Aerospace Conference, Seattle, pp. 2009-2047. 2009.
- [3] Mathew, Neil, Stephen L. Smith, and Steven L. Waslander. "Optimal Path Planning in Cooperative Heterogeneous Multi-robot Delivery Systems". In Algorithmic Foundations of Robotics XI, Springer International Publishing, pp. 407-423, 2015.
- [4] Mellinger, Daniel, Quentin Lindsey, Michael Shomin, and Vijay Kumar. "Design, Modeling, Estimation and Control for Aerial Grasping and Manipulation". In Intelligent Robots and Systems (IROS), 2011 IEEE/RSJ International Conference on, pp. 2668-2673. IEEE, 2011.
- [5] Zahawi, Rakan A., Jonathan P. Dandois, Karen D. Holl, Dana Nadwodny, J. Leighton Reid, and Erle C. Ellis. "Using Lightweight Unmanned Aerial Vehicles to Monitor Tropical Forest Recovery". *Biological Conservation* 186, pp 287-295 2015.
- [6] Bouabdallah, Samir. "Design and Control of Quadrotors with Application to Autonomous Flying". PhD diss., Ecole Polytechnique Federale de Lausanne, 2007.
- [7] Pounds, Paul, Robert Mahony, and Peter Corke. "Modelling and Control of a Large Quadrotor Robot". *Control Engineering Practice* 18, vol. 7, pp 691-699, 2010.
- [8] Bouadi, H., M. Bouchoucha, and M. Tadjine. "Modelling and Stabilizing Control Laws Design Based on Sliding Mode for an UAV Type-Quadrotor". *Engineering Letters* 15, vol. 2, pp 342-347, 2007.

- [9] Alaeddin Bani Milhiml and Youmin Zhang. "Gain Scheduling Based PID Controller for Fault Tolerant Control of a Quad-rotor UAV". In AIAA Infotech Aerospace Conference, 20 - 22 April 2010, Atlanta, Georgia.
- [10] Sadeghzadeh, Iman, Ankit Mehta, Youmin Zhang, and Camille-Alain Rabbath. "Fault-Tolerant Trajectory Tracking Control of a Quadrotor Helicopter Using Gain-Scheduled PID and Model Reference Adaptive Control". In Annual Conference of the Prognostics and Health Management Society, vol. 2. 2011.
- [11] Bi, Yingcai, and Haibin Duan. "Implementation of Autonomous Visual Tracking and Landing for a Low-Cost Quadrotor". *Optik-International Journal for Light and Electron Optics* 124, vol. 18, pp 3296-3300. 2013.
- [12] Leong, Bernard Tat Meng, Sew Ming Low, and Melanie Po-Leen Ooi. "Low-cost Microcontroller-Based Hover Control Design of a Quadcopter". *Procedia Engineering* 41, vol. 4. pp 458-464, 2012.
- [13] Gautam, Deepak, and Cheolkeun Ha. "Control of a Quadrotor Using a Smart Self-Tuning Fuzzy PID Controller". *International Journal of Advanced Robotic Systems* 10, 2013.
- [14] Goodarzi, Farhad, Daewon Lee, and Taeyoung Lee. "Geometric Nonlinear PID Control of a Quadrotor UAV on SE (3)." In *Control Conference (ECC), 2013 European*, pp. 3845-3850. IEEE, 2013.
- [15] Criado, Raúl M., and Francisco R. Rubio. "Autonomous Path Tracking Control Design for a Comercial Quadcopter". *IFAC-PapersOnLine* 48, vol. 9, pp 73-78, 2015.
- [16] Velasco, J., S. Garcia-Nieto, R. Simarro, and J. Sanchis. "Control Strategies for Unmanned Aerial Vehicles under Parametric Uncertainty and Disturbances: a Comparative Study". *IFAC-PapersOnLine* 48, vol. 9, pp 1-6, 2015.
- [17] Khalil, Hassan K. *Nonlinear Systems*. Prentice Hall, Upper Saddle River, Third Edition, New Jersey, 2002.
- [18] Voos, Holger. "Nonlinear Control of a Quadrotor Micro-UAV Using Feedback-Linearization". In *Mechatronics, 2009. ICM 2009. IEEE International Conference on*, pp. 1-6. IEEE, 2009.

- [19] Zemalache, Kadda Meguenni, and Hichem Maaref. "Controlling a Drone: Comparison between a Based Model Method and a Fuzzy Inference System". *Applied Soft Computing* 9, vol. 2, pp 553-562, 2009.
- [20] Luque-Vega, L., B. Castillo-Toledo, and Alexander G. Loukianov. "Robust Block Second Order Sliding Mode Control for a Quadrotor". *Journal of the Franklin Institute* 349, vol. 2, pp 719-739, 2012.
- [21] Benallegue, Abdelaziz, Abdellah Mokhtari, and Leonid Fridman. "High-order Sliding-Mode Observer for a Quadrotor UAV". *International Journal of Robust and Nonlinear Control* 18, vol. 4-5, pp 427-440, 2008.
- [22] Bouabdallah, Samir, and Roland Siegwart. "Backstepping and Sliding-Mode Techniques Applied to an Indoor Micro Quadrotor". In *Robotics and Automation, 2005. ICRA 2005. Proceedings of the 2005 IEEE International Conference on*, pp. 2247-2252. IEEE, 2005.
- [23] Yali, Yu, and Wang Yuanxi. "Controller Design of Quadrotor Aerial Robot". *Physics Procedia* 33 (2012): 1254-1260.
- [24] Zheng, Zhong, and Shenmin Song. "Autonomous Attitude Coordinated Control for Spacecraft Formation with Input Constraint, Model Uncertainties, and External Disturbances". *Chinese Journal of Aeronautics* 27, vol. 3, pp 602-612, 2014.
- [25] Mokhtari, M. Rida, and Brahim Cherki. "A New Robust Control for Minirotorcraft Unmanned Aerial Vehicles". *ISA transactions* 56, pp 86-101, 2015.
- [26] Cabecinhas, David, Rita Cunha, and Carlos Silvestre. "A Nonlinear Quadrotor Trajectory Tracking Controller with Disturbance Rejection." In *American Control Conference (ACC), 2014*, pp. 560-565. IEEE, 2014.
- [27] Madani, Tarek, and Abdelaziz Benallegue. "Control of a Quadrotor Mini-Helicopter via Full State Backstepping Technique". In *Decision and Control, 2006 45th IEEE Conference on*, pp. 1515-1520. IEEE, 2006.
- [28] Yu, Yao, Yukun Guo, Xun Pan, and Changyin Sun. "Robust Backstepping Tracking Control of Uncertain MIMO Nonlinear Systems with Application to

- Quadrotor UAVs". In Information and Automation, 2015 IEEE International Conference on, pp. 2868-2873. IEEE, 2015.
- [29] Li, Yibo, and Gang Wang. "Quad-Rotor Airship Modeling and Simulation Based on Backstepping Control". *International Journal of Control and Automation* 6, vol. 5, pp 369-384, 2013.
- [30] Escareño, Juan, Sergio Salazar, Hugo Romero, and Rogelio Lozano. "Trajectory Control of a Quadrotor Subject to 2D Wind Disturbances". *Journal of Intelligent & Robotic Systems* 70, vol. 1-4, pp 51-63, 2013.
- [31] Benallegue, Abdelaziz, Abdellah Mokhtari, and Leonid Fridman. "High-order Sliding-Mode Observer for a Quadrotor UAV". *International Journal of Robust and Nonlinear Control* 18, vol. 4, pp 427-440, 2008.
- [32] Altuğ, Erdinç, James P. Ostrowski, and Camillo J. Taylor. "Control of a Quadrotor Helicopter Using Dual Camera Visual Feedback". *The International Journal of Robotics Research* 24, vol. 5, pp 329-341, 2005.
- [33] Mahmoud, Magdi S. *Decentralized Systems with Design Constraints*, Springer-Verlag, UK, 2011.
- [34] Mohammadi, Mostafa, and Alireza Mohammad Shahri. "Decentralized Adaptive Stabilization Control for a Quadrotor UAV". In *Robotics and Mechatronics (ICRoM)*, 2013 First RSI/ISM International Conference on, pp. 288-292. IEEE, 2013.
- [35] Belhani, A., F. Mehazzem, and K. Belarbi. "Decentralized Backstepping Controller for a Class of Nonlinear Multivariable Systems". *ICGST ASCE Journal* 6, vol. 2, pp 41-48, 2006.
- [36] Dhaifullah, Mujahid, Abdul-Wahid A. Saif, Mohammad Al-Malki, and Mustafa El Shafie. "Decentralized Backstepping Control of Quadrotor". *Proc. of the 4th International Conference on Underwater System Technology: Theory and Applications 2012 (USYS'12)*, 5th & 6th December 2012, Shah Alam, Malaysia.

- [37] D'Amato, E., G. Di Francesco, I. Notaro, G. Tartaglione, and M. Mattei. "Nonlinear Dynamic Inversion and Neural Networks for a Tilt Tri-Rotor UAV". IFAC-Papers on Line 48, vol. 9, pp 162-167, 2015.
- [38] Oner, Kaan T., Ertugrul Cetinsoy, Mustafa Unel, and Mahmut F. Aksit. "Dynamic Model and Control of a New Quadrotor Unmanned Aerial Vehicle with Tilt-Wing Mechanism". In Proc. of the World Academy of Science, Engineering and Technology, 2008.
- [39] Hancer, Cevdet, Kaan T. Oner, Efe Sirimoglu, Ertugrul Cetinsoy, and Mustafa Unel. "Robust Position Control of a Tilt-Wing Quadrotor". In Decision and Control (CDC), 2010 49th IEEE Conference on, pp. 4908-4913. IEEE, 2010.
- [40] Ryll, Markus, Heinrich H. Bühlhoff, and Paolo Robuffo Giordano. "Modeling and Control of a Quadrotor UAV with Tilting Propellers". In Robotics and Automation (ICRA), 2012 IEEE International Conference on, pp. 4606-4613. IEEE, 2012.
- [41] Hua, Minh-Duc, Tarek Hamel, and Claude Samson. "Control of VTOL Vehicles with Thrust-Direction Tilting". arXiv preprint arXiv:1308.0191, 2013.
- [42] Elfeky, Mahmoud, Moustafa Elshafei, Abdul-Wahid A. Saif, and Mohamed F. Al-Malki. "Quadrotor Helicopter with Tilting Rotors: Modeling and Simulation". In Computer and Information Technology (WCCIT), 2013 World Congress on, pp. 1-5. IEEE, 2013.
- [43] Senkul, Fatih, and Erdinc Altug. "Adaptive Control of a Tilt-Roll Rotor Quadrotor UAV". In Unmanned Aircraft Systems (ICUAS), 2014 International Conference on, pp. 1132-1137. IEEE, 2014.
- [44] Nicol, C., C. J. B. Macnab, and A. Ramirez-Serrano. "Robust Adaptive Control of a Quadrotor Helicopter". Mechatronics 21, vol. 6, pp 927-938, 2011.
- [45] Liu, Hao, Dafizal Derawi, Jonghyuk Kim, and Yisheng Zhong. "Robust Optimal Attitude Control of Hexarotor Robotic Vehicles". Nonlinear Dynamics 74, vol. 4, pp 1155-1168, 2013.
- [46] Waslander, Steven L., and Carlos Wang. "Wind Disturbance Estimation and Rejection for Quadrotor Position Control". In AIAA Infotech@ Aerospace Conference and AIAA Unmanned... Unlimited Conference, Seattle, WA. 2009.

- [47] Kostas, Alexis, Kostas, George Nikolakopoulos, and Anthony Tzes. "Switching Model Predictive Attitude Control for a Quadrotor Helicopter Subject to Atmospheric Disturbances". *Control Engineering Practice* 19, vol. 10, pp 1195-1207, 2011.
- [48] Chen, Yanmin, Yongling He, and Minfeng Zhou. "Modeling and Control of a Quadrotor Helicopter System under Impact of Wind Field". *Research Journal of Applied Sciences, Engineering and Technology* 6, vol. 17, pp 3214-3221, 2013.
- [49] Basri, Mohd Ariffanan Mohd, Abdul Rashid Husain, and Kumeresan A. Danapalasingam. "Enhanced Backstepping Controller Design with Application to Autonomous Quadrotor Unmanned Aerial Vehicle". *Journal of Intelligent & Robotic Systems* 79, vol. 2, pp 295-321, 2015.
- [50] Chen, Yan-min, Yong-ling He, and Min-feng Zhou. "Decentralized PID Neural Network Control for a Quadrotor Helicopter Subjected to Wind Disturbance". *Journal of Central South University* 22, pp 168-179, 2015.
- [51] Solovyev Viktor V., Finaev Valery I., Zargaryan Yuri A. Shapovalov Igor O. and Beloglazov Denis A. "Simulation of Wind Effect on a Quadrotor Flight". *ARNP Journal of Engineering and Applied Science*, vol. 10, pp 1535-1538, 2015.
- [52] Vesterstrøm, Jakob, and Rene Thomsen. "A Comparative Study of Differential Evolution, Particle Swarm Optimization, and Evolutionary Algorithms on Numerical Benchmark Problems". In *Evolutionary Computation, 2004. CEC2004. Congress on*, vol. 2, pp. 1980-1987. IEEE, 2004.
- [53] Paterlini, Sandra, and Thiemo Krink. "Differential Evolution and Particle Swarm Optimisation in Partitional Clustering". *Computational Statistics & Data Analysis* 50, vol. 5, pp 1220-1247, 2006.
- [54] Vu, Vu Truong. "A Comparison of Particle Swarm Optimization and Differential Evolution". *International Journal on Soft Computing* 3, vol. 3, p 13, 2012.
- [55] Salih, Atheer L., M. Moghavvemi, Haider AF Mohamed, and Khalaf Sallom Gaeid. "Modelling and PID Controller Design for a Quadrotor Unmanned Air Vehicle". In *Automation Quality and Testing Robotics (AQTR), 2010 IEEE International Conference on*, vol. 1, pp. 1-5. IEEE, 2010.

- [56] Habib, Manal, Paul W. Quimby, Stephen Chang, Kimberly Jackson, and Mary L. Cummings. "Wind Gust Alerting for Supervisory Control of a Micro Aerial Vehicle". In Aerospace Conference, 2011 IEEE, pp. 1-7. IEEE, 2011.
- [57] Brosilow, Coleman, Joseph Babu. Techniques of Model Based Control, Prentice Hall, Upper Saddle River, New Jersey, 2002.
- [58] "Continuous Gusts." Wikipedia. https://en.wikipedia.org/wiki/Continuous_gusts. Accessed May 12, 2016.
- [59] "Von Kármán Wind Turbulence Model." Wikipedia. https://en.wikipedia.org/wiki/Von_Kármán_wind_turbulence_model. Accessed May 12, 2016.
- [60] Stephanopoulos, George. Chemical Process Control: an Introduction to Theory and Practice, Prentice Hall, Englewood Cliffs, New Jersey, 1985.

Vitae

Name :Abdulrahman Aliyu

Nationality :Nigeria

Date of Birth :4/4/1984

Email :abdulrahman.aliyu007@yahoo.com

Address :No. 336 Maikalwa Yamma, Naibawa, Kano, Nigeria

Academic Background :MS in Systems Engineering

Status of Publications.

1. Abdulrahman Aliyu, Moustafa Elshafei*, Abdul-Wahid A. Saif, Mujahed Aldhaifallah
Performance Evaluation of Quadrotor with Tilted Rotors under Wind Gusts. 2016 IEEE
International Conference on Advanced Intelligent Mechatronics. (Accepted)
2. Abdulrahman Aliyu, Moustafa Elshafei*, Abdul-Wahid A. Saif, Mujahed Aldhaifallah
Decentralized Backstepping Control of a Tiltrotor Quadrotor under Wind Gusts. 2016 To
be submitted to Journal.